Proceedings of the Workshop:

ACTIVE VOLCANISM & CONTINENTAL RIFTING

with special focus on the Virunga (North Kivu, DRC)

November 19-21, 2007

Hotel Parc Belle-Vue
Luxembourg
Grand-Duchy of Luxembourg

Organized by
The European Center for Geodynamics and Seismology (ECGS)

Supported by

European Center for Geodynamics and Seismology (ECGS)
Musée National d'Histoire Naturelle (MNHN)
The Council of Europe (EUR-OPA)
Ministère de la Culture
International Association of Volcanology and Chemistry of the Earth Interior (IAVCEI)
United Nations Educational, Scientific and Cultural Organization (UNESCO)
The Royal Museum for Central Africa, Belgium (RMCA)

Scientific Committee:

E. Calais	Purdue Univ., USA
C. Ebinger	Univ. of Rochester, USA
G. Ernst	Univ. of Ghent, Belgium
F. Lukaya	Goma Volcanological Observatory, RDC
N. Pagliuca	Istituto Nazionlae di Geofisica e Vulacnologia, Italy
D. Tedesco	Univ. of Napoli 2, Italy
T. Wright	Univ of Leeds, UK
G. Yirgu	Univ. Addis Ababa, Ethiopia

Local Organizing Committee:

C. Galassi	ECGS, L
G. Celli	MNHN/ECGS, L
E. Buttini	MNHN/ECGS, L
F. Kervyn	Royal Museum for Central Africa, B
N. d'Oreye	National Museum of Nat. History, L

Edited by:

Nicolas d'Oreye, François Kervyn and Dario Tedesco

Luxembourg - 2010

Workshop organized and Proceedings published
with the support of

MINISTERE DE LA CULTURE

ACCORD PARTIEL OUVERT

en matière de prévention, de protection et d'organisation des secours
contre les risques naturels et technologiques majeurs

du CONSEIL DE L'EUROPE

ISBN N° XXX

Centre Européen de Géodynamique et de Séismologie

Musée National d'Histoire Naturelle
Section Astrophysique et Géophysique, Luxembourg

To Jacques Durieux

We dedicate this volume of the *Cahiers du Centre Européen de Géodynamique et de Séismologie* to **Jacques Durieux,** who passed away on Jun 30th, 2009

For most scientists, talking or hearing about both Nyiragongo and Nyamulagira volcanoes is impossible without thinking of Jacques DURIEUX. For the last 40 years the inhabitants of Goma and its neighbourhoods got used to the presence of Jacques,. Similarly, all scientists working in the region, for a reason or another have come meeting him, knowing him and most of the time enjoying with him the field work, on top - or even inside the crater - of Nyiragongo, or simply sipping a beer in Goma.

Jacques arrived in what is today the Democratic Republic of Congo at the very end of the 60', after his college's years in Bruxelles at the Department of Geology. For young people, those were politically very difficult years in Europe and Jacques had chosen Goma to change his way of life, to meet new challenges and to learn new things. He indeed always had an incredible inner curiosity and thus very naturally immediately got passionate about volcanoes. Soon the Nyiragongo became "his" volcano. During those years, together with Haroun Tazieff - another atypical volcanologist - the most important scientific expeditions since ever were organized .

Durieux and Tazieff shared not only the love for volcanoes, and particularly for the Nyiragongo, but were also both from Belgium.

At this time, as for most of the Belgian citizens just after the independence, Jacques' stay in Congo was not easy, especially at the beginning. His personality did not really help, Jacques was very open and independent minded, very cultured, but he also had a strong and sometimes difficult character. He was not used to add water into his wine, so to speak. No compromises at all. He paid this behaviour repeatedly in his life. Yet, and despite of what most of his friends thought about him, Jacques was extremely shy and very passionate for all what he did and accomplished in his life.

Jacques was mainly a photographer; together with his long time friends, Katia and Maurice Kraft and Jean Louis Cheminé (from IPG-Paris) he pioneered what became common nowadays, that is adventure travelling. He coupled this talent with his fantastic way of writing along with a formidable intuition, and a strong knowledge and impressive memory of the field and its geology.

During the last 40 years, Jacques helped numerous scientists to work on both Nyiragongo and Nyamulagira. He produced the first, and we should say complete, collection of rock samples from the inner part of Nyiragongo's crater. His mountaineer expertise – he was an alpine guide - allowed him to mix his love for the volcanoes with a unique flavour of science.

In January 2002 - during and immediately after the eruption that destroyed part of the city - the United Nations (UN) asked him to contribute assessing the level of hazard for the city of Goma. Ever since he worked closely with Italian volcanologists and participated to several missions in Goma.

In 2005 he was hired by the United Nations to work closely with the Goma Volcano Observatory. That led him back to Goma, the thing he loved and wished the most. Despite inevitable criticisms by few volcanologists who pretended that Jacques did not have the right CV for this work, I personally believe that nobody else would have succeeded a better job. In addition, he helped on a regular basis many scientists to study the Nyiragongo and contributed to produce many scientific articles published in prestigious journals.

In 2004 and 2008, two expeditions were organized by Jacques and his colleagues to work within the crater of Nyiragongo. For the first time since Tazieff's period they were ambitious scientific expeditions, which rendered possible to several researchers, from a variety of fields and nations, to successfully work together.

In February 2009 Jacques was suddenly hospitalized in Kinshasa. Those who knew him say that he started feeling weak for about a year, having continuous pain on his back. But he was "allergic" to doctors and systematically refused any check up.

In March 2009 he was evacuated to Johannesburg. After more than a month without really knowing what was going on, he was finally diagnosed with a terminal cancer and he was again evacuated this time to Lyon in France. He died on June 30, 2009, just a few days after his 60^{th} birthday.

He is survived in Goma by his Congolese wife, Florence, and his three children in France, Héloïse, Arthur and Léonard, and her mother Agnes.

Those who knew him did not believe that such a strong and "invincible" man could possibly disappeared so suddenly, leaving us with such an incredible emptiness in our lifes.

I always thought that I have lost the older brother I never had. He was the person to talk about everything, the one who was always ready to help, to listen and to understand and why not … to argue with!

Since Jacques left from Goma, I have continuously tried - and this was the agreement with the UN -to keep warm his chair, trying to help his project going on and solving the enormous problems Jacques (and other scientists) faced in this environment.
When Jacques asked me to replace him (when he was in Johannesburg and knew to be critically sick) I thought this was an impossible mission. From his office, I was looking at the Nyiragongo. Yet it seemed to me that it was actually the volcano that was watching inside the office … asking where his old friend Jacques was.

I am sure that Jacques in the last months has terribly missed Goma and particularly the Nyiragongo, the only place that made him quiet and raised his mood as nothing else.

All Jacques' friends are terribly missing him. It is not unexpectedly that every time we get together we start talking about him. I am sure that the Nyiragongo also misses Jacques, the unique man that was so intimately related to this majestic mountain.

Dario TEDESCO

Preface

The current 29th Volume of the "Cahier du Centre Européen de Géodynamique et de Séismologie" is dedicated to the proceedings of the workshop entitled « **Active Volcanism & Continental Rifting, with a special focus on the Virunga (North Kivu, DRC) – AVCOR07**» which was held at the Hôtel Parc Belle-Vue in Luxembourg city from 19 to 21 November 2007.

In addition to the dozen contributions included in the current volume of the "ECGS Blue Book", another dozen contributions to the workshop and complementary scientific papers related to continental rifting are published in a special volume of "Journal of African Earth Sciences" (Elsevier).

The AVCOR workshop intended to bring together scientists from different disciplines (geology, volcanology, geodesy, geodynamics, seismology, geochemistry...) to share their knowledge and discuss the complex relationships between continental rifting and magmatism. Continental rifting is indeed one of most complex geodynamical settings of the plate tectonics involving crustal thinning, crustal extension and often a combination of seismic, thermal and/or igneous activity.
Among the places where continents break apart, the pan-African rift valley (or East African Rift) is the largest continental rifting zones on Earth. However it is also one of the less known plate boundaries. Multiple contributions related to continental rifting or rift magmatism in general were presented. Special attention was given to volcanic activity in the Western branch of the East African Rift (EAR) dominated by the Nyamulagira (the most active volcano in Africa) and Nyiragongo volcanoes (North Kivu, DRC). The last 2002 eruption of Nyiragongo reminded the international community what possibly rifting and volcanic eruptions can do in an urban area of several hundreds thousands inhabitants.

Moreover, important discussions took place about the risk and its management thanks to the contributions e.g. from the Italian Civil Protection, the Volcanic Ash Advisory Center in Toulouse, the Italian Institute for Geophysics and Volcanology and the Risk Management Unit from United Nations in Goma, DR Congo.

Other fundamental objectives of the workshop were 1) to stimulate or reinforce scientific collaborations between African countries as well as between Occidental and African countries, and 2) to allow as much African scientists as possible to participate to the meeting. Very few international scientific meeting take place in central Africa and even less in that specific domain and related geohazards notwithstanding the interest it bears for these regions. Too often also, meetings organized abroad are difficult to attend for most colleagues from developing countries, would it be for practical, administrative or economic reasons.

79 participants from 19 countries attended the workshop: 59 participants from 12 European countries (Belgium, France, Germany, Iceland, Italy, Luxembourg, Netherlands, Portugal, Spain, Sweden, Switzerland, UK), 15 participants from 6 African countries (Botswana, Cameroon, DR Congo, Ethiopia, South Africa, Tanzania) and 5 from USA. The program of the meeting comprises 40 oral presentations (including 6 invited keynotes lectures) and about the same amount of posters. A quarter of presentations were made by African scientists directly, and most other contributions included co-workers from across central Africa.

The meeting was also preceded by a 2-day field trip to the East Eifel Volcanic Field led by Dr Gerald Ersnt. It provided a first experience in field-based physical volcanology for 7 young scientists including two Congolese .

The fruitful participation of 15 African colleagues wouldn't have been possible without the financial support from the International Association of Volcanology and Chemistry of the Earth Interior (IAVCEI), the « Geological Applications of Remote Sensing » program from UNESCO, the United Nations' Risk Management Unit in Goma, as well as special budgets from the European Centre for Geodynamics and Seismology and the Royal Museum for Central Africa (Belgium). The official dinner offered by the Minister of Culture, Higher Education and Research in the wonderful Bourglinster Castle was another opportunity to strength the links between the participants and to stimulate numerous fruitful scientific discussions. It was also for many participants a first occasion to get familiar with the gastronomy and the architectural heritage of Luxembourg.

Furthermore we express our warm thanks the scientific committee and the supporting institutes (the National Museum of Natural History, the Royal Museum for Central Africa and the European Center for Geodynamics and Seismology). Without their countless efforts and enthusiasm it wouldn't have been possible to set up such a successful and fertile workshop. The scientific committee was composed of Prof. Eric Calais (Purdue University, USA), Prof. Cynthia Ebinger (University of Rochester, USA), Dr. Gerald Ernst (University of Ghent, Belgium), Dr François Kervyn (Royal Museum for Central Africa, Belgium), Mr François Lukaya (Goma Volcano Observatory, DR Congo), Dr Nicolas d'Oreye (National Museum of Natural History, Luxembourg), Dr Nicola Pagliucia (Instituto Nazionale di Geofisica e Vulcanologia, Italy), Prof. Dario Tedesco (University of Napoli 2, Italy), Prof. Tim Wright (University of Leeds, UK) and Prof. Gezahegn Yirgu (University of Addis Ababa, Ethiopia).

Above all, we also would like to acknowledge the reviewers from the scientific committee and the external reviewers (A. Oth , E. Suh, G. Bianchini, J. Fernandez) for their commitment. Indeed we must here explain the uncommon review process that was occasionally applied for some contributions and which led to the unusual long delay in the publication of the present volume. To stick to the philosophy of the workshop - that is to promote scientific collaboration with African scientists and to offer the opportunity of publishing - a considerable amount of time was dedicated to the pre-reviewing by editors, then to the reviewing process. Some submitted manuscripts didn't lead to publishing and it is hoped that for those authors it was still a valuable exercise —for some of them the first— to share their knowledge and experience in a language they were not familiar with and with sometimes limited scientific means. By the way, some commonly – or hopefully less commonly - encountered problems (such as serious health problems for some authors and reviewers or a dreadful airplane crash) did also slow the process. But all in one, the editors remain convinced that it was worth to proceed that way and we sincerely acknowledge the patience of the majority of authors who were accepted for publication already few months after the onset of collecting the contributions.

Finally, special thanks are sent to the members of the Local Organizing Committee who never spare their efforts to make the meeting a success down to the smallest details: Eric Buttini (National Museum of Natural History, Luxembourg), Corine Galassi (European Center for Geodynamics and Seismology, Luxembourg)

and Gilles Celli (National Museum of Natural History, Luxembourg). The idea of the meeting was raised less than 6 months prior the workshop took place. Organizing from scratch the venue of 80 people from three continents and ensure a smooth progress of the meeting was a real challenge.

In conclusion, we believe that AVCOR was a rich scientific workshop about a “hot topic”. But most of all we believe it was more than simply “yet another” scientific meeting. We are glad to see how some other initiatives bearing similar philosophy were blooming the last few years.

Nicolas d’Oreye
National Museum of Natural History, Luxembourg

François Kervyn
Royal Museum for Central Africa, Belgium

Dario Tedesco
University of Napoli 2, Italy

June 2010

Post Scriptum:

The present volume is dedicated to Jacques Durieux who was heading the Risk Management Unit in Goma. Jacques passed away prematurely on June 30 2009. He was involved in the monitoring of the volcanism in the Virunga since 1974. We loose a friend and with him invaluable field knowledge.

The volume is also dedicated to David Bizima, the chief of the porters that used to accompany all of the expedition to the Nyiragongo volcano. He was assassinated in October 2007. His tragic murder witness only part of the violence that affects the Eastern Congo.

European Center for Geodynamics and Seismology

26th ECGS Workshop

Co-organized with the National Museum of Natural History of Luxembourg and
The Royal Museum for Central Africa, Belgium

Active Volcanism & Continental Rifting
with special focus on the Virunga (North Kivu, DRC)

---- November 19-21, 2007 ----

- PROGRAM -

Monday November 19th

Chair: d'Oreye and Kervyn

13:30 - 13:50 Opening session: welcome and short allocutions by
M. Feider (ECGS), G. Bechet (Mnhn), J. Lavreau (MRAC), R. Bausch (FNR) and N.d'Oreye

Chair: Ebinger and Yirgu

13:50 - 14:30 Ebinger C. et al.
Time and Length Scales of Extension and Magmatism in the East African Rift System

14:30 - 14:50 Bryan S. and Ernst R.
Revised Definition of Large Igneous Provinces (LIPs)

14:50 - 15:10 Meyer R. et al.
Crustal-mantle interaction during a continental rift phase and its rift to drift evolution

15:10 - 15:30 Tentler T.
Dynamics of magma emplacement in controls of rift segmentation and propagation

15:30 -15:50 Sigmundsson F.
Multi-mode magma storage in volcano roots : Physical aspects and examples from Iceland

15:50 - 16:20. Coffee break and Posters session

Chair: Calais and Kervyn

16:20 - 17:00 Stamps S. et al. (speaker : Calais E.)
Present-day kinematics of the East African Rift

17:00 - 17:20 Delvaux D. et al.
Fault control of the Ngozi-Songwe geothermal system in the Rungwe Volcanic Province (East African rift, SW Tanzania)

17:20 - 18:30 Poster presentation session (2 min. oral presentation per poster)

18:30 - 19:30 Posters session

Tuesday November 20

08:00 - 08:30 Welcome

Chair: Ernst and Ebinger

08:30 - 08:50 Sebagenzi S.
The NE-SW nascent branch of the East African Rift system in the southeastern DR Congo and Zambia : geophysical evidences

08:50 - 09:10 Bauer F. et al.
Denudation history of the Rwenzori Mountains, Albertine Rift, Uganda

09:10 - 09:30 Ernst G. et al.
Research and Monitoring at Oldoynio Lengai Volcano, N. Tanzania: Review of recent advances

09:30 - 09:50 Basu A. et al.
Petrochemical Geodynamics of Nyiragongo and Nyamuragira Volcanoes in the Western Rift of the East African Rift System (EARS).

09:50 - 10:20 Coffee break and Posters session

Chair: Wright and Calais

10:20 - 11:00 Yirgu G. et al.
The Da'Ure volcanic eruption during the September 2005 Dabbahu rifting episode, Afar, Ethiopia

11:00 - 11:20 Gonzales P. et al.
Three dimensional volcanic deformation fields at Tenerife Island : integration of GPS and Time Series of InSAR (SBAS)

11:20 - 11:40 Van Cranenbroeck J.
Single to multi frequency GNSS signal processing solutions for active volcanism and continental rifting monitoring applications.

11:40 - 12:00 d'Oreye N. et al.
The November 2006 Nyamulagira eruption revealed by InSAR

12:00 - 13:30 Lunch

Chair: Tedesco and Lukaya

13:30 – 14:10 Tedesco D. et al.
The January 2002 Volcano-Tectonic Eruption of Nyiragongo volcano, Democratic Republic of Congo

14:10 - 14:30 Durieux J.
Preliminary Hazard Map of the Nyiragongo – Goma area (D.R. Congo)

14:30 - 14:50 Papale P. et al.
Hazard by lava flows at Nyiragongo volcano, West Virunga, from numerical simulations of lava flow paths.

14:50 - 15:10 Wadge G.
Temporal and spatial analysis of the eruptions of Nyamuragira

15:10 - 15:30 Vaselli O. et al.
Environmental impact of the Nyiragongo volcanic plume after the 2002 eruption

15:30 - 16:00 Coffee break and Posters session

Chair: Kervyn and d'Oreye

16:00 - 16:20 Husson P.
Operation of the VAAC Toulouse related to African Volcanoes

16:20 - 16:40 Kervyn F. et al.
Towards the progressive setup of a GIS platform integrating major monitored volcanic parameters of the GORISK project, Nyiragongo (DR Congo).

16:40 - 17:00 Reiter E.
Use of GIS and XML for geochemical data survey : information for public health issue, transfer to research

17:00 - 17:20 De Bernardinis B. et al. (speaker: V. Bosi)
Civil protection organization in volcanic emergency

17:20 - 18:20 Posters session

19:00 - 20:00 City Tour (included in the transportation to the official dinner)

20:30 - 00:30 Official dinner in the Medieval Castle of Bourglinster

Wednesday November 21

08:00 - 08:30 Welcome

Chair: d'Oreye and Wright

08:30 - 09:10 Wright T. et al.
Pre- co- and post-dyking deformation in the Dabbahu rift segment (Afar, Ethiopia) observed with satellite geodesy

09:10 - 09:30 Wauthier C. et al.
Modelling of InSAR displacements related with the January 2002 eruption of Nyiragongo volcano (DRC)

09:30 - 09:50 Heleno S. et al.
Discrimination between tropospheric effects and crustal deformation in SAR interferograms of Fogo volcano, Cape Verde Islands (1993 - 2006)

09:50 - 10:10 Yirgu G.
The August 2007 fissure eruption on the Dabbahu magmatic segment

10:10 - 10:30 Oyen A. et al.
InSAR monitoring of Ol Doinyo Lengai (Tanzania) : the March 2006 and July 2007 events

10:30 - 11:00 Coffee break and Posters session

<u>Chair: Pagliuca and Lukaya</u>

11:00 -11:40 Pagliuca N. et al.
The monitoring of seismic activity at Nyiragongo volcano through telemetered seismic network, Goma Volcano Observatory (Democratic Republic of the Congo)

11:40 - 12:00 Mavonga T. et al.
Seismic Activity prior to the recent eruptions of volcano Nyamuragira, Western Rift Valley of Africa

12:00 - 12:20 Shuler S. and Ekström G.
Anomalous Earthquakes in the Virunga

12:20 - 12:40 Kavotha et al.
Recent major magmatic processes at volcano Nyiragongo inferred from long-period earthquakes

12:40 - 14:00 Lunch

<u>Chair: Tedesco and Pagliuca</u>

14:00 - 14:20 Lukaya F. et al.
Recent seismic activity at volcano Nyamulagira, Western Rift Valley of Africa

14:20 - 14:40 Ferdinand R.
Lake Natron (Tanzania) earthquake of 17th July 2007: First Report

14:40 - 15:00 Tedesco D. et al.
Active and passive margins of the Western African Rift: Helium and Carbon Isotopic Signatures in the Lake Kivu Region (D.R.C)

15:00 - 15:20 Bobrowski N. et al.
Nyiragongo - A huge global bromine and sulphur emission into the free troposphere

15:20 - 15:50 Coffee break and Posters session

<u>Chair: Yirgu and Ernst</u>

15:50 - 16:10 Rouwet D. and Kusakabe M.
He-C-N isotope systematics of dissolved gases in Lake Nyos and Monoun (Cameroun, Western Africa)

16:10 - 16:30 Rosenthal A. et al. (speaker : Link K.)
Geochemical constraints on the origin of silica-poor alkaline volcanic rocks in the Toro-Ankole and Bufumbira regions of western Uganda

<u>Chair: d'Oreye and Kervyn</u>

16:30 - 17:30 Discussion and closing session

POSTERS

01	Albaric J. et al.	*SEISMO-TANZ'07: A dense seismological broadband network for a seismotectonic and structural study of the North Tanzanian Divergence*
02	Atanga M. et al. (speaker: <u>Ernst G.)</u>	*Health and environmental impact from basaltic ash falls : The case of the 1999 eruption of Mt Cameroon*
03	Chakrabarti R. et al. (speaker: Basu A.)	*Determining Eruption Ages and Timescales of Magmatic Processes in the Nyiragongo and Nyamuragira volcanics from U-Th-Ra disequilibria*
04	Chakrabarti R. et al. (speaker: Basu A.)	*Isotopic and Geochemical study of the Nyiragongo and Nyamuragira volcanics in the western rift, East African rift system*
05	van Cranenbroeck J. et al.	*Deployment of a GNSS volcano monitoring network on Nyiragongo.*
06	Croi et al.	*Feasibility Study on the Use of Available Geo satellite based Ranging Technologies for Monitoring Volcano Activities*
07	Durieux J.	*Nyiragongo volcano crisis: implication of United Nations in risk management*
08	Ernst G. et al.	*Morphometry and dynamics of a basaltic eruption: The case of the 1999 SW rift zone eruption of Mount Cameroon*
09	Fontijn K. et al.	*Volcanotectonic architecture of Rungwe Volcanic Province (SW Tanzania) : Low cost remote sensing study.*
10	Fontijn K. et al.	*A review on recent volcanology and volcanic hazards in the Rungwe Volcanic Province (SW Tanzania).*
11	Frischknecht C. et al.	*Challenges of SAR interferometry on Mount Cameroon*
12	Galle B. et al.	*Installation and first results from sulfur dioxide gas measurements on Nyiragongo within the Novac Project*
13	Hashimoto M. et al. (speaker: d'Oreye N.)	*Coseismic and Postseismic Displacements From the Mozambique Earthquake of 22 February 2006 Detected by InSAR*
14	Head E. et al.	*Eruptions of Nyamuragira Volcano, D.R. Congo (1980-2006)*
15	Kervyn M. et al.	*Analogue modelling of magma ascent and how it can be used to anticipate outbreak location at Central African volcanoes*
16	Kies A. et al.	*CO2 and radon measurements around Nyiragongo volcano*
17	Lukaya F.et al.	*Are seismicity and magma output at Nyamuragira in an increasing stage ?*
18	Mafany G.et al.	*Using lightning detection for a low cost monitoring of explosive eruptions in Sub-Saharan Africa: The case of Mount Cameroon*

19	Mathieu L. and van Wyk de Vries B.	*Sub-volcano complexes morphology and deformations that their formation induce in a volcanic edifice*
20	Modisi M. et al.	*Trans-Kalahari rifting: the case of the Okavango and Makgadikgadi basins, northern Botswana*
21	Njome S. et al. (speaker: Ernst G.)	*Mineral Chemistry and Whole Rock Geochemical Data of the Mount Cameroon Rift Basalts: Implications for Petrogenetic and Geotectonic Evolution*
22	Njome S. et al.	*Loading And Structural Instability At The Mount Cameroon Volcano, West Africa.*
23	Nkono C. et al.	*Geodynamic framework of Cameroon Volcanic Line highlighted by Shuttle Radar Topography Mission (SRTM) Digital Elevation Models (DEMs)*
24	Ntasin G. et al.	*Bambouto Caldera Formation and the 20th July 2003 landslides phenomena along the volcanic line, Cameroon*
25	d'Oreye N. et al.	*A major rifting event detected by InSAR : The Lake Natron (Tanzania) July 2007 crisis.*
26	Pasche N. et al.	*Methane in Lake Kivu: risks of gas eruption?*
27	Savelli C. (no speaker)	*Oligo-Miocene rift of the West Mediterranean area and the subsequent onset of westwards subduction*
28	Sawyer G. et al.	*Investigation into magma degassing at Nyiragongo volcano, Democratic Republic of Congo*
29	Smets B. et al.	*The "Mazukus" in south of Nyiragongo and Nyamulagira (Democratic Republic of Congo) : hypothesis of formation and first risk assessment.*
30	Tassi F. et al. (speaker: Vaselli O.)	*Chemical and isotopic stratigraphy of water and dissolved gases at Lake Kivu*
31	Trefois J.	*The International Charter of Space and Major Disasters: the 2002 Nyiragongo Emergency, city of Goma, North Kivu, D.R. Congo*
32	Tsafack J. et al.	*Occurrence of a sedimentary basement under the Mount Cameron active volcano (Cameroon Volcanic Line)*
33	Wafula M. et al.	*Seismic activity associated to the Nyamuragira eruptions for the period from 2000 to 2006, Virunga Region, D.R. Congo*
34	Wafula M. et al.	*Impacts of the eruptions of Nyiragongo on January 17, 2002 and Nyamuragira November 27, 2006 on the environment*
35	Wandji P. et al.	*The mount Manengouba, a mio-quarternary horst stratovolcano of the Cameroon Volcanic Line (Central Africa) : new volcanic successions, geochemical evidence and isotopic data*

List of Participants

Albaric Julie
Université Bretagne Occidentale
IUEM, UMR 6526 CNRS Domaines Océaniques
Place Nicolas Copernic
F-29280 Plouzane
France
Julie.Albaric@univ-brest.fr

Badryio Innocent
UNOPS
Risk Management Unit
07, avenue Loashi, Q. Murara
Commune de Karisimbi
Ville de Goma
D.R. Congo
ibadriyo@yahoo.fr

Bagalwa Monfort
Goma Volcanogical Observatory
CRSN
Rond Point 142
Mt. Goma, Goma
D.R. Congo
louisbagalwa@yahoo.fr

Basu Asish
University of Rochester
Dep.of Earth & Environmental Sciences
227, Hutchison Hall
Rochester, NY 14627
USA
abasu@earth.rochester.edu

Bauer Friederike
University of Heidelberg
Geological-Paleontological Institute
Im Neuenheimer Feld 234
D-69120 Heidelberg
Germany
Friederike.Bauer@urz.uni-hd.de

Bechet Georges
National Museum of Natural History
Director
Luxembourg
georges.bechet@mnhn.lu

Bennati Laura
Purdue University
2, Ter Rue du Docteur Rondeau
F-72220 Ecommoy
France
laura.bennati@gmail.com

Bobrowski Nicole
Istituto Naz. di Geofisica e Vulcanologia
INGV
Via Ugo la Malfa 153
I-90146 Palermo
Italy
n.bobrowski@pa.ingv.it

Bosi Vittorio
Italian Civil Protection
Via Vitorchiano 2
I-00189 Roma
Italy
Vittorio.Bosi@protezionecivile.it

Bryan Scott
Kingston University
School of Earth Sciences and Geography
Penrhyn Road
Kingston Upon Thames, Surrey KT1 2EE
United Kingdom
S.Bryan@kingston.ac.uk

Buttini Eric
National Museum of Natural History
Dept. of Geophysics / Astrophysics
19, rue Josy Welter
L-7256 Walferdange
Luxembourg
ebuttini@ecgs.lu

Calais Eric
Purdue University
Dept. of Earth & Atmospheric Sciences
West Lafayette, IN 47907
USA
ecalais@purdue.edu

Cayol Valérie
Université Blaise Pascal
Laboratoire Magmas et Volcans
5, rue Kessler
F-63038 Clermont-Ferrand Cedex
France
V.Cayol@opgc.univ-bpclermont.fr

Celli Gilles
National Museum of Natural History
Dept. of Geophysics / Astrophysics
19, rue Josy Welter
L-7256 Walferdange
Luxembourg
gilles.celli@ecgs.lu

List of Participants

Croi Willibald
Luxspace
Château de Betzdorf
L-6815 Betzdorf
Luxembourg
croi@luxspace.lu

Delvaux Damien
Royal Museum for Central Africa
Dept of Geology and Mineralogy
Leuvensesteenweg 13
B-3080 Tervuren
Belgium
damien.delvaux@africamuseum.be

d'Oreye Nicolas
National Museum of Natural History
Dept. of Geophysics / Astrophysics
19, rue Josy Welter
L-7256 Walferdange
Luxembourg
ndo@ecgs.lu

Durieux Jacques
UNOPS
Risk Management Unit
c/o Observatoire Volcanologique de Goma
Rond Point 142
Mt. Goma, Goma
D.R. Congo
jdurieux@chello.fr

Ebinger Cindy
University of Rochester
Earth & Environmental Sciences
227, Hutchison Hall
Rochester, NY 14627
USA
ebinger@earth.rochester.edu

Ernst Gerald
University of Ghent
Mercartor & Ortelius Research Centre
Eruption Dynamics
Krijgslaan 281 S8
B-9000 Ghent
Belgium
Gerald.Ernst@ugent.be

Feider Michel
Administration des Services de Secours
Directeur
Luxembourg
michel.feider@protex.etat.lu

Ferdinand Richard
University of Dar es Salaam
P.O. Box 35052
Uvumbuzi Road
Dar es Salaam
Tanzania
rf@udsm.ac.tz

Ferguson David
University of Oxford
Dept. of Earth Sciences
Patricks Road
Oxford OX1 3PR
United Kingdom
davidjferguson@gmail.com

Fontijn Karen
University of Ghent
Geology & Soil Sciences
Krijgslaan 281 S8
B-9000 Ghent
Belgium
Karen.Fontijn@Ugent.be

Frischknecht Corine
University of Geneva
Earth Sciences
13, rue des Maraîchers
CH-1205 Geneva
Switzerland
corine.frischknecht@terre.unige.ch

Galassi Corine
European Centre of Geodynamics and Seismology
ECGS
19, rue Josy Welter
L-7256 Walferdange
Luxembourg
corine.galassi@ecgs.lu

Galle Bo
Chalmers University of Technology
Dept. of Radio and Space Science
Horsalsvagen 11
412 96 Gothenburg
Sweden
bo.galle@rss.chalmers.se

Giuffrida Giovanni Bruno
Istituto Naz. di Geofisica e Vulcanologia
INGV
Via Ugo la Malfa 153
I-90146 Palermo
Italy
g.giuffrida@pa.ingv.it

List of Participants

Gonzalez-Mendez Pablo
University of Madrid
Institute of Astronomy and Geodesy
Faculty of Mathematical Science
Plaza de Ciencias 3
E-28045 Madrid
Spain
pjgonzal@mat.ucm.es

Gryuseels Guido
Royal Museum for Central Africa
General Director
Belgium
guido.gryseels@africamuseum.be

Head Elisabet
Michigan Technological University
Dept. of Geological & Mining Engineering & Sciences
1400 Townsend Dr., 630 Dow
GMES Department
Houghton, MI 49931
USA
emhead@mtu.edu

Heleno Sandra
Instituto Superior Tecnico
Dep. Fisica
Av. Rovisco Pais 1
P-1049-001 Lisboa Codex
Portugal
sandra.heleno@ist.utl.pt

Husson Philippe
VAAC Toulouse
Meteo France
42, Avenue Gaspard Coriolis
F-31057 Toulouse Cedex 1
France
philippe.husson@meteo.fr

Kavotha Déogratias
Goma Volcanogical Observatory
CRSN
Rond Point 142
Mt. Goma, Goma
D.R. Congo
ovggoma@yahoo.fr

Keller Joerg
Universität Freiburg
Mineralogisch-Geochemisches Institut
Albertstrase 23b
D-79104 Freiburg
Germany
Joerg.Keller@minpet.uni-freiburg.de

Kervyn Francois
Royal Museum for Central Africa
Centre d'Information Géographique
13 Leuvensesteenweg
B-3080 Tervuren
Belgium
francois.kervyn@africamuseum.be

Kervyn Matthieu
University of Ghent
Geology & Soil Sciences
Krijgslaan 281 S8/A.309
B-9000 Ghent
Belgium
Matthieu.KervynDeMeerendre@UGent.be

Kies Antoine
University of Luxembourg
162a, avenue de la Faïencerie
L-1511 Luxembourg
Luxembourg
antoine.kies@uni.lu

Klaudius Jurgis
Universität Freiburg
Mineralogisch-Geochemisches Institut
Albertstrase 23b
D-79104 Freiburg
Germany
Klaudius@uni-freiburg.de

Kraml Michael
BGR
Stilleweg 2
D-30665 Hannover
Germany
m.kraml@bgr.de

Link Klemens
University of Mainz
Dept. Geosciences
Becherweg 21
D-55099 Mainz
Germany
linkk@uni-mainz.de

Lukaya Francois
Goma Volcanogical Observatory
CRSN
Rond Point 142
Mt. Goma, Goma
D.R. Congo
lukayan@yahoo.fr

List of Participants

Mathieu Lucie
Université Blaise Pascal
Laboratoire Magmas et Volcans
5, rue Kessler
F-63000 Clermont-Ferrand
France
L.Mathieu@opgc.univ-bpclermont.fr

Mavonga Tuluka Georges
Wits University
CRSN
Private Bag X3
Wits 2050, Johannesburg
South Africa
mavotul@yahoo.fr

Meyer Romain
K.U. Leuven
Geo-Instituut
Afd. Geologie
Celestijnenlaan 200 E (02.202)
B-3001 Leuven-Heverlee
Belgium
mail@romain-meyer.eu

Modisi M.P.
University of Botswana
Dept of Geology
Privat Bag UB00704
Gaborone
Botswana
MODISIMP@mopipi.ub.bw

Nechia-Wantim Mabel
Cameroon
mabnechia@yahoo.com

Njome Stephen
University of Buea
P.O. Box 63
Buea S.W.P.
Cameroon
mnjome@yahoo.com

Nkono Collin
Université libre de Bruxelles
Lab.de Géochimie Isotopique et Géodyn.Chimique
17, Avenue des Attelages
Chaumont Gistoux
B-Dion-Valmont
Belgium
cnkono@ulb.ac.be

Oyen Anneleen
Technical University Delft
Kluyverweg 1
Nl-2629HS Delft
The Netherlands
A.M.Oyen@student.tudelft.nl

Paganelli Flora
European Centre for Geodynamics and Seismology
ECGS
19, rue Josy Welter
L-7256 Walferdange
Luxembourg
flora.paganelli@ecgs.lu

Pagli Carolina
University of Luxembourg
Faculty of Sciences
Technology and Communication
162a, rue de la Faiencerie
L-1511 Luxembourg
Luxembourg
carolina.pagli@uni.lu

Pagliuca Nicola
Istituto Naz. di Geofisica e Vulcanologia
INGV
Via di Vigna Murata 605
I-00143 Roma
Italy
pagliuca@ingv.it

Papale Paolo
Istituto Naz. di Geofisica e Vulcanologia
INGV
Via della Faggiola 32
I-56126 Pisa
Italy
papale@pi.ingv.it

Pasche Natacha
Swiss Federal Institute of Aquatic Science and Technology
Seestrasse 79
CH-6047 Kastanienbaum
Switzerland
Natacha.Pasche@eawag.ch

Pik Raphael
Centre de Recherche Pétrographiques et Géochimiques
CRPG
15, rue Notre-Dame
F-54501 Vandoeuvre-les-Nancy
France
rpik@crpg.cnrs-nancy.fr

List of Participants

Reiter Eric
2, rue des Abeilles
F-57440 Algrange
France
ereiter@free.fr

Rouwet Dmitri
Istituto Naz. di Geofisica e Vulcanologia
INGV
Via Ugo la Malfa 153
I-90146 Palermo
Italy
dmitrirouwet@gmail.com

Santo Alba
Università di Firenze
Dipartimento di Scienze della Terra
Via la Pira 4
I- 50121 Firence
Italy
alba.santo@unifi.it

Savelli Carlo
ISMAR-CNR (Geologia Marina)
Via Gobetti 101
I-40129 Bologny
Italy
carlo.savelli@bo.ismar.cnr.it

Sawyer Georgina
University of Cambridge
Dept of Geography
Downing Site
Cambridge CB2 3EN
United Kingdom
gms26@cam.ac.uk

Sebagenzi Stanislas
University of Lubumbashi
Boîte Postale 1825
Lubumbashi
D.R. Congo
ssebagenzi@yahoo.fr

Shuler Ashley
Columbia University
Lamont-Doherty Earth Observatory
548 Riverside Dr., Apt. 3C
New York, NY 10027
USA
ashuler@ldeo.columbia.edu

Sigmundsson Freysteinn
University of Iceland
Nordic Volaconologial Center
Askja, Sturlugata 7
101 Reykjavik
Iceland
fs@hi.is

Smets Benoît
Royal Museum for Central Africa
Dept. of Geology
13 Leuvensesteenweg
B-3080 Tervuren
Belgium
benoit@reaj.org

Tedesco Dario
University of Napoli 2
Dipartimento di Scienza Ambientali
Via Vivaldi 43
I-81100 Caserta
Italy
dtedesco@unina.it

Tentler Tatiana
Institute of Earth Sciences Jaume Almera
Barcelona
Spain
tatiana_tentler@hotmail.com

Toombs Andrew
University of Reading
Whiteknights
PO Box 217
Reading, Berkshire, RG6 6AH
United Kingdom
gw@mail.nerc-essc.ac.uk

Trefois Philippe
Royal Museum for Central Africa
Dept. of Geology
13 Leuvensesteenweg
B-3080 Tervuren
Belgium
ptrefois@africamuseum.be

Tsafack Ferdinand
Université de Paris Sud
Orsay
s/c Mr. Ouema, Socaver
B.P. 1456
Douala
Cameroon
ftsafack2000@yahoo.fr

List of Participants

Van Cranenbroeck Joël
Leica Geosystems
Rue du Tienne de Mont 11
B-5530 Moont
Belgium
Joel.VanCranenbroeck@leica-geosystems.com

Van Overbeke Anne-Catherine
Royal Museum for Central Africa
Dept. of Geology
13 Leuvensesteenweg
B-3080 Tervuren
Belgium
vanoverbeke@hotmail.com, anne-catherine.van.overbeke@africamuseum.be

Vaselli Orlando
Università di Firenze
Dipartimento di Scienze della Terra
Via la Pira 4
I- 50121 Firence
Italy
orlando@geo.unifi.it

Wadge Goeff
University of Reading
Environmental Systems Science Center
Whiteknights
PO Box 217
Reading, Berkshire, RG6 6AH
United Kingdom
gw@mail.nerc-essc.ac.uk

Wafula Mifundu Dieudonne
Goma Volcanogical Observatory
CRSN
Rond Point 142
Mt. Goma, Goma
D.R. Congo
dmwafula@yahoo.fr

Wandji Pierre
Univeristé de Yaoundé I
Laboratoire de Géologie
Boîte Postale 47
Yaoundé
Cameroon
pierrewandji@yahoo.fr

Wauthier Christelle
Royal Museum for Central Africa
Dept. of Geology
13 Leuvensesteenweg
B-3080 Tervuren
Belgium
c.wauthier@gmail.com

Wright Tim
University of Leeds
School of Earth and Environement
Leeds LS2 9JT
United Kingdom
eartjw@earth.leeds.ac.uk

Yirgu Gezahegn
University of Addis Ababa
Department of Earth Sciences
P.O. Box 1176
Addis Ababa
Ethiopia
gezahegnyirgu@yahoo.com /
yirgu.g@geol.aau.edu.et

Automatic InSAR systematic processing and web based tool for efficient data mining: application to volcano monitoring in Africa.

N. d'Oreye[1] and G. Celli[1]

[1]Geophysics/Astrophysics Dept., National Museum of Natural History of Luxembourg; ndo@ecgs.lu

Abstract

For the need of volcano monitoring in Africa, all possible ENVISAT ASAR data is systematically programmed and ordered for a given set of Modes, Tracks and Swaths. This data is processed using a (semi-)automated procedure based on the DORIS InSAR open source software (TU Delft), Mathematica© routines and shell scripts running on Mac OS X environment. This mass processing produces thousands of phase interferograms, coherence maps, amplitude images and deformation maps (in cm). The results are available as Sun-Rasters in radar geometry or as geocoded images in conventional GIS format (ENVI© or GMT grid).
A web-based tool was developed for visualizing the rapidly increasing number of conventional differential SAR Interferograms (InSAR) and related products.
More than a simple visualization tool, it also helps to easily discriminate artifacts from deformations, to detect seasonal variations or continuous slow phenomena, or to detect timing errors or frame shifts.
Eventually potentially interesting interferograms, identified thanks to this bulk procedure are re-processed using manually fine-tuned parameters.

Key words: InSAR, volcano monitoring, Open source software

Introduction:

A possible way (at least partly) to overcome the vegetation-induced decorrelation within differential SAR interferograms is to increase the number of SAR acquisitions. This will in principle increase the chances of producing interferograms with favorable small temporal and spatial baselines.
This method has been applied successfully since 2005 at the National Museum of Natural History in Luxembourg for studying and monitoring a.o. some active African volcanoes in Cameroon, Democratic Republic of Congo, Cape Verde and Tanzania (d'Oreye et al. 2008).
The drawback of this method is of course the number of interferograms (and associated maps) that will obviously increase roughly as $(n-n^2)/2$, where "n" is the number of available SAR scenes in a given Mode, Track and Swath.
A web-based tool has hence been developed for helping with both monitoring and data mining.
More than being a tool for quickly and efficiently looking through the thousands of InSAR products, it also helps to easily discriminate artifacts from deformations, to

detect seasonal variations or continuous slow phenomena, and to detect timing errors or frame shifts. The web tool is also password-protected allowing an easy and secure way to share the information through the Internet.
The semi-automated InSAR processing:

All possible ENVISAT ASAR data is systematically programmed and ordered for a given set of Modes, Tracks and Swaths over some tectonically active targets. When an e-mail issued by ESA announces the availability of a new scene, an automated script downloads and archives the corresponding files. Since the data is only made available for 10 days on the ESA FTP server such a script avoids loosing the data in case of the operator being absent.

For each target (i.e. each volcanic or tectonic area in the present case) a set of optimized parameters is pre-defined for automated processing: crop size, multilook factor, Digital Elevation Model (DEM), maximum spatial baseline, file naming and locator, etc…
Based on these parameters, a single command line will either allow for computing a single interferogram or all the possible combinations of a given scene, with each compatible scene in the database. The command line calls more scripts, duplicates and modifies input cards, modifies, renames or copies input and output files, following the needs to execute the different Doris steps up to the production of geocoded relevant InSAR products and maps.
To avoid crashing computers, freezing the bulk process within an infinite loop and filling hard disk with error logs, scripts are equipped with watchdog functions that would abort a failed process. It would then rename the corresponding directory according to the reason of the failure and step to the next InSAR pair to process. Large computations can then be safely launched unmonitored.

Instead of triggering the automated bulk processing by the notification mail issued by ESA, the launch procedure is kept manual in order 1) to avoid too many simultaneous launches on a given computer and 2) for the operator to choose between a few options such as:
- The type of precise orbit(s) to use. Since the DEOS precise orbits are not produced anymore on a regular basis, one can choose to use either Preliminary or Verified precise orbits provided by ESA. These are available respectively about 3 days and 1 Month after the SAR acquisition. A Mathematica routine interpolates, resamples and transforms them in the appropriate format. The corresponding information is then inserted in the results file and the Doris processing is carried out. Other Mathematica programs are available to remove manually possible orbital residual lefts in the interferograms.
- Modify the default list of masters or slaves scenes to combine with the given image.
- Choosing to unwrap the final residual phase. Given the time required for unwrapping large scenes with large decorrelated patches (as for the highly vegetated areas under equatorial latitudes) it is usually not advised to run that option by default. For interferograms that would require it, another single command line script can be launched afterward.

The web-based visualization tool:

Yet another group of automated scripts will collect the results of all the pairs processed for a given Mode, Track and Swath. The Sun-Raster figures in radar geometry are converted to JPG and renamed with relevant information such as the volcano name, the Master and Slave orbit numbers and their dates, the perpendicular and temporal baselines and the altitude of ambiguity.
Filtered phase interferograms, filtered phase interferograms wrapped on the amplitude and coherence maps are stored in distinct directories either at low resolution (for web thumbnails icons) or medium resolution (for visualization). The automated conversion and down-sampling is made using shell scripts and open source software (ImageMagick, http://www.imagemagick.org/).
A cron job checks every 30 minutes if new figures are available and transfers them from the mass storage hard disks up to the Web server (hosted on a Mac OS X Server) using an open source synchronization tool (rsync, http://samba.anu.edu.au/rsync/).
An InSAR XHTML table is then created making use of CSS (Cascading Style Sheet) features for the design of the Web pages.

When logged in using the appropriate password, the first page allows the user to choose a target (i.e. a volcano) and a Mode/Track/Swath in the column to the left, then the type of product to display (coherence, phase or phase wrapped on the amplitude) in a new dialog box. A first triangular table pops up (See figure 1) filled with small yellow-green icons. These icons refer to computed interferograms. The column and line headers are respectively the Master and Slave characteristics (date and orbit number). Empty cells mean that no interferogram could be computed for that given pair (usually because the perpendicular baseline is too large). The table allows the user to view on a single page which products are available vs. time.

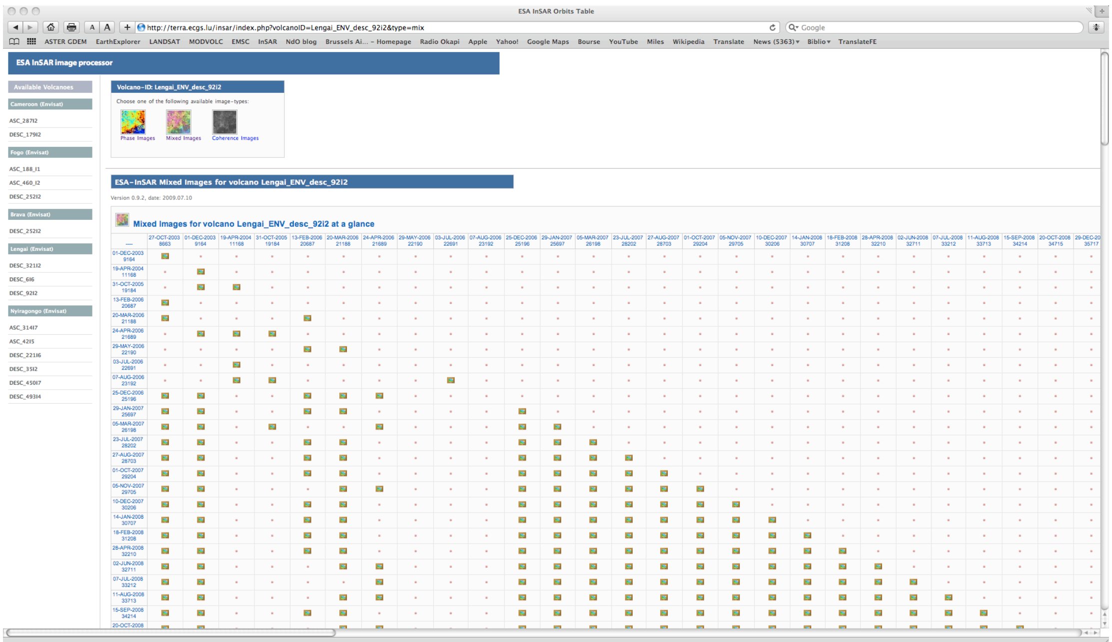

Figure 1: Web tool for InSAR product visualization. The operator selects a target (i.e. a volcano) in the column to the left and a Mode/Track/Swath. Three kinds of product to display are offered in the small upper window: the coherence maps, the phase interferograms, or the phase wrapped on the amplitude. The table displays all the

interferometric pairs computed in the database.

When the operator moves the mouse pointer over one of these yellow cells, a low-resolution preview of the interferometric product pops up. Clicking on the icon opens a new page displaying the medium resolution product. Relevant information about interferometric parameters and processing is given in the name of both the low and medium resolution images.
A second table similar to the first one is also displayed. It shows low-resolution thumbnails instead of the yellow icons. The table is then obviously much larger but offers a global view and the possibility to compare many products at a glance (See figure 2).

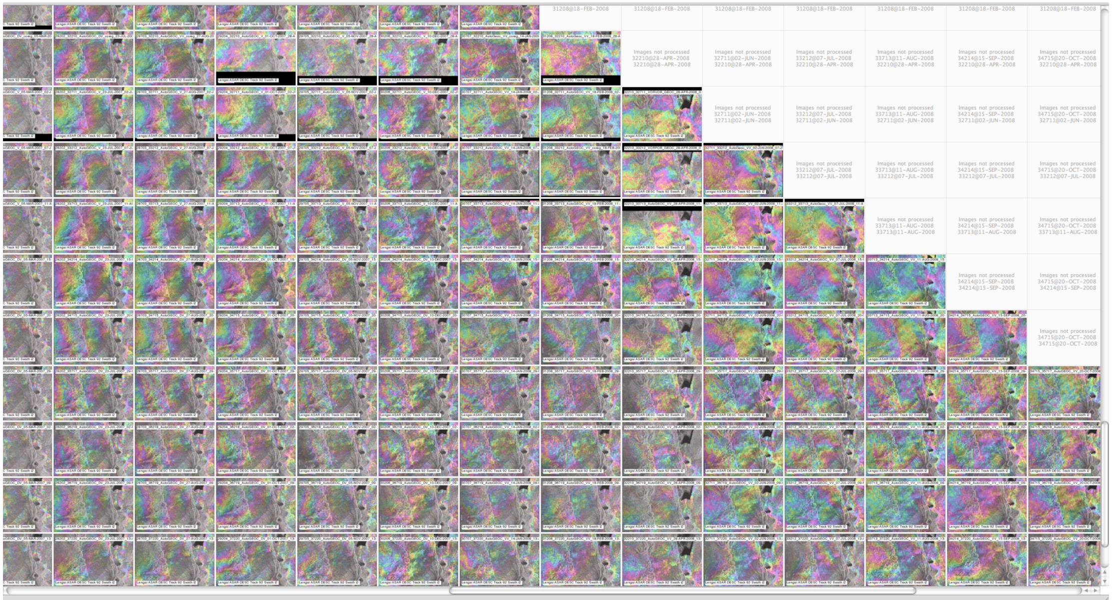

Figure 2: Extract of the table provided by the visualization web tool for InSAR products. The table shows here phase interferograms wrapped on the amplitude images (Tanzania: Lengai Descending Track 92 Swath i2). Clicking on one of the low-resolution products displays it in a new window at higher resolution.

The position of each interferometric product in the tables (based on its Master and Slave orbit numbers) is computed using the open source PHP language combined with the "jquery" java script library (http://www.jquery.org, mainly used to make the figures to pop up under the mouse pointer).

For the sake of transfer/display speed, the visualization is limited to medium resolution images. The full resolution Sun-Rasters or geocoded products are (so far) only accessible by ftp on request.

Application for data mining and events discrimination:

The web tool is more than a simple interface to visualize a large amount of data and look through the thousands of different interferograms. It offers the possibility of quickly and easily discriminating atmospheric artifacts from deformations, to detect seasonal variations and continuous slow phenomena, or to detect timing errors or frame shift.

For instance, when an atmospheric artifact affects an image, all and only the interferograms combining that image will display that signal (that is one line and one column in the table). Moreover, the sign of phase delay will be reverted when the affected images are used as the Master or the Slave in the interferogram. Figure 3 shows an example of an atmospheric artifact localized on the Nyiragongo volcano in DR Congo. Since the neighboring Nyamulagira volcano does not shows similar features despite its proximity (15 km) and similar dimensions, and since that behavior hasn't been observed in past data, at a first glance, one could easily misinterpret that signal as an inflation/deflation of the volcano.

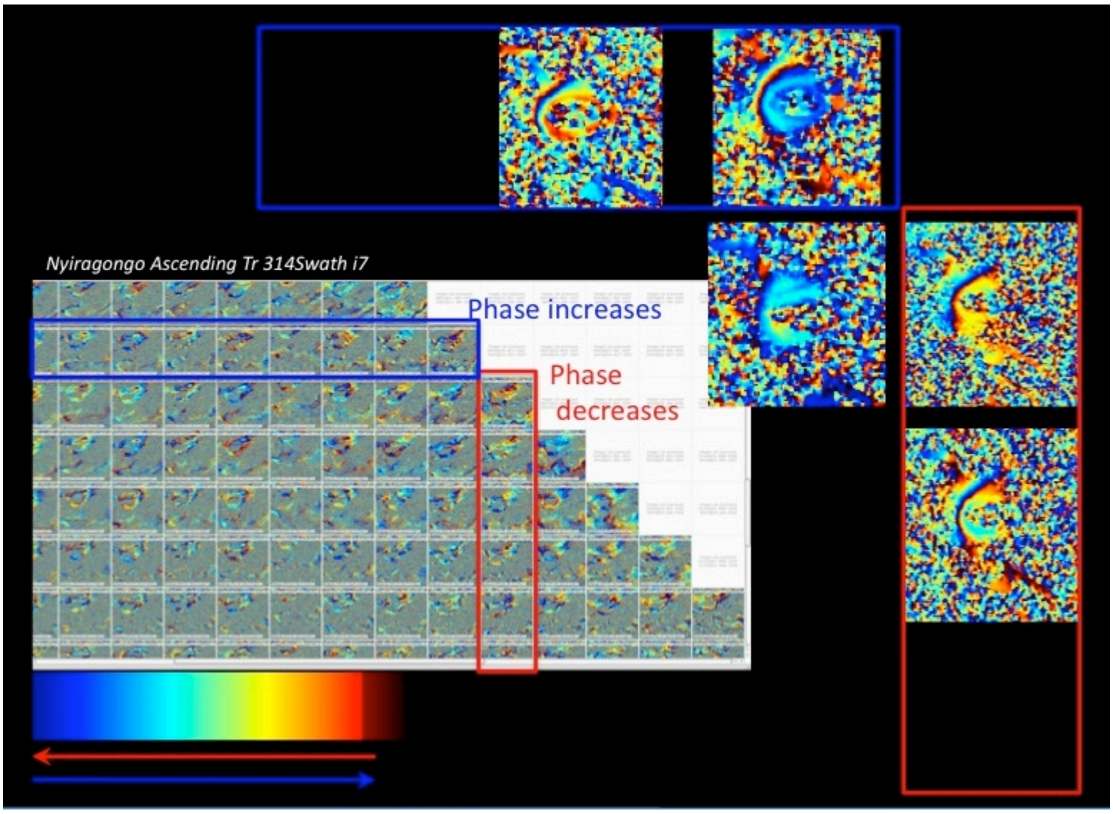

Figure 3: Table on white background: extract of web tool showing phase interferograms of the Nyiragongo area, DR Congo (Nyiragongo Ascending Track 314 Swath i7). Interferograms framed in Blue and Red show an atmospheric artifact affecting the Nyiragongo volcano (too small to be seen in the table – see enlargements to the right instead). The sign of phase delay observed on the crater area is reverted when the affected image is used as a Slave (line framed in Blue; phase increases) or a Master (column framed in red; phase decreases).
The two interferograms shown in the upper blue frame are enlargements of only the Nyiragongo crater area. These are extracted from the two interferograms at the right of the blue-framed interferograms in the table. Similarly the two interferograms shown in the red frame to the right of the figure are similar zooms extracted from the two interferograms at the top of the red-framed interferograms in the table. The amplitude of the signal (about 1,5 color cycle in the present case) is about the same on every affected interferogram (see blue and red frames) whatever the altitude of

ambiguity is. This rules out possible DEM related errors. The unframed zoom is the enlargement of the same crater area, taken from the interferogram just below the contact point between the blue and red frames in the table. None of the independent interferograms spanning the affected image show similar signal (see unframed interferograms).

Such artifacts are easily discriminated from the real deformations as a deformation will affect all and only the interferograms spanning a given epoch, whatever the combination of (independent) images is. As it can be seen from the example on Figure 4, the signal is not only visible in one column and one line of the table, but in the entire box below a given date.

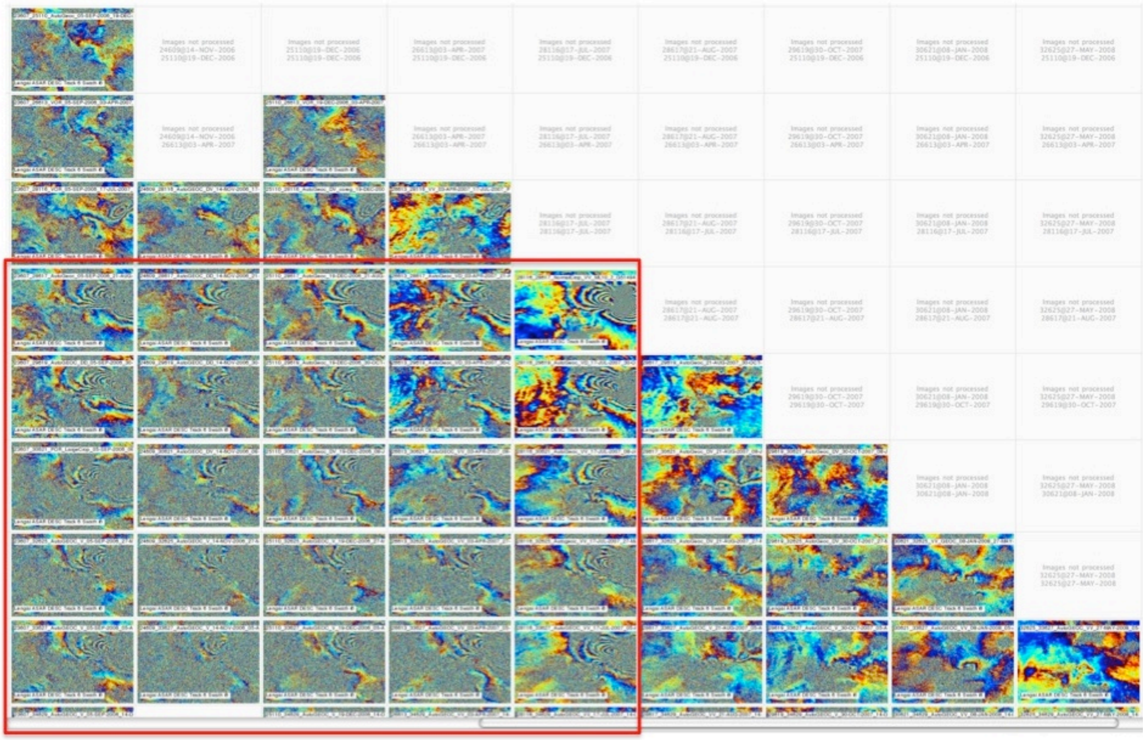

Figure 4: Extract of web tool showing phase interferograms of the Lengai volcano and Lake Natron area, Tanzania. (Lengai Ascending Track 6 Swath i6). All the interferograms spanning July 17th 2007 (framed in red) show an extensive ground deformation related to a dyking event (Calais et al. 2008). Unlike the atmospheric artifact no phase reversal is observed in the present case.

Obviously the tools will easily allow the detection of slow progressing phenomena such as lava compaction. It also facilitates the detection of seasonal variations (see figure 5).

Finally, the web tool can also help to detect timing errors or frame shifts. Every scene from a given Mode, Track and Swath is ordered with the same frame along the orbital path. The Master scene is always cropped at the same line and pixel numbers. When a timing error or a frame shift occurs, the image will appear shifted in the interferometric products (see figure 6).

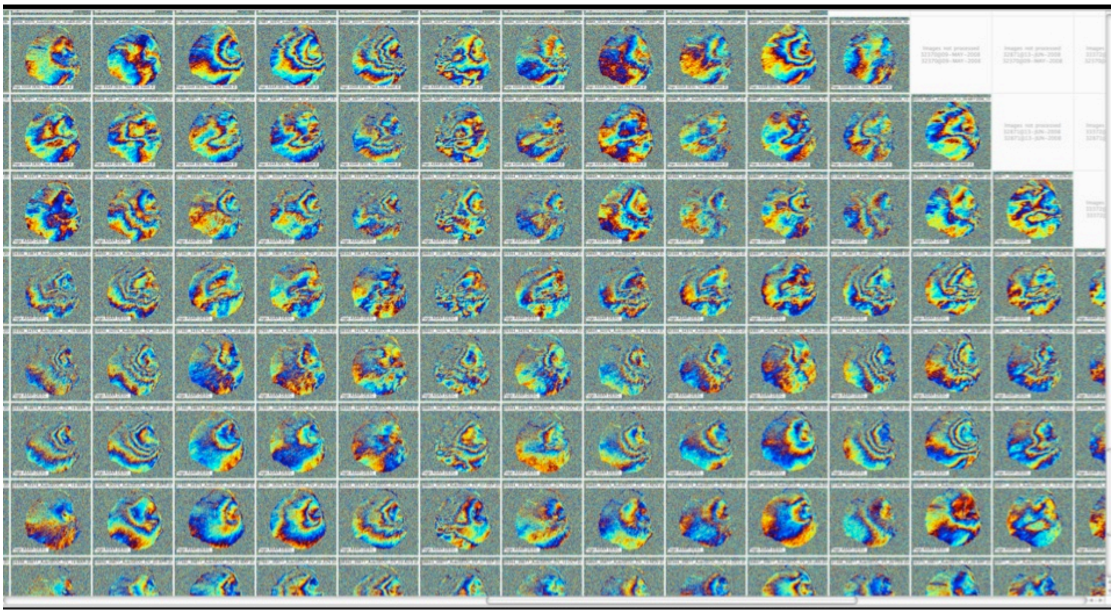

Figure 5: Extract of web tool showing phase interferograms of the Fogo volcano, Cape Verde. (Fogo Descending Track 252 Swath i2). Clear phase delays with different signs can be observed over time. Although these signals have a clear correlation with the topography, no correlation can be seen with the altitude of ambiguity, ruling out DEM errors. It was shown that these variations are attributed to variations of precipitable water vapor in the troposphere due to the Inter-Tropical Convergence Zone (ITCZ) seasonal variations (Heleno et al., in press).

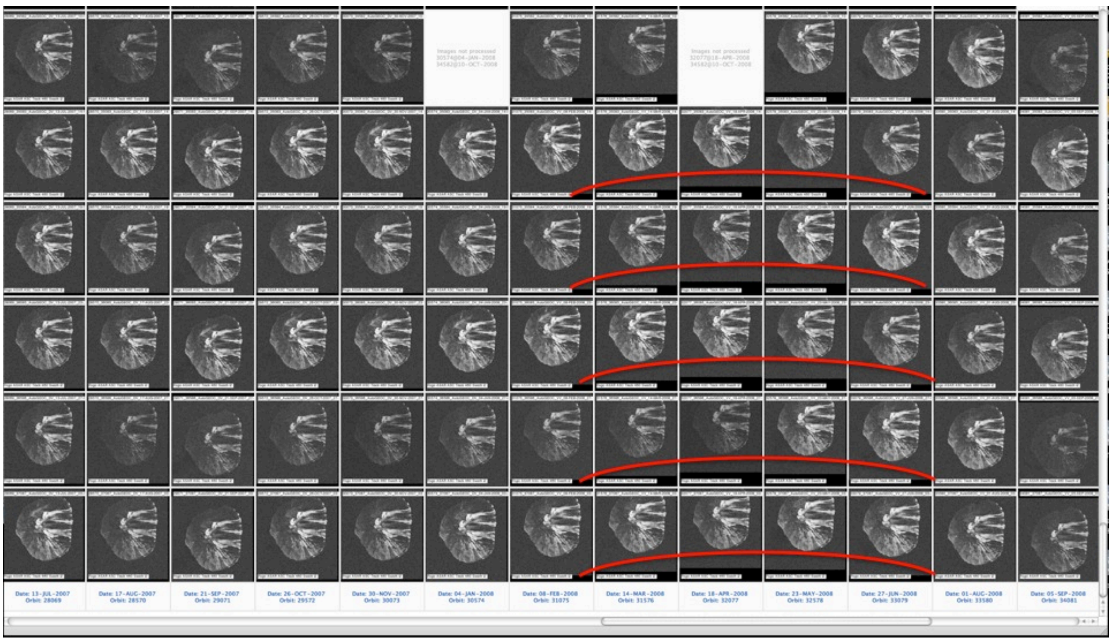

Figure 6: Extract of web tool showing coherence maps of the Fogo volcano, Cape Verde. (Fogo Ascending Track 460 Swath i2). The scenes are always processed with the same crop counted in lines and pixels in the Master image. One can clearly see the shift of the volcanic island in the frame of the scene as underlined by the red curves.

Conclusions:

The automated bulk processing and the web interface have proven to be a simple, quick and efficient tool for the management of the large InSAR data base. It also helps to easily discriminate artifacts from deformations, to detect seasonal variations or continuous slow phenomena, or to detect timing errors or frame shift.
Thanks to the pre-defined parameters and the automated procedure, the tools are also useful for fast response in case of a crisis. Usually each new scene can be combined with the previous most recent compatible image from the database to produce the last interferogram within less than 30 minutes.

Scripts and Mathematica routines may be made available on request to the corresponding author although without the manual but containing the documentation written in the scripts. The procedure was set up and upgraded step by step during the growth of the project(s) and tailored for our needs and hardware, based on our configurations. It is hence not portable "as it is" and could certainly be optimized.

Acknowledgements:

SAR data are provided in the frame of ESA Cat-1 project nr 3224 and ESA-JAXA Cat-1 project nr 3690. Precise orbits are provided by the Delft Institute of Earth Observation and Space Systems (DEOS) and ESA. Interferograms are computed with the DORIS open source software, TU Delft (Kampes and Usai, 1999). Phase data are unwrapped using SNAPHU (Chen and Zebker, 2001). SRTM digital elevation models are provided by USGS (Far et al., 2004).

The automated mass processing and web tool were developed in the frame of the SAMAAV projects (supported by the Belgian Science Policy), the GORISK projects (supported by the STEREO-II program of the Belgian Ministry of Science Policy and the Luxemburg National Research Fund), and the CORSAIR project (supported by the European Center for Geodynamics and Seismology).

References:

Calais E., N. d'Oreye, J. Albaric, A. Deschamps, D. Delvaux, J. Déverchère, C. Ebinger, R. W. Ferdinand, F. Kervyn, A. S. Macheyeki, A. Oyen , J. Perrot, E. Saria, B. Smets, D. S. Stamps & C. Wauthier
Aseismic strain accommodation by slow slip and dyking in a youthful continental rift, East Africa
Nature, Vol. 456, Iss. 7223, 2008

Chen C. W., H. A. Zebker, "Two-dimensional phase unwrapping with use of statistical models for cost functions in nonlinear optimization," J. Opt. Soc. Am. Opt. Image Sci., 18(2), 338–351, 2001.

Farr T.G., P.A. Rosen, E., Caro, R., Crippen, R., Duren, et al., "The Shuttle Radar Topography Mission", Review of Geophysics., 45, RG2004, doi:10.1029 /2005RG000183, 2007

Heleno S., FrischknechtC., d'Oreye N., Lima N., Faria B., Wall R., Kervyn F. Seasonal Tropospheric Influence on SAR Interferograms near the ITCZ - the case of Fogo Volcano and Mount Cameroon. *Journal of African Earth Sciences, in Press.*

Kampes B., S. Usai, "Doris: The Delft Object-oriented Radar Interferometric software," Proc. ITC 2nd ORS symposium, August 1999, The Netherlands, 1999.

d'Oreye N., Kervyn F., Calais E., Cayol V., Fernández J., Frischknecht C., Gonzales P., Heleno S., Oyen A., Wauthier C. (2008)
Systematic InSAR Monitoring of African Active Volcanic Zones: What we have learned in three years, or a harvest beyond our expectations.
Proc. Second workshop on USE of Remote Sensing Techniques for Monitoring Volcanoes and Seismogenic Areas (USEReST 2008), Naples, Italy, November 11-14, 2008, 1-4244-2547-1/08/$20.00 ©2008 IEEE, pp57-62

CHALLENGES OF SAR INTERFEROMETRY ON MOUNT CAMEROON

C. Frischknecht[1], N. D'Oreye[2], F. Kervyn[3]

[1]CERG, Section of Earth and Environmental Sciences, University of Geneva, 13, rue des Maraîchers, CH-1205 Geneva, Switzerland
[2]Dept.of Geophysics/Astrophysics, National museum of natural history, 19 rue Josy Welter, L-7256 Walferdange
[3]Dept. of cartography and remote sensing, Royal Museum for Central Africa, Leuvensesteenweg 13 3080 Tervuren, Belgium

Abstract

Mount Cameroon is the only active volcano of the Cameroon Volcanic Line and is located in an inhabited area. Consequently ground deformation monitoring is crucial. DinSAR has demonstrated its capability in various volcanic contexts. However Mount Cameroon is located close to the Equator and is under the influence of the Africa branch of the Inter-Convergence Tropical Zone (ICTZ), which plays a major role on the precipitable water vapor content in the atmosphere. This volcano also exhibits an elliptical shape and strong slope gradients. We discuss these factors that may hamper the use of radar images on Mount Cameroon.

Introduction

Monitoring volcanoes located close to populated areas is a necessity in order to provide warnings in time, when possible. However a ground-based monitoring network must be dense enough to obtain a spatial coverage precise enough to follow the deformation evolution. Such a network requires a lot of economical and human resources that can rarely be supplied. Differential Interferometry synthetic aperture radar (DInSAR) is an alternative way and has demonstrated its capability to monitor volcanic activity over broad areas and over time (e.g. Pritchard and Simons, 2002; Froger et al, 2007). However several factors that are mainly related to volcano surface characteristics (e.g. presence of vegetation), radar system (e.g. look angle) and noise produced by variation in the water vapor content of the lower part of the troposphere (Stevens and Wadge, 2004) can impede its use.

Mount Cameroon exhibits some of the challenges encountered when using DINSAR in a volcanic context, the most critical being the coherence and the water vapor content in the troposphere. Nevertheless this volcano is of special interest because it is an active volcano closed to populated areas and with reduced ground-based monitoring systems.

General context

Located on the western coast of Cameroon (figure 1), Mount Cameroon is a volcanic horst that belongs to the continental part of the Cameroon Volcanic Line (CVL), a 1600 km-long chain. The origin of the CVL is still uncertain. Various hypotheses include a hot spot, a hotline generated by the upwelling flow from the upper mantle, an intraplate shearing zone and the early stages of rifting (Fitton et al., 1985; Deruelle et al., 1987).

This basaltic edifice gradually rises up to 1000m, then exhibits a strong slope gradient, up to 40° on the northwestern and southeastern flanks (figure 2) before reaching its maximum altitude of 4095 m. Its shape is elliptical with a major axis oriented northeast-southeast. This stratovolcano is the most active volcanic center of the CVL (figure 1), with 7 eruptions over the last 100 years. The most recent eruption was in 2000 (Suh et al., 2003). Its volcanic activity produced basanite to hawaiite lava (Fitton et al., 1985; Suh et al, 2003; Herrero-Bervera et al., 2004).

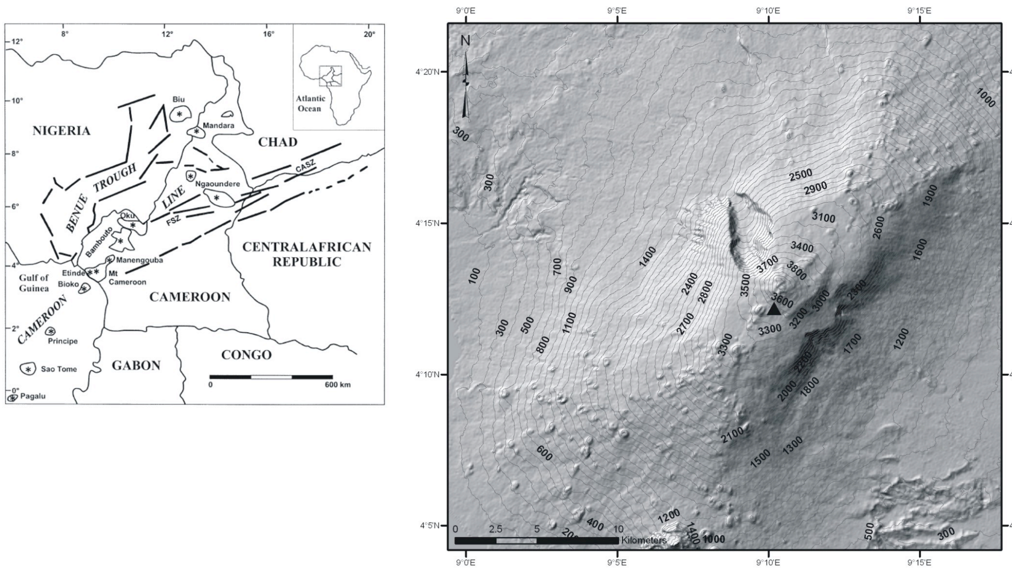

Figure 1. Location of Mount Cameroon (Shuh et al., 2003) and shaded relief produced from SRTM data

Due to its location closed to the Equator, the climate in the region of Mount Cameroon is influenced by seasonal oscillations of the Africa branch of the inter-convergence tropical zone (ICTZ). This induces a bimodal rainfall distribution (McGregor and Nieuwolt, 1998). Maxima rainfalls occur in April/June and in September/October, when the Africa branch is near, whereas minima occur in December/January and July or August, when the Africa branch is located further north (Mc Gregor and Nieuwolt, 1998). On Mount Cameroon itself, precipitations on its southwest flank can reach up to 12000 mm/year, whereas on the opposite flank, the level is around 1800 mm/year (Chauvel et al., 2005). This amount of rain facilitates the growth of various types of vegetation, from mosses and lichens to rain forest, which distribution varies in function of altitude and volcanic rocks ages. Consequently, Mount Cameroon is covered by abundant vegetation, except on the summit.

SAR Data acquisition and processing

All available images have been collected either from ERS 1/2 or ENVISAT ASAR (Advanced Synthetic Aperture Radar). Computed interferograms span the time period from 1995 up to 2008, with a gap between 2000 and 2003, and in 2005 (figure 2).

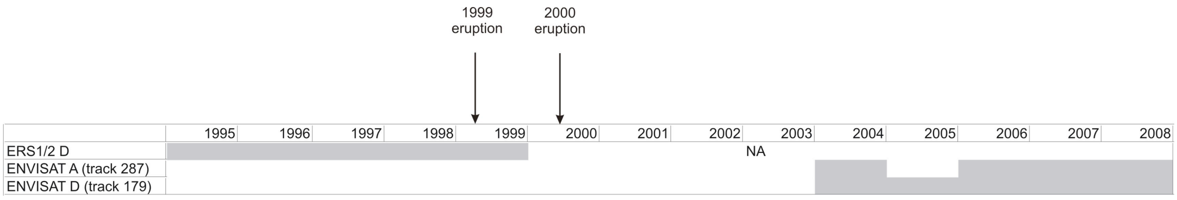

Figure 2. Availability of ERS and ENVISAT SAR images

Interferograms were calculated with DORIS software (Kampes et al., 2003) from SLC images using the standard two-pass method. Orbital errors are corrected using DEOS and ESA precise orbit state vectors. Removal of topographic contribution is achieved by using a 90m-resolution digital elevation model produced from SRTM radar data (Farr et al., 2007).

Results

The initial objective of investigating on Mount Cameroon was to determine whether deformation signal linked with volcanic activity could be detected with satellite radar images. Regarding past events, it was not possible to produce valid ERS nor ENVISAT interferograms spanning the 1999 or the 2000 eruptions. This was due either to data unavailability, too large baselines, or Doppler frequency incompatibility due to ERS2 navigation problems.

Thanks to the few archives and the systematic acquisition planning started in 2005, more than 315 different ENVISAT ASAR interferograms were computed for the post-eruption period (March/July 2004 up to July 2008), considering descending and ascending paths. Only interferograms with perpendicular baselines greater than 500m were considered. In order to understand challenges of InSAR on Mount Cameroon we discuss the effect of surface geometry, coherence and atmospheric effects.

Surface geometry

The geometry of Mount Cameroon, with its main axis almost oriented at almost 45 degrees and its steep slopes on each side, and the existence of a through on the north-western flank poses a real challenge for interferometry for it alters the quality of radar images. Figure 3 demonstrates the effect of the geometry and the slopes on radar images. Shadow effect can be seen on ascending path (dark tones) whereas layover effects can be noticed on descending path (white).

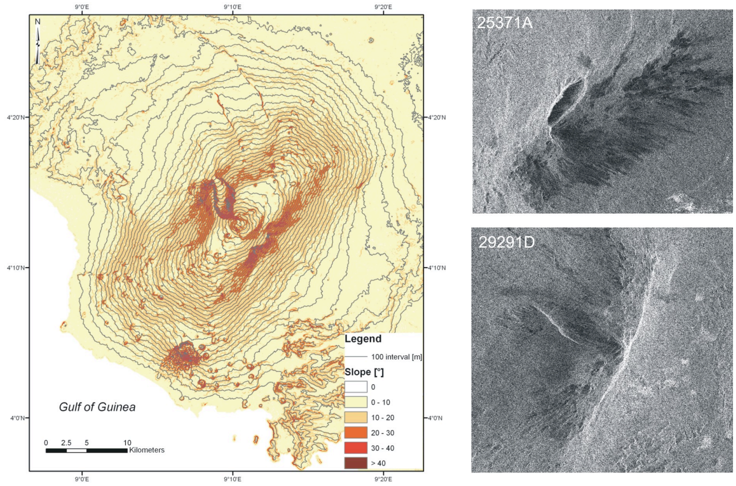

Figure 3. Slopes of Mount Cameroon (left) and amplitude images in radar geometry of ascending (upper right) and descending (lower right) paths.

Coherence evolution

The Mount Cameroon area is located in a tropical humid climate and covered by dense vegetation, which exhibits seasonal variations. Such an environment in InSAR domain inhibits coherency (Stevens and Wadge, 2004). On Mount Cameroon, detection of signal is restricted to the upper part. Coherence remains high over time only for inhabited areas or recent lava flows (figure 4).

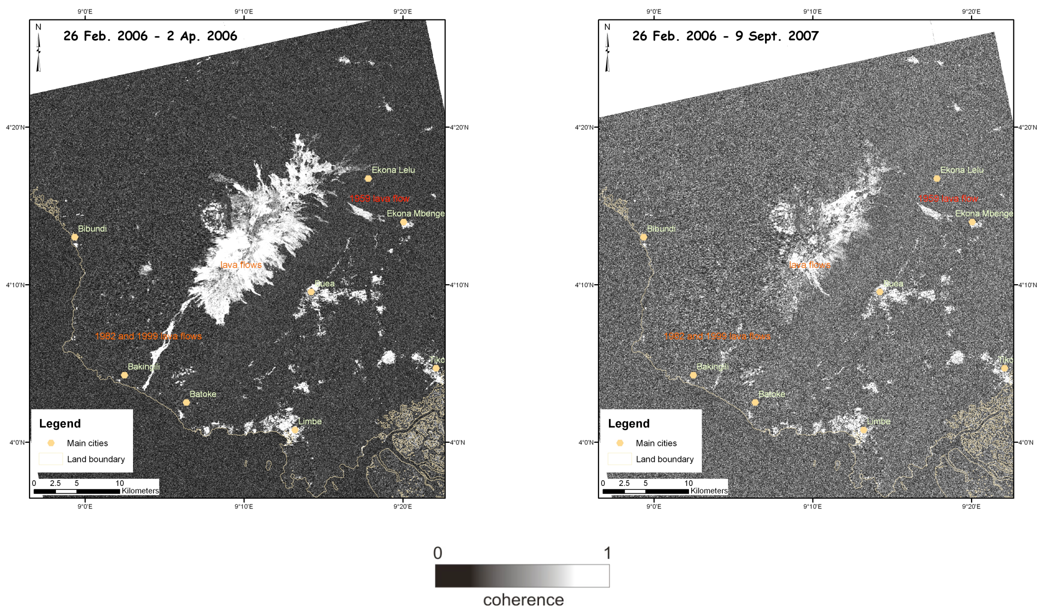

Figure 4. Decorrelation over time. Left: despite the short time span (35 days) and a highly favorable 46m perpendicular baseline, most of the volcano suffers from decorrelation (black area). Only the summital regions and the recent bear lava flows present a high coherence (white areas). Right: situation becomes obviously worst when time span and perpendicular baseline increase (560 days and 359m respectively). Images are in true geometry and georeferenced.

Atmospheric effects

On the bare summit of Mount Cameroon, where the backscattering properties of the ground are not affected by vegetation, ellipsoidal interferometric fringes can be observed up to 4 fringes on both ascending and descending paths (figure 5). Each full color cycle (RBY) represents a signal delay equivalent to half the radar wavelength that could be miss(-interpreted as a range change of 2.8 cm in the satellite line of sight. The fringe pattern follows the general shape of the volcano.

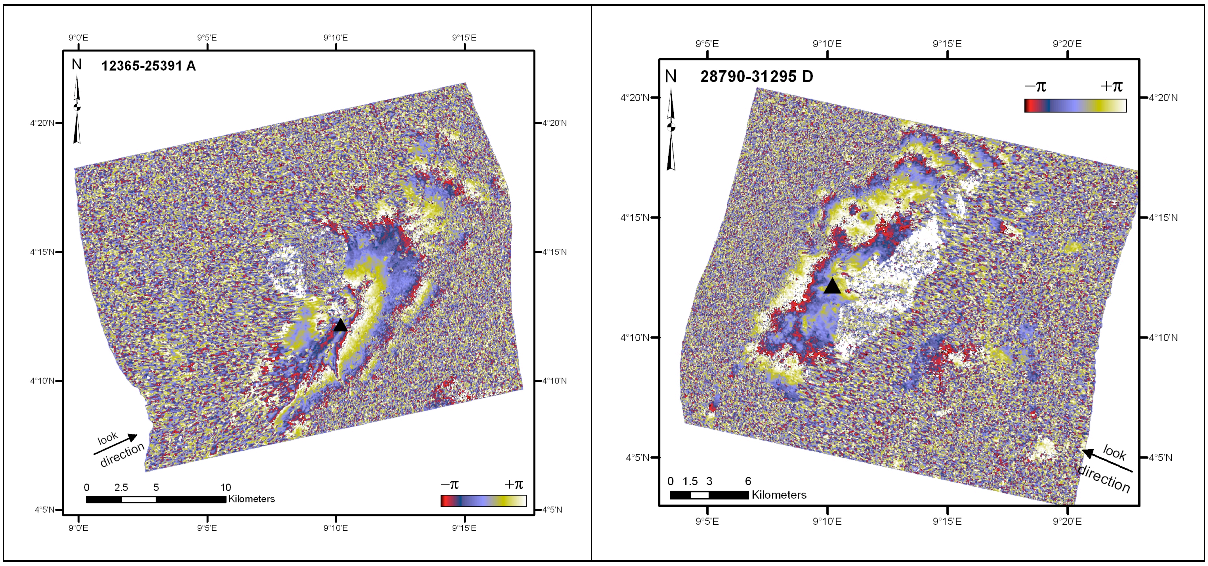

Figure 5. Ellipsoidal interferometric fringes detected on wrapped filtered georeferenced interferograms for ascending (12365-25391 A) and descending paths (28790-31295 D).

Patterns are dissimilar when considering ascending and descending paths, which is induced by the irregular topography of Mount Cameroon and the difference of looking geometry (figure 1).

Potential causes of these signals could be DEM errors, volcano unrest or atmospheric effects. Regarding DEM errors, this hypothesis can be discarded since the amplitude of the observed signal is not proportional to the altitude of ambiguity (figure 6).

12365-25391A	**13367-25391A**
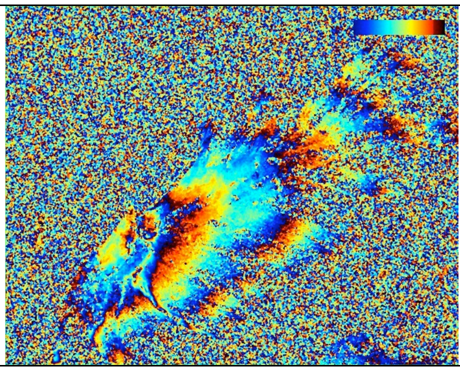	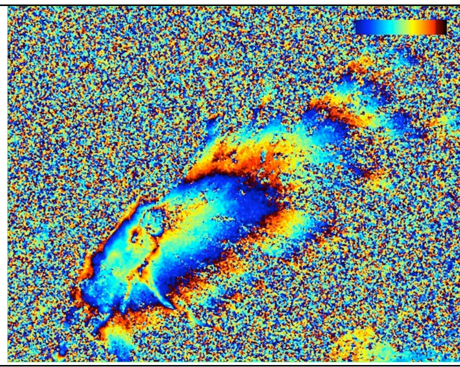
Bp : -120.9m, ha : 77.8m, ΔT : 910 days	Bp : 18.3m, ha : -512.9m, ΔT : 840 days

Figure 6. Wrapped interferograms on track 367, ascending path. Both images (in radar geometry) show the same amount of phase delay, independently from the altitude of ambiguity.

Regarding volcano unrest, no activity was reported between 2000 and 2008 (Global Volcanism Program, 2009).

The latest hypothesis is related to atmospheric artifacts. It has been noticed on other high altitude volcanoes (e.g. Etna, Sakurajima) that topographic-like atmospheric effects can be significant (e.g. Delacourt et al., 1998; Remy et al., 2003), inducing several artifactual fringes.

Mount Cameroon does not differ. On ascending and descending path, the observed signal can reach up to 4 fringes over 2000 m, which represents about 11 cm of pseudo ground deformation. Moreover these observed phase delay fringes are strongly correlated with topography as shown on figure 7.

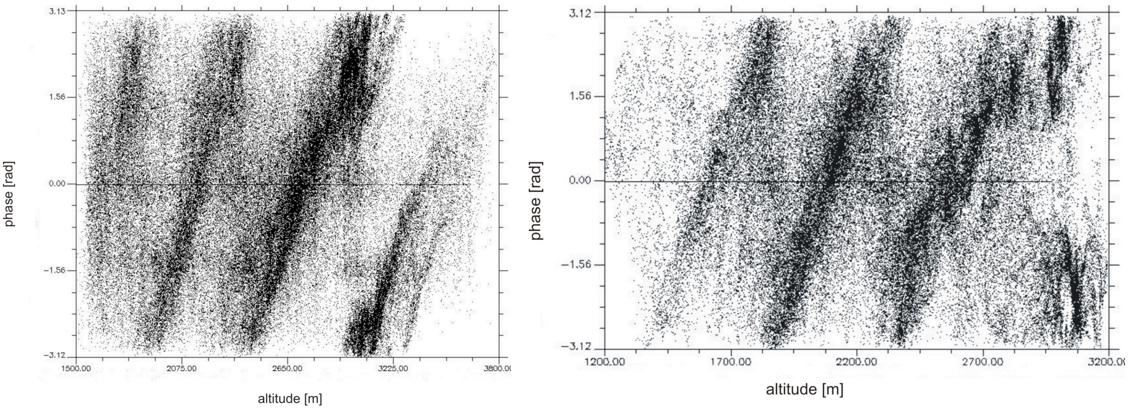

a) b)

Figure 7. Scatterplot between altitude and phase delay obtained on wrapped filtered interferograms a) 13367 (Sept.04)-25391 (Jan.07) and altitude and b) 28790 (Sep07)-31295 (Feb.08) and altitude

The number of fringes seems to be independent of the time difference between images, but is closely related to the variation of water vapor content in the troposphere between acquisitions of images.

Retrievals of the water vapor content in the atmosphere can be obtained using satellite instruments such as the moderate resolution imaging spectroradiometer (MODIS). Using near-infrared channels, column water vapor amounts can be derived (Gao & Kaufman, 2003).

To examine the variation of the precipitable water vapor (PWV) in the area of Mount Cameroon, we extracted mean PWV value from MODIS level 3 atmosphere monthly product (MOD08_M3) for years where InSAR data are available, i.e. 2004, 2006, 2007 and 2008. This MODIS product is available on a global scale at 1° resolution and georeferenced.

These time-series (figure 8) show the bimodal behavior, with minimum precipitable water vapor in December-February and August and maximum in May/June and September/October. It can also be seen that there are some fluctuations from year to year. This is induced by the ICTZ migration pattern which can exhibit year variability (McGregor and Nieuwolt, 1998).

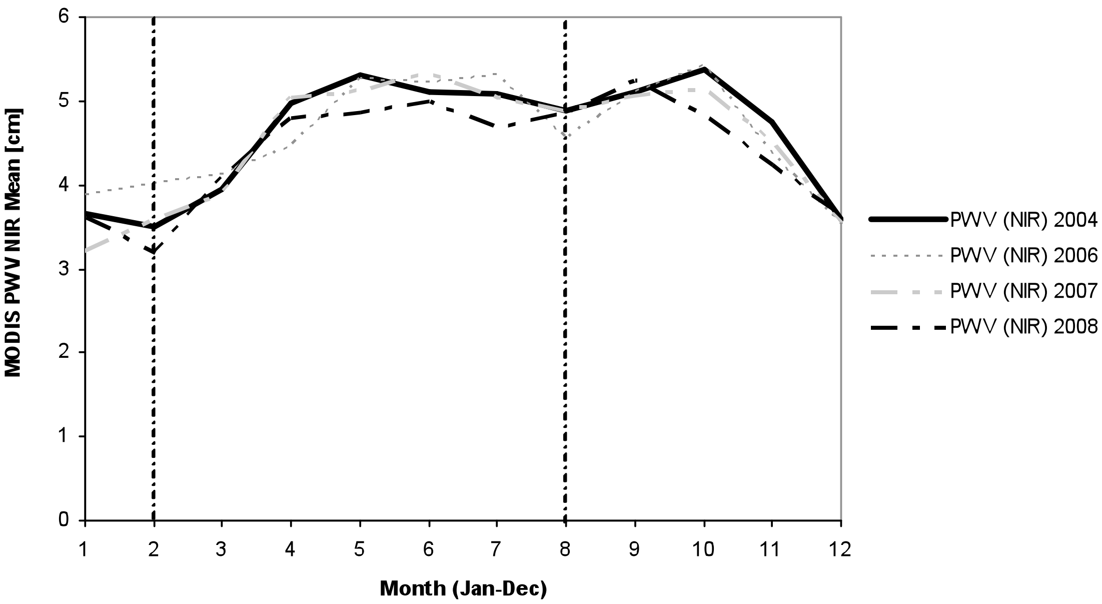

Figure 8. MODIS PWV monthly mean value retrieved from near-infrared channels.

Looking at data acquired on ascending path, maximum phase delay can be observed on pairs involving December and January (2006, 2007, 2008) combined with images acquired during June 06, September 06/07 and October 07. Similar maxima are observed on descending interferograms involving February 2008 and combined with December 05, September 06/07, April 07, May 07, October 07. Phase delays are maximum when involving images acquired during period of contrasted wet atmosphere. More detailed investigation on the relationship between season variability induced by the migration of the ICTZ and magnitude of phase delays observed on interferograms acquired for Fogo and Mount Cameroon volcanoes is described in Heleno et al, submitted.

Conclusion

This study presents key elements that hamper DInSAR on Mount Cameroon. Those elements are :
1) the high vegetation-induced decorrelation rate over a short period of time,
2) the geometric effects (layover and shadowing) due to its peculiar topography and
3) the substantial phase delays induced by the variation of precipitable water vapor content in the troposphere.

These observations demonstrate that DInSAR analysis on Mount Cameroon to detect potential deformation is challenging. Considering these elements should help to improve the interpretation of future ground deformation analysis.

Acknowledgements

The ENVISAT ASAR images used in this analysis are copyright of the European Space Agency. They were acquired through the SAMAAV project (ESA Cat-1 project N°3224 and 3690). Precise orbits are provided by the Delft Institute of Earth Observation and Space Systems (DEOS) and ESA. Interferograms are computed with the DORIS open source software (TUDelft). The Cameroon Digital Elevation model was extracted from SRTM radar data distributed by USGS. MODIS data were downloaded from NASA MODIS website. Automated InSAR mass-processing procedure (up to the production of geo-referenced deformation and coherence maps) was developed at the MNHN, Luxembourg.

References

Chauvel C., Dia A. N., Bulourde M., Chavaux F., Durand S., Ildefose P., Gerard M., Deruelle B., Ngounouno I., 2005, Do decades of tropical rainfall affect the chemical compositions of basaltic lava flows in Mount Cameroon ?, J. Volc. Geoth. R., 141, 195-223

Delacourt C., Briole P., Achache J.,1998, Tropospheric corrections of SAR interferograms with strong topography. Application to Etna, Geophys. Res. Lett. 25 (1998) 2849-2852.

Deruelle B, N'Ni J., Kambou R., 1987, Mount Cameroon : an active volcano of the Cameroon Line, J. African Earth Sciences, vol. 6 (2), 197-214

Farr, T.G., Rosen, P.A., Caro, E., Crippen, R., Duren, R., Hensley, S., Kobrick, M., Paller, M., Rodriguez, E., Roth, L., Seal, D., Shaffer, S., Shimada, J., Umland, J., Werner, M., Oskin, M., Burbank, D., Alsdorf, D., 2007. The Shuttle Radar Topography Mission, Review of Geophysics 45, RG2004, doi:10.1029/2005RG000183.

Fitton J. G. and Dunlop H. M., 1985, The Cameroon line, West Africa, and its bearing on the origin of oceanic and continental alkali basalt, Earth Plan. Sc. Let., 72 (1), 23-38

Froger, J. L., D. Remy, Bonvalot, S.Legrand, D., 2007, Two scales of inflation at Lastarria-Cordon del Azufre volcanic complex, central Andes, revealed from ASAR-ENVISAT interferometric data, Earth and Planetary Science Letters 255(1-2): 148-163.

Gao, B.-C., Kaufman, Y.J., 2003. Water vapor retrievals using Moderate Resolution Imaging Spectroradiometer (MODIS) near-infrared channels. Journal of Geophysical Research 108 (D13), 4389 doi:10.1029/2002JD003023.

Global Volcanism Program, 2009, Cameroon, http://www.volcano.si.edu/world/volcano.cfm?vnum=0204-01=, as seen on 26.02.2009

Heleno S.I.N., Frischknecht C., d'Oreye N., Lima J.N.P., Faria B., Wall R. and Kervyn F.,

Seasonal Tropospheric Influence on SAR Interferograms near the ITCZ – the case of Fogo Volcano and Mount Cameroon, Journal of African Earth Sciences, special issue : AVCOR, *in press.*

Herrero-Bervera E., Richard Ubangoh, F.T. Aka, Jean-Pierre Valet, 2004, Paleomagnetic and paleosecular variation study of the Mt. Cameroon volcanics (0.0–0.25 Ma), Cameroon, West Africa Emilo Herrero-Bervera, Physics of the Earth and Planetary Interiors 147 (2004) 171–182

Kampes, B.M., Hanssen, R.F., Perski, Z., 2003. Radar interferometry with public domain tools. Proc. of FRINGE 2003 Workshop, Frascati, Italy, 1-5 December 2003

McGregor, G. R., Nieuwolt S., 1998, Tropical Climatology, second edition, John Wiley & Sons, Ltd, 339p.

Pritchard, M.E., Simons, M., 2002. A satellite geodetic survey of largescale deformation of volcanic centres in the central Andes. Nature 418, 167-171

Remy, D., S. Bonvalot, et al. (2003). "Accurate measurements of tropospheric effects in volcanic areas from SAR interferometry data: application to Sakurajima volcano (Japan)." Earth and Planetary Science Letters **213**(3-4), 299-310

Suh C.E., Sparks R.S.J., Fitton J.G., Ayonghe S.N., Annen C., Nana R., Luckman A., 2003, The 1999 and 2000 eruptions of Mount Cameroon: eruption behaviour and petrochemistry of lava, Bull. Volcanol. 65, 267-281

Stevens, N.F., Wadge, G., 2004, Towards operational repeat-pass SAR interferometry at active volcanoes, Natural Hazards 33, 47-76

3D volcanic deformation fields at Tenerife Island: integration of GPS and Time Series of DInSAR (SBAS)

Pablo J. González[1], Sergey V. Samsonov[2], Mariarosaria Manzo[3], Juan F. Prieto[4], Kristy F. Tiampo[2], Pietro Tizziani[3], Francesco Casu[3], Antonio Pepe[3], Paolo Berardino[3], Antonio G. Camacho[1], Ricardo Lanari[3] and José Fernández[1]

1. Instituto de Astronomía y Geodesia, CSIC-UCM, 28045-Madrid, Spain. (pjgonzal@mat.ucm.es; pabloj.glez@gmail.com)
2. Department of Earth Sciences, Univ. of Western Ontario, London, Ontario, Canada.
3. Istituto per il Rivelamento Elettromagnetico dell'Ambiente, CNR, Napoli, Italy.
4. Dept. Ingeniería Topográfica y Cartografía, Univ. Politécnica de Madrid, Madrid, Spain.

Abstract

Surface ground deformation have been used to imaging complex magmatic plumbing systems. At Tenerife Island the magmatic plumbing system is highly complex with the coexistence of low and high compressible magmas. In this context an accurate knowledge of the 3D deformation field could help to assess possible magmatic sources. Combining survey-mode GPS and SBAS DInSAR data the present work aims at studying the time evolution of the ground deformation at Tenerife Island in relation with the anomalous seismicity recorded in 2004. We found that deformation patterns reversed polarity between periods of quiescence and period characterized by a large number of earthquakes. This could be related with active deformation sources acting before, during and after the 2004 seismic crisis.

Keywords: Ground deformation, GPS, SBAS DInSAR time series, Tenerife Island

Introduction

Ground deformation volcano monitoring (such as at oceanic-island volcanoes) is a key tool to investigate the behaviour of the magmatic plumbing systems. Buoyancy of basaltic melts with low compressibility is capable to produce large surface displacements. In contrast more evolved magmas are less efficient to produce surface ground displacements (*Johnson et al., 2000*). At Tenerife Island, both types of magmas coexist resulting in a complex volcanic system (*Marti et al., 1994*). In such a context the interpretation of volcanic unrest (i.e. defined as departures from usual behaviour or background level) could potentially be difficult. In addition, magmatic intrusions imprint very different patterns on the ground deformation depending on their geometries and volumes at depth. To decipher the responsible mechanism of magma transport and/or emplacement, we need an accurate knowledge of the full three-dimensional deformation field caused by the volcanic activity. In this work, such a three-dimensional deformation field is estimated through the combination of GPS and SBAS-DInSAR data, using a modification of technique of *Samsonov and Tiampo,* (*2006)*, which basically jointly optimize a kriging interpolated 3D GPS deformation field with a DInSAR deformation map.

Tenerife (Canary Islands, Fig. 1) is formed by a Shield Volcanic Complex (SVC) (*Ablay and Keary, 2000*) and a Central Volcanic Complex (CVC) (*Marti et al., 1994*). The SVC is mostly submerged, forming about 90% of the island volume. SVC formed during the last 10 Ma, as the accretion of mantle-derived basaltic material along two main rift zones trending NE and NW and on a third subsidiary S-trending rift (*Carracedo et al., 2007*). The CVC comprises the Las Cañadas composite volcano (from more than 3.5 Ma to 0.18 Ma) and the Teide-Pico Viejo strato-volcano (from 0.18 Ma to present) (Fig. 1). The CVC is mostly composed of lavas that evolved from basaltic to phonolitic composition and is characterized by abundant explosive eruptions. CVC suffered several vertical collapses following explosive withdrawal of high-level magma chambers, occasionally accompanied by lateral collapses (*Marti et al., 1994*).

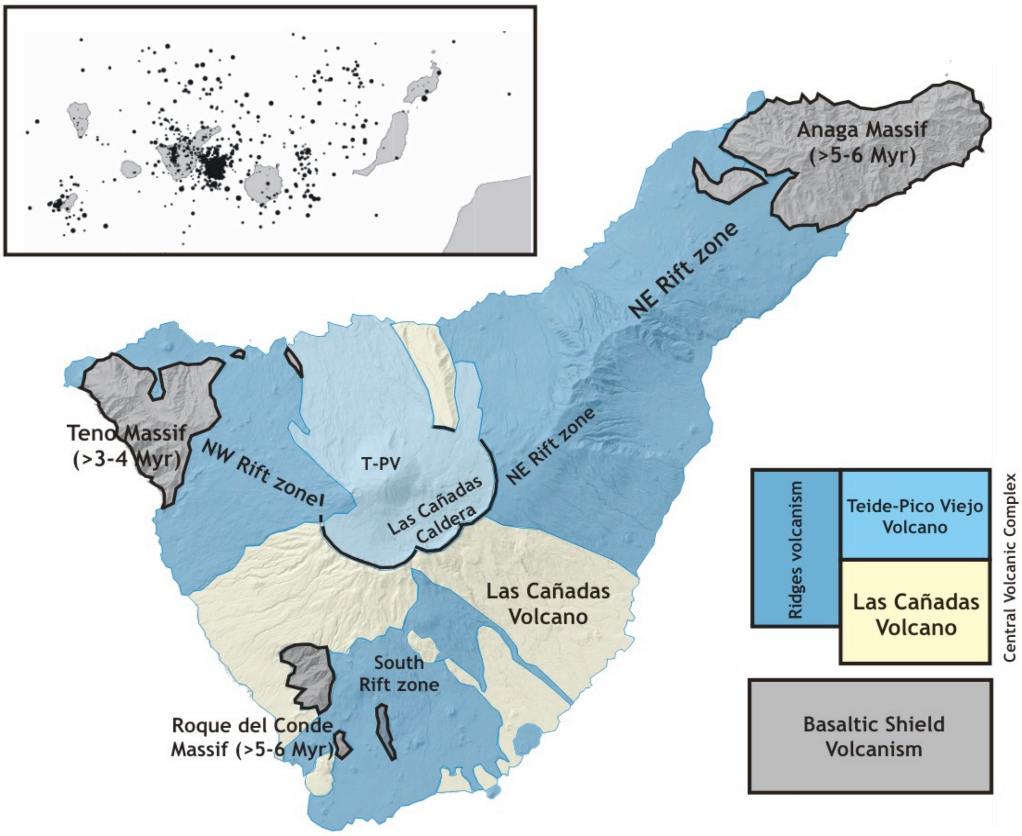

Figure 1. Simplified geological setting of Tenerife Island and a simplified stratigraphic column of the main volcanic edifices, after Ablay and Marti (2000), T-PV is acronym for Teide-Pico Viejo volcano. Upper inset shows the location in the Canary Islands and the recorded seismicity for the period 1980-2007 by the IGN.

In April 2004 began an unusual relatively high seismicity activity located NW of Teide volcano, whereas for the last 20 years, the seismicity usually concentrated offshore to the SE of Tenerife (inset of Fig 1). Over the next 22 months more than 3.000 earthquakes were recorded. See e.g., *Gottsmann et al. (2006), Almendros et al. (2007)* or *Fernández et al. (2008)*.

In this paper, we estimate three dimensional motion deformation maps using survey mode GPS data and SBAS DInSAR time series for the period 2000-2005. We divided the studied period in three phases using seismicity recorded inside the island (NW sector), as a proxy of the volcanic activity that could reflect in different volcanic deformation patterns (red line in Fig. 2a). First period ranges from the second half of 2000 to March 2004 and is characterized by a rather quiescence period with almost no seismicity detected by the available regional seismic network (www.ign.es). Second period runs from April to September 2004 when more than 90% of the total seismic strain energy released and several (M>3) were felt by the population. The third period, from October 2004 to December 2005, is characterized by a slowly decrease of seismicity rate to pre-April 2004 levels (Fig. 2). Note that the detected rate of seismic strain release will not be expected to return to pre-2004 levels due to improvements in the volcano seismic monitoring network.

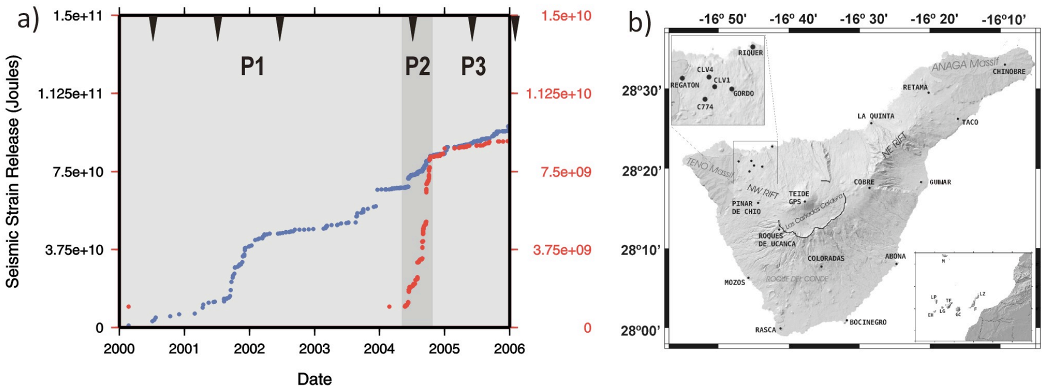

Figure 2. a) Seismic strain release (in Joules) in Tenerife island region (blue) and NW region of Tenerife for the period 2000 to end 2005 (red). It is shown the three considered periods (P1, 2000-2004; P2, 2004; and P3 2004-2006), we also indicate with botton pointing arrows the time of the GPS surveys. b) Tenerife GPS network (Fernandez et al., 2003).

Data Analysis and methods

2000-2006 GPS surveys

In 2000, an island-wide GPS benchmarks network was installed in Tenerife (Fig. 2b). It purpose was to serves as routine yearly-monitored ground deformation network (*Fernández et al., 2003*) and a validation tool for deformation detected by DInSAR [Fernandez et al., 2005]. Since 2000, the network has been re-observed 7 times (Aug. 2000, Jul. 2001, Jul. 2002, May 2004, Jul. 2005, Jan. 2006 and Sept. 2007), except for 2006 all GPS campaign were carried out at the summer/dry season (*Fernández et al, 2008*). In 2000, data were acquired with geodetic double frequency receivers during measurement sessions of 3 to 6 hours depending on the baseline length. From 2001 and onwards all the sessions lasted at least 6 hours. Data were processed using differential positioning technique with Bernese 5.0 software (*Dach R. et al., 2009*) and precise ephemerides. The IGS station located in the nearby island of Gran Canaria (MAS1) was considered as the reference station with coordinates in ITRF2000 reference system, epoch 1997.0. The overall precision obtained for all surveys is of the order of a few mm for horizontal components, and better than 1 cm for the vertical one. For this study we select a time span that covers the 2000 to 2006 GPS surveys, we exclude the 2007 survey due to non-overlapping period with the SBAS-DInSAR results, we also included the 2006 survey because it was performed on January 2006 only a few weeks after the last available ERS-SAR acquisition processed with SBAS. We do not include in the analysis the GPS station CHINOBRE due to the lack of neighbour SBAS coherent pixels. We also note that GUIMAR GPS station was destroyed by the tropical weather depression Delta in November 2005 (Seco et al., 2009).

SBAS DInSAR (1992-2005)

We use the DInSAR technique [Gabriel et al., 1989] that analyzes the phase difference (interferogram) of temporally separated SAR image pairs to measure ground deformation with centimetre to millimetre accuracy; the estimated displacements represent the projection of the surface deformation in the radar line-of-sight (LOS). In particular, we apply the Small BAseline Subset (SBAS) approach (*Berardino et al., 2002*) to determine the spatial distribution of the displacement rates and to generate the deformation time series of coherent pixels. SBAS technique uses a temporal low-pass filter to reduce artefacts due to atmospheric inhomogeneities (*Ferretti et al., 2000*). This filtering step also includes the compensation for the topography-correlated atmospheric phase artefacts characterized by a very limited temporal correlation. We used a set of 55 descending radar images acquired by the ERS-1/2 satellites during the period 1992–2005 for the present SBAS analysis and analysed only the period 2000-2005 overlapping the GPS surveys. A separated paper has deeply discussed the data processing and interpretation of the SBAS results for the whole period (*Fernandez et al., 2009*).

Validation: Correlation analysis

To check wether both data sets are consistent and comparable we perform a linear correlation analysis between SBAS-DInSAR and GPS deformation measurements. Both geodetic techniques are aimed at imaging (at least) the same phenomena (ground deformation). They are highly complementary [*Puglisi and Coltelli, 2001*; *Fernández et al., 2003*], however they dramatically differ in how they sample the deformation field. On one hand, GPS captures three-dimensionally spatial positions at sparsely distributed fixed benchmarks, resulting in three-dimensional deformation measurements through time-spanned comparisons. On the other hand, DInSAR data accounts for a spatial quasi-continuous scalar sampled version of the deformation field (in the line-of-sight, LOS, direction). In consequence, both techniques can be compared if we project the GPS measurements onto the LOS to check for their inner consistency. A figure with the comparison of the corresponding time series could be found in the on-line material in Fernández et al., (2009), http://www.agu.org/journals/gl/gl0904/2008GL036920/2008gl036920-fs01.jpg).

Because of the low number of available GPS data points, only basic statistics can be performed. To strength somehow our analysis, we have correlated a) a linear velocity estimation for the whole period (2000-2006), and b) the deformation time series on each station. We show in Figure 3, results of both analyses. Long term velocity deformation shows a high linear correlation index (R=0.76) and both dataset seems consistent at the level of 3-5 mm/yr (Figure 3a). In the time series comparisons case, correlation is much lower (R=0.37) and show less agreement (Figure 3b). In the light of these results, we calculate a correlation index for each GPS point time series, to separate the most consistent stations (Figure 3c). Correlation index map from each station shows that the deformation registered at the NW part of the island seems much more linearly correlated between both dataset. A first reason for that effect is that the GPS network in the NW part of the island was observed in all campaigns. A second one, would be the fact that significant deformations were only registered with both techniques (GPS and SBAS DInSAR) in this area. For this reason, we include in the 3D map estimation method (next section) only the stations surveyed in the NW part of Tenerife, what indeed were surveyed in the 6 campaigns (2000-2006).

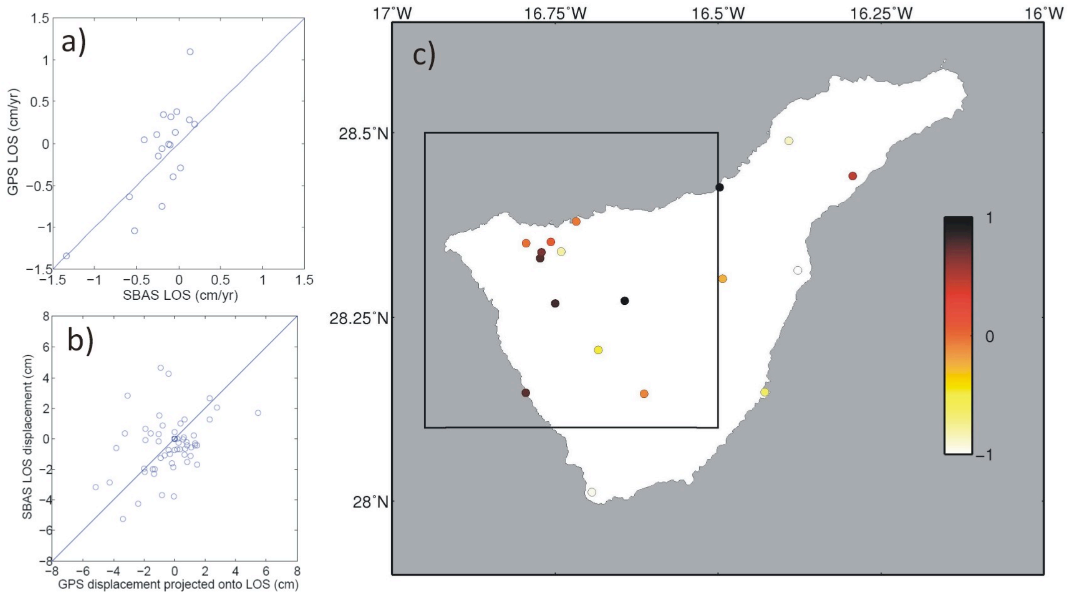

Figure 3. Correlation analysis. a) 2000-2006 LOS velocity estimation correlation between SBAS and projected GPS (R = 0.76), b) Time series data correlation between SBAS and projected GPS (R = 0.37). There are 71 points available due to the different temporal sampling at the GPS benchmarks and c) Correlation index map for each time series and GPS point, black rectangle shows more reliable region, used to estimate the 3D deformation fields.

Three-dimensional deformation field solutions

Volcanic ground deformation is a non-linear process with time. So, we prefer to study the ground deformation splitting the data in the above mentioned periods. For each of the 3 selected periods, we estimate a linear ground displacement velocity using each component of the GPS and the LOS SBAS-derived deformation. Using these data, we used a method based on the Gibbs-Markov random field equivalency within the Bayesian statistical framework (*Samsonov and Tiampo, 2006*) to account for sparse surveyed GPS measurements and time series of DInSAR to derive the full volcanic three-dimensional ground deformation maps. Solution involves the analytical minimization of a Gibbs energy function, under the assumption of independency on neighbouring points. Together with the estimation of the three-dimensional ground deformation, this technique allows the computation of error estimation at each point (*Samsonov et al., 2007).*

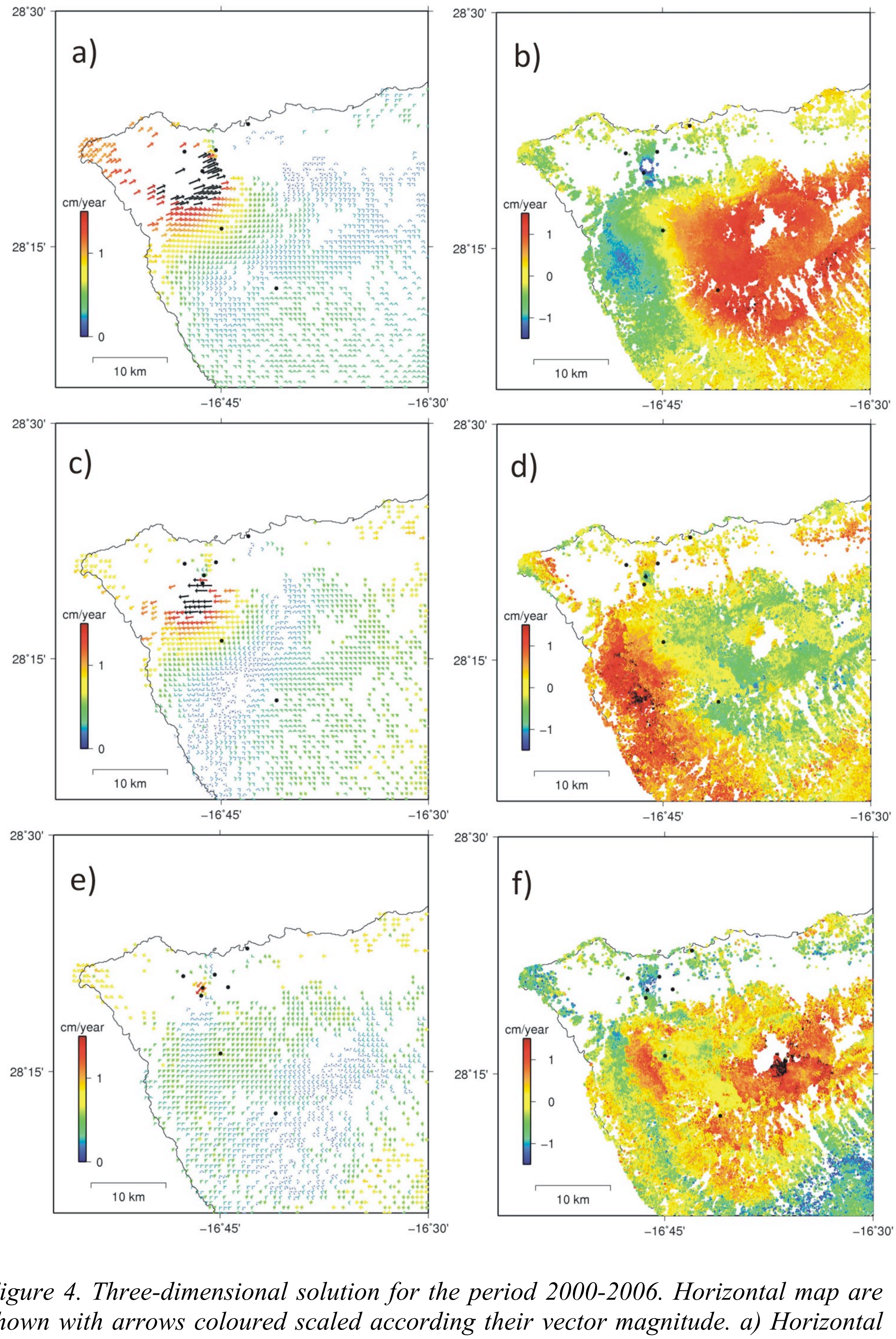

Figure 4. Three-dimensional solution for the period 2000-2006. Horizontal map are shown with arrows coloured scaled according their vector magnitude. a) Horizontal 2000-2002, b) Vertical 2000-2002, c) Horizontal 2002-2004, d) Vertical 2002-2004, e) Horizontal 2004-2006 and f) Vertical 2004-2006.

Discussion and Conclusions

In Figure 4, we show the horizontal and vertical solutions obtained using the above mentioned method for the three different periods. Vertical (4b, 4d and 4f) and horizontal (4a, 4c and 4e) motion maps showed strong changes in polarity between 2000-2002 and 2002-2004, meanwhile the 2004-2006 period show less magnitude motions. 2000-2002 period is characterized by broad uplift in the central part of the island, followed with a rather large NE motion in the area of the largest subsidence detected by InSAR data (*Fernández et al., 2003*). The 2002-2004 period shows a quite different pattern of subsidence in the central part of the island and an uplift area in the south-western part of the NW rift zone. Moreover the horizontal component shows a clear dilatation motion along a rough NS striking orientation (clearly correlated with the anomalous seismicity recorded in this period). Finally, the 2004-2006 period shows insignificant horizontal motions and a diffuse uplift signal in the vertical component in the central volcanic system. It is noted that in every vertical motion map is possible to recognize the previous reported Garachico and Pinar de Chio subsidence areas (*Fernández et al., 2003, 2005*). In this study, we present complete three dimensional motion maps obtained with a combination of GPS and SBAS DInSAR time series for the period 2000-2006. These results would allow us to model of the ground deformation motion maps in relation with the active processes acting beneath the NW and central part of Tenerife to obtain insight in its complex magmatic plumbing system. A further analysis using ground source modelling should be carrying out to explore the possible nature of the deformation processes.

Acknowledgements

Large part of the work was carried out during a research stage at the Earth Sciences department at UWO (Canada). This work has been partially sponsored by the European Community on Provision 3.15, under the project of the Regional Center of Competence ‘‘Analysis and Monitoring of the Environmental Risk’’ (CRdC-AMRA) and by the Eurorisk Preview Project. We thank the European Space Agency (ESA), which has provided the SAR ERS data within the Category-1 Project n. 3560 relevant to the Eurorisk Project. Research by JF, PJG, AGC, SS, and KFT has been also supported by Research Project and CGL2005-05500-C02, CGL2008-06426-C02 and PCI2006-A7-0660. PJG was funded by a UCM predoctoral research fellowship. The work of KFT was accomplished under an NSERC Discovery Grant. GMT software was used in this paper (Wessel and Smith, 1998). We used the SRTM 3-arcsecond Digital Elevation Model (ftp://e0srp01u.ecs.nasa.gov/srtm/version2/SRTM3/). We thank Nicolas d'Oreye for the numerous and interesting comments and suggestions, that improved the original manuscript.

References

Ablay G.J. and Keary P., (2000). Gravity constraints on the structure and volcanic evolution of Tenerife, Canary Islands, *J. Geophys. Res.*, 105, 5783-5796.

Ablay G.J. and Marti J., (2000). Stratigraphy, structure, and volcanic evolution of the Pico Teide-Pico Viejo formation, Tenerife, Canary Islands. *J. Volcanol. Geotherm. Res.*, 103, 175-208.

Almendros, J., et al., (2007). Array analyses of volcanic earthquakes and tremor recorded at Las Canadas caldera (Tenerife Island, Spain) during the 2004 seismic activation of Teide volcano. *J. Volcanol. Geotherm. Res.*, 160, 285-299.

Berardino et al., (2002) A new Algorithm for Surface Deformation Monitoring based on Small Baseline Differential SAR Interferograms. *IEEE TGARS.*, 40, 11, 2375–2383.

Carracedo et al., (2007) Eruptive and structural history of Teide Volcano and rift zones of Tenerife, Canary Islands. *GSA Bulletin*, 119, 1027–1051.

Dach R. , et al., (2009) Bernese GPS Software Version 5.0. University of Bern. 640 pp.

Fernandez et al., (2003) New geodetic monitoring system in the volcanic island of Tenerife, Canaries, Spain: Combination of InSAR and GPS techniques. *J.Volc. Geotherm. Res.*, 124, 241-253.

Fernandez et al., (2005) Detection of displacements in Tenerife Island, Canaries, using radar interferometry. *Geophys. J. Intern.*, 160, 33-45. doi:10.1111/j.1365-246X.2005.02487.x.

Fernández, J., et al., (2008). Integration of two line-of-sights classical DInSAR and GPS data to study the 2004–2006 Tenerife volcanic unrest. *Geophys. Res. Abstracts*, 10, EGU2008-A-10611.

Fernández, J., et al. (2009), Gravity-driven deformation of Tenerife measured by InSAR time series analysis, *Geophys. Res. Lett.*, 36, L04306, doi:10.1029/2008GL036920.

Ferretti et al., (2000) Non-linear subsidence rate estimation using Permanent Scatterers in Differential SAR Interferometry. *IEEE TGARS*, 38, 5, 2202−2212.

Gabriel et al., (1989) Mapping small elevation changes over large areas: Differential interferometry. *J. Geophys. Res.*, 94, 9183-9191.

Gottsmann, J., et al., (2006). New evidence for the reawakening of Teide volcano. *Geophys. Res. Lett.*, 33, L20311, doi:10.129/2006GL027523.

Johnson D.J. et al., (2000) Comment on “Volume of magma accumulation or withdrawal estimated from surface uplift or subsidence, with application to the 1960 collapse of Kilauea volcano” by P. T. Delaney and D. F. McTigue, *Bull. Volcanol.* 61, 491-493.

Marti et al., (1994) Stratigraphy, structure and geochronology of the Las Cañadas Caldera (Tenerife, Canary Islands). *Geol. Mag.*, 131, 715-727

Puglisi G. and Coltelli M. (2001). SAR interferometry applications on active volcanoes: state of the art and perspectives for volcano monitoring. *Il Nuovo Cimento*, 24, 1, 133-145.

Samsonov, S. and Tiampo, K.F. (2006) Analytical optimization of InSAR and GPS dataset for derivation of three-dimensional surface motion, *IEEE GRSL*, 3, 1, 107-111.

Samsonov et al., (2007) Application of DInSAR-GPS Optimization for Derivation of Fine-Scale Surface Motion Maps of Southern California, *IEEE TGARS*, 45, 2.

Seco, A., et al., (2009) GPS monitoring of the tropical storm Delta along the Canary Islands track, November 28-29, 2005, *Pure Appl. Geophys.*, 166, *in press*.

Wessel, P. and Smith, W.H.F. (1998), New, improved version of the Generic Mapping Tools released, EOS Trans. AGU 79, 579.

VOLCANO NYIRAGONGO: ANALYSIS OF LONG-PERIOD EARTHQUAKES AND VOLCANIC TREMORS.

Kavotha,K. S., N. Lukaya, T. Mavonga, B. K. Rusangiza and A.M. Syavulisembo.

Goma Volcano Observatory, Democratic Republic of Congo.

Abstract

Earthquake-hypocenter data collected by the Goma Volcano Observatory during 2002-09 provide information on some characteristics of the Long-Period seismicity of Volcano Nyiragongo:

- The epicentres of these earthquakes are clustered around the central crater of the volcano particularly at the Northern and Eastern of the Central crater.
- The Long-Period earthquakes originating from Nyiragongo occur rarely and no episodic earthquake swarm could be recognized. It seems however that the seismicty of Nyiragongo can be triggered by major tectonic and /or volcanic events in and around the Virunga volcanic area.
- The vertical magma conduit, as defined by earthquake foci, is rather obscure due to the poor knowledge of the velocity structure. Nevertheless, the vertical distribution of conduit earthquakes shows foci at depths from 0 to 27 km without any pronounced seismic gap that can represent the shallow magma chamber.

The RSAM technique was, for the first time, applied to the digital seismic signals recorded at Kibumba and Rusayo observation points close the volcano. A promising result is that drastic increases in RSAM amplitudes of volcanic tremors corresponded to increases of the surface level of the lava lake within the Nyiragongo main crater. This suggests the possibility that the lava lake level can be monitored according to seismic data.

Introduction

Volcano Nyiragongo, a strato-volcano at the northern end of Lake Kivu (Fig.1), is the south-westernmost of the eight edifices of the Virunga volcanic complex of the Western Rift Valley of Africa.

Mount Nyiragongo is famous for its lava lake type of eruptions: a lava lake has persisted in its summit crater (3,465m in altitude) in the period from 1928 till the 1977 flank eruption (Tazieff, 1977, Hamaguchi et al, 1982). After only six years dormancy, lava fountaining reappeared on June 21, 1982 and a lava lake covered again the crater floor for four months (SEAN Bull. Vol.7, N° 7). In 1994, a renewal of activity was observed at Nyiragongo with the reappearance of an active lava lake which was later covered by a 24m thick crust of solidified lava until January 2002. Today a lava lake is growing up into the central crater giving rise to a vaporous cloud of volcanic gases from a body of molten lava.

Volcano Nyiragongo is also well known for its recent catastrophic fissure eruptions. In January 10th, 1977, the volcano erupted an estimated 22 millions m^3 of lava (Tazieff, 1977) that originated from the central crater and from lateral fissures at the southern, western and northern flanks of the volcano. The lava lake was then completely drained out. Another lateral eruption on January 17th 2002 erupted 20 millions m^3 of fluid lava emptying, once again, the lava lake that has been feeding the crater since 1994.

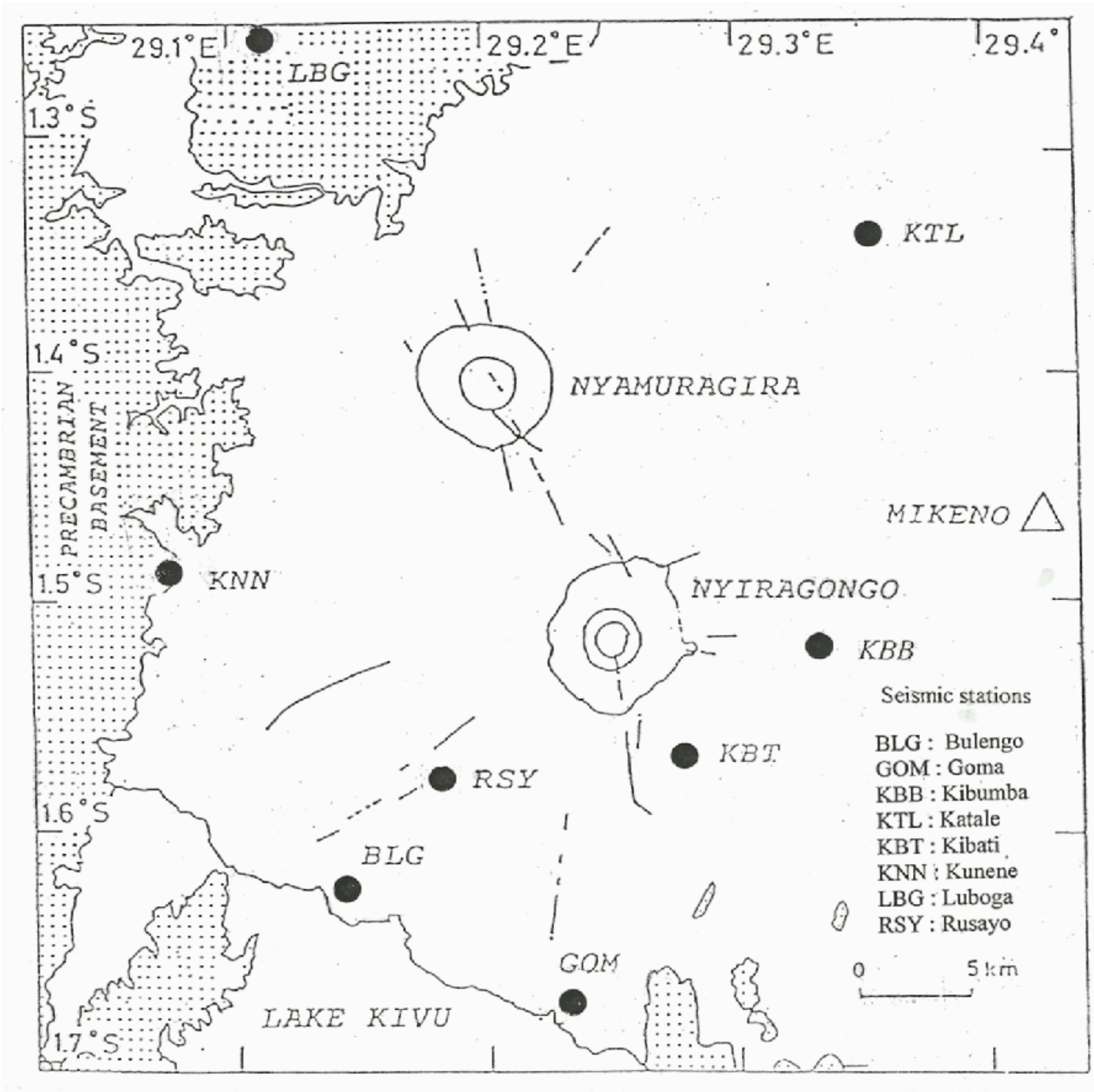

Fig.1: GVO analogue seismic network around volcanoes Nyiragongo and Nyamulagira (2002-2009). KNN, KBB, RSY, BLG and GOM were supplied with digital stations in the period November, 2003 to September, 2006.

Although Nyiragongo is located at a distance of only 13km from Nyamulagira, these two volcanoes have different features in the chemical composition of Lava (Denaeyer and Schellink, 1965; Hayashi et al, 1992). A summary of historical eruptive activity of Nyiragongo (Chakrabarti et al, 2009) indicates that the volcanic complex consists of three overlapping large strato-volcanoes aligned roughly N-S and exhibiting summit craters, the Baruta volcano (3,148 m) to the north, the Nyiragongo main cone located 1.5 km south and the Shaheru volcano (2,600 m) located 2 km to the south of Nyiragongo. At least a hundred scoria cones (among which about half have been buried by giant lava flows) are distributed south of the main cone. From these considerations, we call Nyiragongo area the surface where the historic eruptive cones of the volcano are found. This area, bounded by latitude 1.46S, is delineated to the west by the alignment of scoria cones through Bulengo and Rusayo with, however, no clear limit at the junction of the alignment and the fractures connecting Nyiragongo to Nyamulagira.

Seismological observation provides an efficient means to evaluate the activity inside a volcanic edifice (Shimozuru, 1971; Gasparini et al, 1992). This evaluation deals mainly with two characteristic seismic signals at active volcanoes: Volcanic tremors (Benoit and McNutt, 1977; McNutt, 2000) and Long- and Very-Long-Period volcanic earthquakes (Chouet, 1996).

- A volcanic tremor is a continuous signal with duration of minutes to days or even more and having characteristic dominant frequencies between 1 and 5 Hz. A volcanic tremor is noted to be generated by magmatic motion under an active volcano or by molten lava motion beneath a crater surface. The vibrations of magma in columnar form (Shimozuru, 1961) or in spherical form (Kubotera, 1974) were proposed as models of the origin of the volcanic tremors. Aki et al.(1977) and Aki and Koyanagi (1981) proposed a model of volcanic tremor generated by jerky motions of magma through cracks and discussed the model with reference to the tremors observed at Kilauea in Hawaii.

- A Long-Period earthquake has also dominant frequencies similar to that of a volcanic tremor; in addition, it shows emergent P-waves, obscure S-waves and its duration is controlled by the magnitude of the event. Long-Period earthquakes are though to be caused by fluid pressurization and by shear failure, tensile fail or nonlinear flow processes at very shallow depths (McNutt, 2000). Over the past two decades, deployment of broadband seismometers has resulted in the observation of peculiar volcanic earthquakes with period contain up to 270s (McNutt, 2000). Such Very-Long-Period events are now an exciting part of volcano seismology and have been reported at some volcanoes including Aso (Kaneshima et al, 1996), Kilauea Hawaii (Ohminato et al, 1998) and Nyiragongo (Shuler and Ekström, 2009). Very-Long-Period events at volcanoes are believed to be produced as magma moves through a flapper valve in distinct pulses.

  Volcanic tremors and Long-Period earthquakes have indicated some correlations with magma activities and have been reported to be typical precursors of volcanic eruptions at volcano Nyiragongo.

- Shimozuru and Berg (1961) reported on the nature of volcanic tremors at various locations inside the crater in connection with the continuous activity of the lava lake and compared the results with those of other volcanoes. They recognized a finite cycle of tremor amplitude variation, which seemed to have close relation with the cycle of energetic transport from the magma reservoir.

- Hamaguchi et al.(1992) also analysed the volcanic tremors which were associated with the Nyiragongo eruption in 1977: they indicated that volcanic tremors preceded the eruption by four days. They also found out that, during the eruption, vigorous magma movements in the deeper conduit of the volcano excited continuous intense volcanic tremors that were recorded at very distant seismic stations such us NAI (Nairobi) at 841 km from Nyiragongo.

- Recently, Kavotha et al.(2003) stated that, although the 2002 eruption of Nyiragongo may have been triggered by a rifting process [hundred of tectonic earthquakes including events of magnitude greater then 5 and a subsidence of the ground of up to 37 cm (Komorowski et al, 2003) along the Lake Kivu shore were extraordinary phenomena associated with the eruption], volcanic tremors were a noticeable precursor of the eruption of Nyiragongo in 2002.

- As a precursory phenomenon of the eruption of Nyiragongo in 1977, Hamaguchi et al.(1982) pointed out that shallow seismic activity of Long-Period earthquakes began to occur three to four days before the eruption. Taking the analytical results of seismic events in consideration, they concluded that repeated visiculations at the top of the magma chamber during the eruption resulted in the generation of Long-Period earthquakes.

- In November 18th to 25th 1990, a swarm of Long-Period earthquakes, including a magnitude ML=4 tectonic earthquake that killed one women, was observed in the Monigi area located just about 1km NE of Goma city (Zana, 1992). This was a confirmation of the existence there of a magma chamber detected as a geomagnetic anomaly by Masaaki et al.(1983).The lava flow that devastated in 2002 the economic center of Goma city originated mainly from this magma chamber, killing at least 100 people (Tedesco et al, 2002).

- Approximately one year before the 2002 Nyiragongo eruption, the seismic stations began to record series of Long-Period earthquake swarms that mainly originated from Nyiragongo (Kavotha et al, 2003). Although, tectonic earthquakes with local magnitudes around 4 on January 4 and 7, 2002 were the best indications of the incoming eruption [they were accompanied with dark plume, and rumbling sounds on top of Nyiragongo and a reactivation of fumarolic activity (Kavotha et al.2002)], it was noted that occurrence of Long-Period earthquakes remained at high level until January 16th 2002.

- Recently, Shuler and Ekström (2009) studied a series of five Very-Long-Period earthquakes related to the activity of Nyiragongo. They concluded that these events were generated by the collapse of the roof of the Nyiragongo shallow magma chamber along an inward-dipping cone-shaped fault. They also suggested that the diking events associated with magma shallow chambers could trigger such earthquakes.

In view of the above results obtained on the basis of irregular observations, it is now important to document the seismic behaviour of the volcano using data now continuously available at Goma Volcano Observatory (GVO).

The authors (Kavotha et al, 2003) have already examined the tectonic seismic activity that accompanied the 2002 Nyiragongo eruption. In this short study, the attention is focussed on the Long-Period earthquakes that followed this eruption. The amplitude variations of volcanic tremors are also analysed and interpreted in relation with the lava lake level within the main crater of Nyiragongo.

Data And Procedure Of Analysis.

The seismograms used in this study were provided by the seismological network of Goma Volcano Observatory. The observation network (Fig.1) consists of 8 seismic stations equipped with short-period Kinemetrics vertical SS-1 ranger pick up (T_0=1s) connected to PS-2 portable seismic recorder instruments. Signals from the sensors are amplified and filtered in amplifier modules. The overall maximum of PS-2 is 1mm deflexion for 1μV of input voltage. Each amplifier panel has controls for amplifier gain and filter setting. At our stations, the low-pass and the high-pass filters are set to 12.5 and 0.1 Hz and the amplifier gain can be varied from 36 to 66 dB according to the response of the site.

In November 2003, an acquisition system recording seismic data in continuous mode and in real time at high sampling rate was deployed in some GVO seismic stations, allowing pertinent analysis such as Real-Time Seismic Amplitude measurement [RSAM (Endo and Murray, 1991)] and Real-time Seismic Spectral Amplitude Measurement (SSAM) (Rogers and Stephens, 1995). It was expected for all GVO stations to be equipped of such stations and to be relayed to Goma base station: unfortunately this could not be possible for KTL and LBG due to transmission problems. Then, the GVO digital system consists of three-component Lennartz LE-3D/5s seismometers ($T_{0=}$1sec, upper corner frequency 40Hz) at BLG, RSY, GOM and broadband trillium 40 seismometers ($T_{0=}$ 20 sec, lower corner frequency=0.025 Hz, upper corner frequency=50Hz) at KNN and KBB stations. Signals from these stations are locally digitized from a data logger at a sampling frequency of 50 Hz and an A/D resolution of 24 bits and are telemetered to the Goma base station where they are recorded in triggered and continuous files.

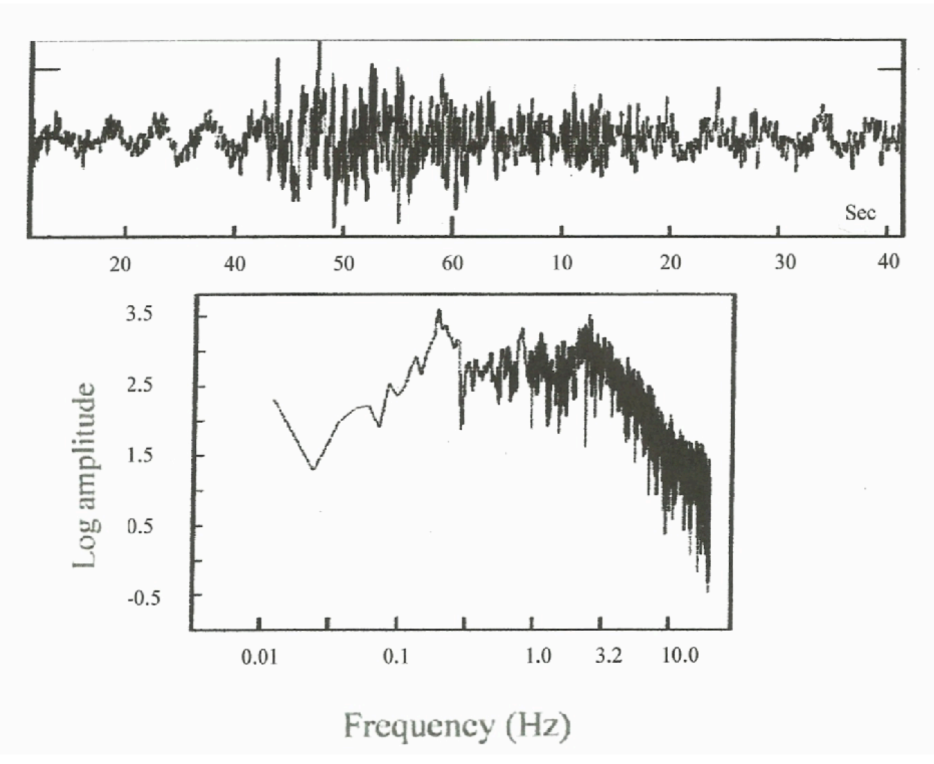

Fig.2: Typical waveform (top) and velocity spectra (bottom) of a Long-Period Earthquake recorded by the digital acquisition system on January 15, 2005.

It is well known that the accuracy of epicentre determination is performed when the seismic source (here volcano Nyiragongo) is located inside the network: this is fulfilled by the analogue network while it is not by the digital one which is mainly south of Nyiragongo. Moreover, the period September 2004-September 2006 during which the digital system worked normally is not long enough to give a comprehensive panorama of the seismic activity at Nyiragongo. Then, in this study, only the analogue records are used to locate events. The digital records are however useful particularly for early alert in case of volcanic crisis and when spectral (Fig.2) or RSAM analyses are concerned.

The accuracy of phase reading is about 0.5s for Long-Period earthquakes. The events that occurred in the study area in the period from March, 2002 to October, 2009 were located using the hypocenter 3.2 location program by Lienert and Havskov (1995). In the computation of earthquake epicenters, it would be desirable to consider a P and S velocity structure specific for the Virunga region. Since these parameters are not available, we assumed a simple model which is the average model of Bonjer et al.(1970), Bram (1975) and Nolet and Mueller (1982). This simplified P-waves velocity model includes an upper 0 to 3 km thick surface layer, a 3 to 20 km and 20 to 40 km thick layers with P-velocities varying linearly with depth from 3 to 4 km/s, 4 to 6 km/s and from 6 to 7.2 km/s respectively. The S-wave velocities are calculated using a VP/VS ration of 1.73.

To reduce bias due to uncertainty in phase reading at the time of intense volcanic tremor and velocity model, phase reading was conducted repeatedly (when necessary) for each event until standard error in epicenter determination becomes less than 0.027 ° (about 3.0 km) in longitude and latitude and the standard root mean square (RMS) error on the travel time residual remains less than 0.5 s.

Mavonga et al.(2006) has already indicated that, using our analogue seismic network, the computed focal depths are fair for deep earthquakes (depth range of 10 to 30 km). In order to obtain an optimal maximum error in the focal depth (erz), he varied the error from erz=10 km by decrementing it in steps of 1 km and concluded that the maximum accuracy on focal depth of deep events was obtained for erz=5 km.

Real-time Seismic Amplitude Measurement (Endo and Murray 1991) is a powerful tool for detecting increase in seismicity regardless of event type. The RSAM system provides consecutive 10 minutes average absolute amplitude for a seismic station and averaged data are plotted as time series for individual station. In the RSSAM technique, two measurements are computed for each incoming signal:

(1) the 1-minute average amplitude (absolute voltage) for an incoming signal is computed by summing the measurements made in the minute and dividing by the number of measurements.

To reduce the amount of data, a 10 minute average amplitude is computed using the 1-minute averages.

(2) the number of events for an incoming signal occurring in 10 minutes period are counted by comparing successive 2-second average amplitudes.

According to Murray and Endo (1992) when the following conditions are met, the Event counter for an input is incremented:

if A(n) is greater than ß
and
if A(n) is greater than θ times A(n-2)

where A(n), n=1,2,3… are the successive 2-second averages, ß is the minimum amplitude for a event and θ defines how much greater than background the amplitude must be to be considered an event.

RSAM cannot discriminate earthquakes from other events such us landslides, rockfalls and surface noise. The data from the RSAM are shown in RSAM units. RSAM units are the average value of the output of the analogue-to-digital converter multiplied by 10 so as to be an integer.

Although Vila et al.(2008) presented recently a new software-based quality control system that monitors volcano activity in near real-time, RSAM techniques remain a powerful and effective tool for monitoring volcanoes and forecasting eruptions: RSAM is widely used at many volcanoes showing excellent performance (Sparks, 2003). We applied this RSAM techniques on the digital data acquired in the period from September 2004 until the acquisition system fell down on September 2006 by analysing the variations in the background level (which varies with the amplitudes of volcanic tremors) of RSAM graphs.

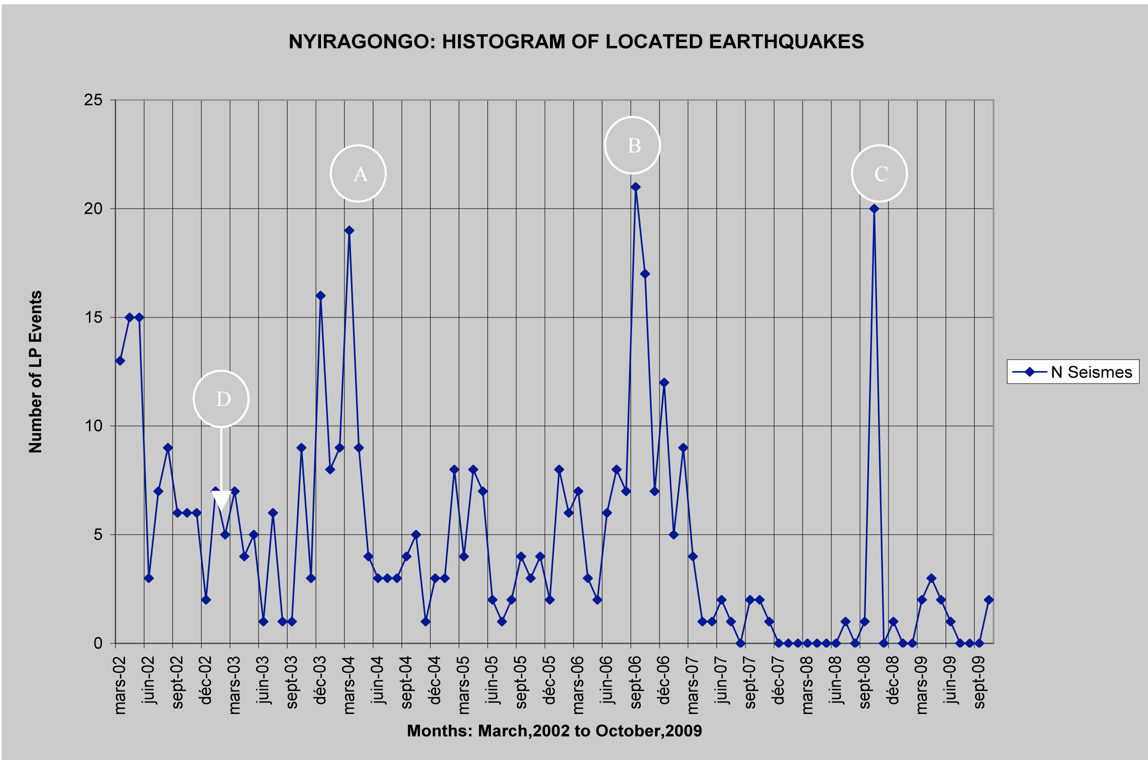

Fig.3-a: Monthly number of located Long-Period earthquakes related to the activity of Volcano Nyiragongo (March 2002-September 2009).

Results And Discussion.

Only epicentres of Long-Period earthquakes that fall in the Nyiragongo area are concerned here. Fig.3-a shows the history of these earthquakes for the period 2002 to 2009: clearly the seismicity that accompanied the 2002 eruption of Nyiragongo declined progressively until it almost vanished in May, 2003 (Position D). It is also clear in this figure that the number of volcanic earthquakes increased significantly (A, B and C) in the periods December 2003-May, 2004; September-December, 2006 and October, 2008. These increases occurred randomly with no outstanding swarm of earthquakes. The most significant result here is that Long-Period earthquakes are not so numerous at volcano Nyiragongo: a count of less than 10 located earthquakes per month is typical at this volcano. This is in a marked contrast with the neighbouring Nyamulagira volcano that commonly give rise to hundreds of located Long-Period earthquakes per month and to earthquake swarms of hundreds of events per day (Lukaya et al, 2009). This behaviour of Nyiragongo can be attributed to the fact that, due to its almost permanent lava lake, the seismic activity of Nyiragongo undergoes mainly through eruption tremors.

It has been demonstrated convincingly that a moderate earthquake with m_b=5.2 located about 130 km South of Nyiragongo triggered volcanic tremors, Long-Period earthquakes and the spectacular 1977 eruption of the volcano (Hamaguchi et al., 1982). A new example of seismic activity of Nyiragongo (sharp increase C in Fig.3-a) triggered by a regional earthquake is presented here: Long-period earthquakes suddenly affected (Fig.3-b) the Nyiragongo crater after the occurrence of a tectonic event (with m_b=5.1) located about 70 km North of the volcano on October 05, 2008. According to McNutt (2000) such volcano seismicity triggered by major tectonic earthquakes can be explained by the rectified diffusion mechanism in which oscillatory strain caused by the passage of seismic waves make existing bubbles expand and contract causing pressure increase.

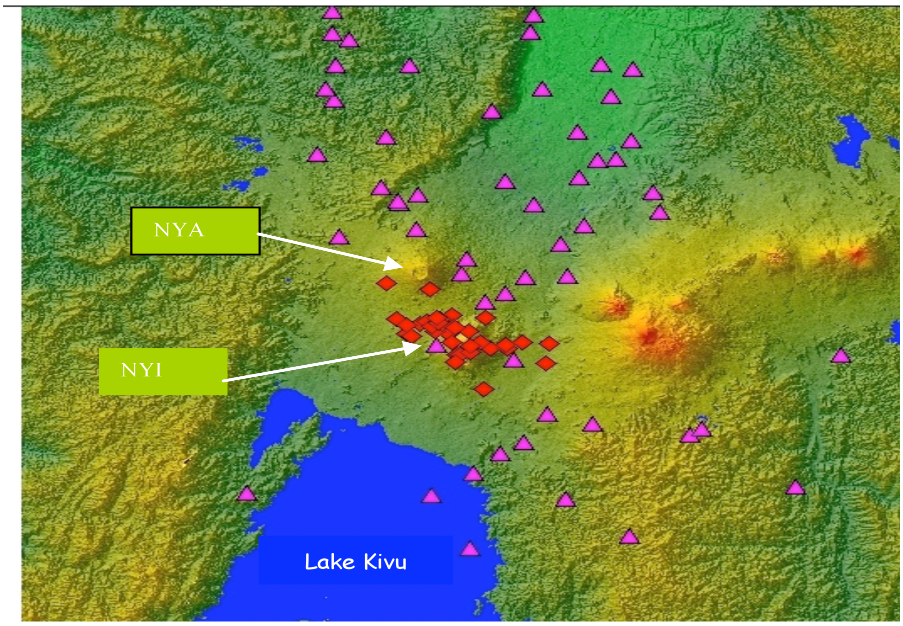

Fig.3-b: Unusual Long-Period seismicity (red lozenges) of volcano Nyiragongo (NYI) in the month following the major tectonic Earthquake on October 05, 2008. Triangles are locations of tectonic earthquakes. Note a cluster of epicentres at and just around, the Nyiragongo main crater. For coordinates, refer to Fig.4

Volcano Nyamulagira is among the most active volcanoes in the world as indicated, since 1901, by a sequence of 30 flank eruptions (Pouclet, 1975; Smets et al, 2010).

Specifications of the major eruptions of Nyamulagira include the eruptions on May 08, 2004 at the NW flank and that on November 27, 2006 at SW of the volcano some 15.5 and 7.5 km from the main crater of volcano Nyiragongo respectively. According to Wafula et al. (2009) and Mavonga et al. (2010), these eruptions were characterized by precursory and post-eruption intense Long-Period earthquake swarms just in the time intervals of the seismicity increases A and B in Fig. 3-a). Although the problems of earthquake location and of velocity structure are interdependent (Chiarabba et al, 2000; Stephen, 2005), error in location of earthquakes originating, for instance, from 15.5 km during the episode of the 2004 Nyamulagira eruption cannot be evocated to explain increase A at volcano Nyiragongo. Thus, the seismicity increases A and B in Fig.3 may be interesting observations requiring more detailed investigations and suggesting that transient stress changes associated with the activity of Nyamulagira can also trigger significant changes in the seismicity of Nyiragongo.

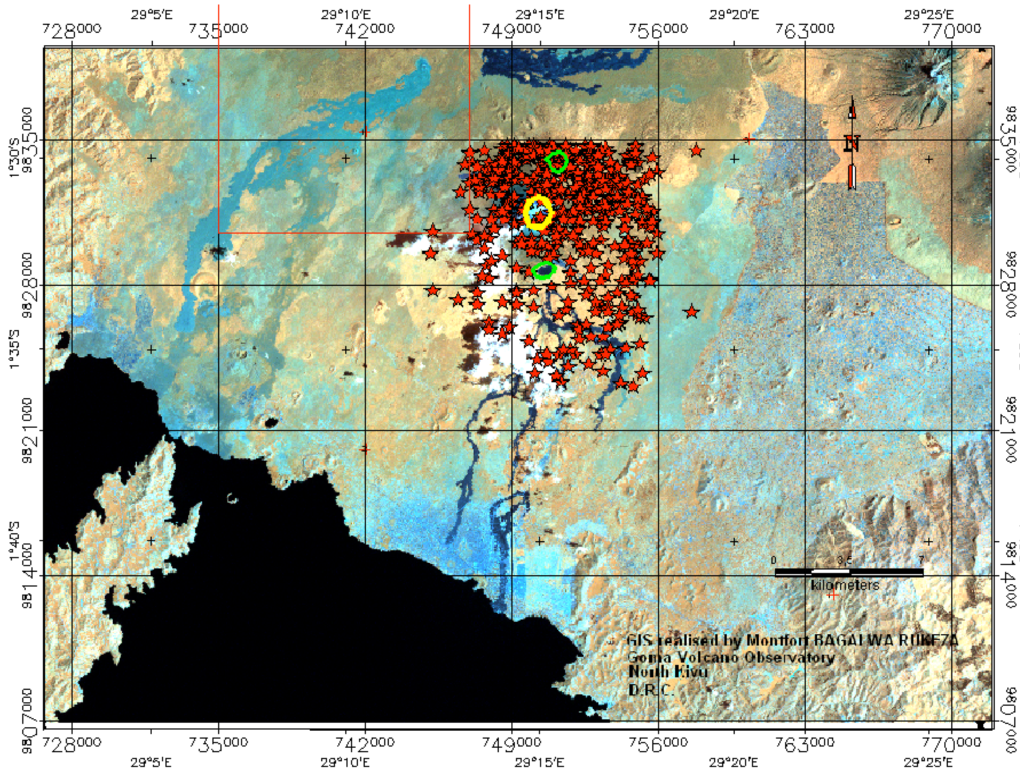

Fig.4: Map of epicentres (stars) of long-period earthquakes for the period March 2002 to October 2009. Yellow line is the contour of the Nyiragongo main crater, green ones are contours of Baruta and Shaheru craters.

We could locate 469 Long-Period earthquakes regardless of their magnitudes. From the seismic map (Fig.4), it is noted that these earthquakes have had a monotonous occurrence just around the central crater of Nyiragongo particularly at its northern and eastern flanks and that southwards, the seismicity extends less densely for about 10 km. It is also important to note that the volcanic earthquakes were not clustered along the main N-S fissures (Komorowski, 2003) which are supposed to be the main lines of weakness in the area. Roughly speaking, the epicenters extended from the crater to mid-distance between the Nyiragongo main crater and Goma city.

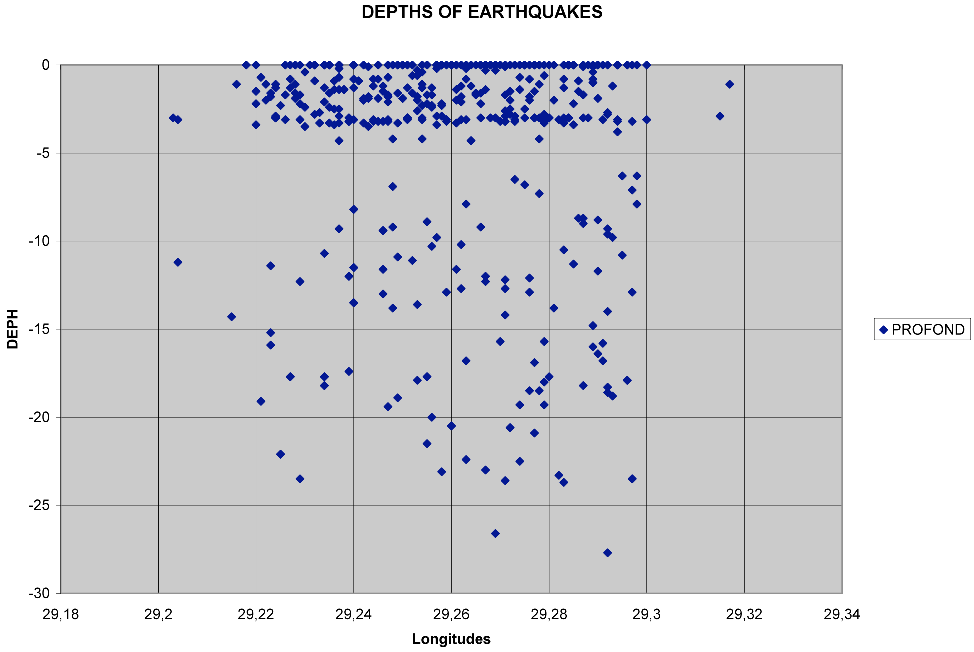

Fig.5: Depth distribution of Earthquakes at volcano Nyiragongo.

It is worthy to note that this activity was associated with the activity of magma from the deep part of the conduit to the lava lake at the surface. This interpretation prevails because the depth distribution of the earthquakes in Fig.5 shows events at all depth from 27 km to the surface. Following Fred et al.(1987) it was expected that Fig. 5 would show a seismic gap that could be interpreted as representative of the shallow magma chamber. Actually, such a gap is not found, possibly due to the poor accuracy of seismic focal depths.

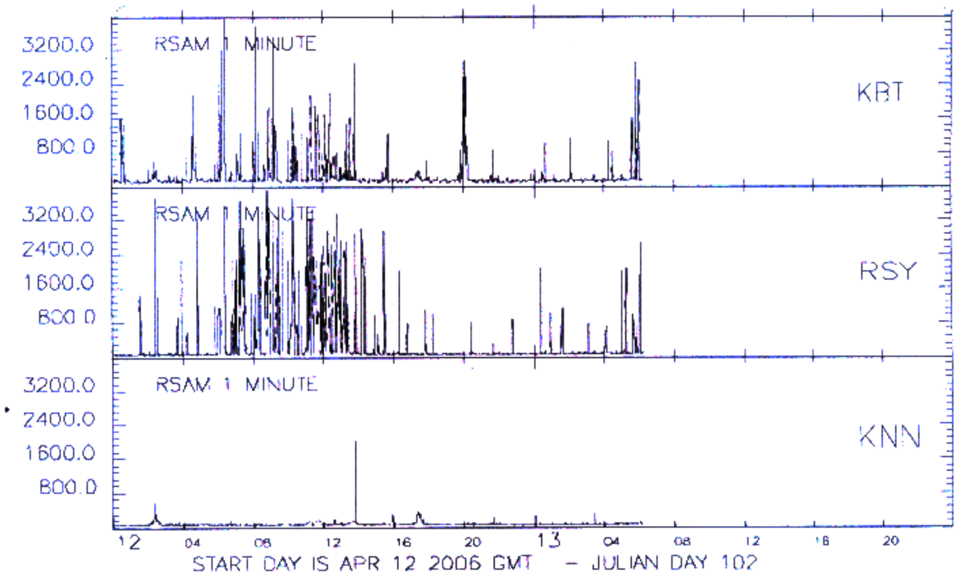

Fig.6: Examples of RSAM graphs on April 12, 2006-Julian time at Kibati (KBT), Rusayo (RSY) and Kunene (KNN) seismic stations. Y axis is in digital Counts.

An example of a RSAM graphs is shown in Fig.6. In general, regardless of volcanic activity, each station has its background noise level which results from site effects. At the time of volcanic tremors, additive amplitude from tremors is added to natural background level at each station, the additive increment being function of the epicentral distance of the station relative to the source of the volcanic tremors.

A careful analysis of the RSAM data (Fig.7) indicates that, at the time of moderate activity of Nyiragongo lava lake, RSAM background level remain at less than 500 digital counts per day. However, at specific episodes that can last for weeks, this background level can reach very high level up to more 1500 digital counts per day. Examples of such anomalies A (on November 07 to December, 2004) and B (on February, 03 to May, 15, 2006) stand out clearly in Fig.7.

It has been emphasised by McNutt (1992) that, in most cases, the strongest tremors at a given volcano occur during the most vigorous eruptions. During the years 2004-2006, GVO team conducted by J. Durieux and/or M. Kasereka used to monitor, twice a month, the surface level of the lava lake by photographing from the same point the lava lake and using as references two benchmarks on the first and the second platforms inside the crater. It was then estimated by them that the RSAM anomalies A and B corresponded to increases, of about 120m and 150m respectively, in the lava lake level within the Nyiragongo crater. It is proposed here that those tremors anomalies were associated with magma transport from depth.

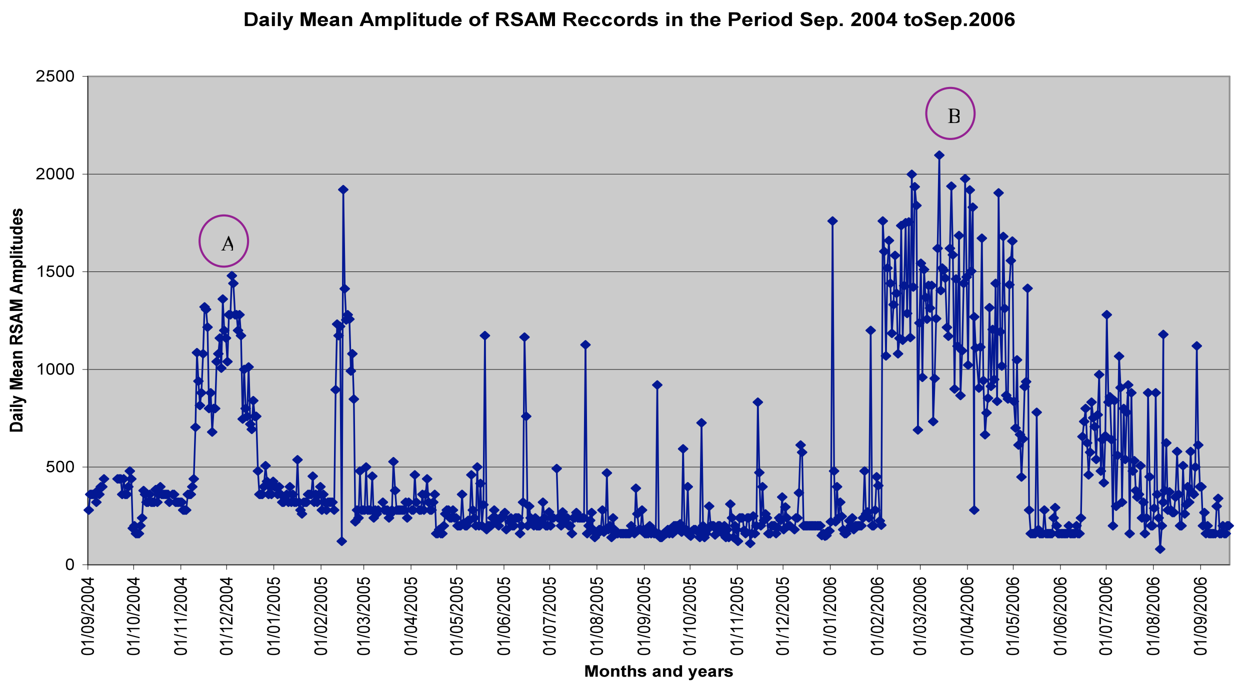

Fig.7: Daily variation of the mean RSAM amplitudes of tremors at Kibumba seismic stations. Note RSAM anomalies A_2 and B_2 on November 07 to December 04, 2004 and B2 on February, 03 to May15, 2006 respectively.

Conclusion.

The major purpose of this analysis was to study the nature of the volcanic activity at volcano Nyiragongo through an investigation on the Long-Period earthquakes and on the volcanic tremors originating from the volcano.

During the 7 years period from 2002, the Long-Period earthquakes, which are locatable manifestations of magma activity, were restricted to a conduit of 27km deep with the epicentres mainly around the Central crater of the volcano. This activity, however, extends southwards for about 10 km from the central crater.

Some interesting aspects such as influences of tectonic activity and volcanic activity of Nyamulagira on the seismic behaviour of Nyiragongo could be recognized. Although these aspects may need more detailed analysis, they may be of importance for risk mitigation at volcano Nyiragongo.

The RSAM of volcanic tremors presented here explains the two observed increases of the lava lake level in term of drastic increases of the tremors amplitudes. This first experience may be of great interest in the future as far as the Nyiragongo lava lake level is concerned. The question however arise as to whether a lava lake increase is controlled by the jamb in the RSAM amplitudes of tremors or whether it is function of the duration of the tremor anomaly: this, obviously, cannot be answered without a continuous and simultaneous observation, in the future, of both volcanic tremors and the lava lake level.

Acknowledgments

I wish to express my hearty thanks to all GVO technicians (Etoy Osodundu, Muhindo Syaghuswa) and operators for their effort to maintain the GVO seismic network in continuous operation.

The GIS plot of the epicentres by Bagalwa Rukeza Monfort is also greatly acknowledged.

References.

Aki, K., M. Felher and S. Dass (1977): *Source mechanism of volcanic Tremors: Fluid-driven crack model and their application to the 1963 Kilauea eruption, J.* Geotherm. Res. **2**, 259 - 287.

Aki, K and R. Koyanagi (1981): *Deep volcanic tremors and magma ascent Mechanism under Kilauea, Hawaii,* J. Geophys. Res. ***86***, 7095-7109.

Benoit, J. P. and S. R. McNutt (1977): *New constraints on source processes of volcanic tremors at Arenal volcano, Costa Rica, using broadband seismic data, Geophys. Res. Lett.* ***24,*** *449-452.*

Bonjer, K.P, Fucha, K. and J. Wohlenberg (1970): *Crustal structure of the East African Rift System for Spectral Response Ratios of Long-Period Body Waves,* Zeitschr. Geophys., **36**, 287-297.

Bram, K. (1975): *Zun Aufbau der kruste und Oberen Mantels im Bereigch des Westlichen Grabens des Ostafrikanisichen Graben systems und im Ostinchen Zaire-Becken Ergebnisse Einer Untersuchung der Raumwellem von Nah-Erdbeben."Geophysikalische Abhandlungen ,* Heft, **4**, 1-65.

Chakrabarti, R., K. W. W. Sims, A. R. Basu, M. Reagan, and J. Durieux (2009): *Timescales of magmatic processes and eruption ages of the Nyiragongo volcanics from 238U-230Th-226Ra-210Pb disequilibria,* Earth and Planetary Science Letters, **288**, 149-157.

Chiarabba, C., A. Amato, A. Boschi and E. Berberi (2000): *Recent Seismicity and tomohgraphic modelling of Mont Etna plumbing system*, J. Geophys. Res. **105**, 10923-10938.

Chouet, B. A. (1996): *Long-Period Volcano Seismicity: Its source and use in Eruption forecasting*, Nature **380**, 309-316.

Denaeyer, M. N. and F. Schellink (1965): *Recueil d'Analyses des Laves du Fossé Tectonique de l'Afrique Centrale (Kivu, Rwanda, Toro-Ankore), M.R.A.C*, 234pp.

Endo, E.T. and T. Murray (1991): *A Real-Time Seismic Amplitude Measurement (RSAM): A volcano monitoring and Prediction Tool,* Bull. Volcanol. **53,** 533-545.

Fred, W. K., Y. R. Koyanagi, S. N Jennifer and R.T. Wilfred (1987): *The seismicity of Kilauea's magma system*, USGS professional paper **1350**, 1019-1185.

Gasparini, P., R. Scarpa and K. Aki (Editors) (1992): *Volcanic Seismology*, Springer Verlag. Berlin.

Hamaguchi, H., T. Nishimura and N. Zana (1992): *Process of the 1977 Nyiragongo eruption Inferred from the Analysis of Long-Period Earthquakes and Volcanic Tremors,* Tectonophysics, **209,** 241-254.

Hamaguchi, H., N. Zana, K. Tanaka, M. Kasahara, M. Mishina, S. Ueki, K. Sawa-Sawa and K. Tachibana (1982): *Observation of Volcanic Earthquakes and Tremors at Volcanoes Nyiragongo and Nyamulagira in the Western Rift Valley of Africa.* Tohoku Geophys. Jour. **29**, 41-56.

Hayashi, S., M. Kasahara, K. Tanaka, H. Hamaguchi and N. Zana (1992): *Major Element of Recent Eruptive Products from Nyamuragira Volcano, Africa (1976-1989),* in *Geophysical Study on the Hotspot Volcanoes in the African Continent* (Ed.: Hamaguchi), Tohoku University, Sendai, Japan.

Kaneshima, S., H. Kawasaki, H. Matsubayashi, Y. Sudo, T. Tsutsui, T. Ohminatu, to, K. Uhira, H. Yamasoto, J. Oikawa, M. Takeo and T. Iidaka (1996): *Mechanism of phreatic eruptions at Aso volcano inferred from neat-field broadband seismic observations*, science **273**, 842-645.

Kavotha, K.S., M. Kasereka, K. Mukambilwa and M.Ciraba (2002): *A propos des Précurseurs de l'éruption latérale du Nyiragongo du 17/01/2007*, Rapport Annuel 2002 du Département de Géophysique, CRSN-Lwiro, 18-19.

Kavotha, K. S., T. Mavonga, J. Durieux and K. Mukambilwa (2003): *Towards a More Detailed Seismic Picture of the January 17th, 2002 Nyiragongo Eruption*, Acta volcanologica **15** (1-2), 87-100.

Komorowski, J.C., D. Tedesco, M. Kasereka, P. Allard, P. Papale, O. Vaselli, J. Durieux, P. Baxter, M. Halbwachs, M. Akumbe, B. Baluku, P. Briole, M. Ciraba, J-C. Dupin, O. Etoy, D. Garcin, H. Hamaguchi, N. Houlié, K. S. Kavotha, A. Lemarchand, J. Lockwood, N. Lukaya, T. Mavonga, M. de Michelle, S. Mpore, K.Mukambilwa, F. Munyololo, C. Newhall, J. Ruch, M. Yalire and M. Wafula (2003): *The January 2002 Flank Eruption of Nyiragongo Volcano (Democratic Republic of Congo): Chronology, Evidence for a Tectonic Rift Trigger and Impact of Lava Flows on the City of Goma*, Acta Volcanologica **15** (1-2), 27-61.

Kubotera, A., (1974): *Volcanic Tremor at Aso Volcano* in *Physical Volcanology*, (Eds.: Civetta, L., J. Luango and A. Rapolla) Elsevier, Amsterdam, 29-48.

Lienert, B.R.E and J. Havskov (1995): *Hypocenter 3.2, A computer Program for locating Earthquakes Locally, Regionally and Globally*, Seismol. Res. Lett. **66**, 26-36.

Lukaya, F. N, K.S. Kavotha, T. Mavonga, N. d'Oreye, F. Kervyn, J .Durieux, R. *Nyamuragira, Western Rift Valley of Africa, IASPI Gen. Ass., Cape Town*

McNutt, S.R. (1992): *Volcanic Tremor*, Encyclopedia of Earth System Sciences, Vol.4, Acad. Press, 417-425.

McNutt, S.R. (2000): Terminology and Types of Volcanic Earthquakes, Encyclopedia of Volcanoes, Academic Press, 1100-1103.

Masaaki, M, N. Zana and K. Sawa-Sawa (1983): *Geomagnetic Anomalies in the Virunga Volcanic Area and their Volcanological Implications*, in Volcano Nyiragongo and Nyamulagira: Geophysical Aspects, (Editor: Hamaguchi), Tohoku University, Sendai, Japan.

Mavonga, T., S. K. Kavotha, N. Lukaya, O. Etoy and J. Durieux (2006): *Seismic activity prior to the May 8, 2004 eruption of Volcano Nyamuragira, Western Rift Valley of Africa*, J. Volcanol. Geoth. Res. **158**, 355-360.

Mavonga, T., K.S. Kavotha, N. Lukaya, O. Etoy M. Wafula, R. K. Rusangiza and J.Durieux (2010): *Same Aspect of seismicity prior to the 27 November 2006 eruption of Nyamulagira Volcano and its implication for Volcano monitoring and Risk Mitigation in the Virunga area, Western Rift Valley of Africa*, J. Afr. Earth Sci., in press.

Murray, T. L. and E. T. Endo (1992): *A Real-time Seismic-Amplitude Measurement System,* in *Monitoring Volcanoes: Techniques and Strategies Used by the Staff of the Cascades Volcano Observatory, 1980-1990* (Editors: Ewert, J.W. and D.A. Swanson), USGS Bull. **1966**, 5-10.

Nolet, G and S. T. Mueller (1982): *A model for the deep structure for the deep structure of the East Africa rift system from simultaneous inversion of teleseismic data,* Tectonophysics **84**, 151-178.

Ohminato, T., B. Chouet, P. Dawson, and S. Kedar, Waveform inversion of very-long-period impulsive signals associated with magmatic injection beneath Kilauea volcano, Hawaii, *J. Geophys. Res.*, **103**, 23839–23862, 1998.

Pouclet, A. (1975): *Contribution à la connaissance du Volcan Nyamuragira (Rift Oust de l'Afrique Centrale), Evaluation des volumes des Matériaux émis*, Bull. Volcanol. **39**, 466-478

Roger, J. A. and C. D. Stephens (1995): *SSAM Real-time Seismic Spectral Amplitude Measurements on a PC and its Application to volcano Monitoring,* Bull. Seim. Soc. Amer. **832**, 632-639.

Shimozuru, D. and E. Berg (1961): *Seismological Study of the Nyiragongo Volcano,* Acad. Roy. Sci. Outre-mer, **VII-4,** 686-711.

Shimozuru, D. and E. Berg (1961): *Volcanic micro-Seisms, - Discussion on the Origin,* Bull. Volcanol. Soc. Japan **5,** 154-162.

Shimozuru, D. (1971): *A seismological Approach to the prediction of volcanic eruptions,* in *The surveillance and prediction of volcanic eruptions,* (Unesco-Paris), 19-45.

Shuler, A. and G. Ekström (2009*): Anomalous earthquakes associated with Nyiragongo volcano: Observation and potential mechanisms*, J. Volcanol. Geoth. Res. **181**, 219-230.

Smets, B., C. Wauthier, N. d'Oreye (2010): A new map of the lava flow field of Nyamulagira (D.R.Congo) from satellite imagery *J. of Afr. Earth Sc., In press*.

Sparks, S. R. J. (2003): *Forecasting Volcanic Eruptions*, Earth Planet. Sci. Lett. **210**, 1-15.

Stephen, R. M. (2005): *Volcanic Seismology*, Ann. Rev. Earth Planet. Sci. **33**, 461-492.

Tazieff, H. (1977): *An exceptional Eruption: Mt. Nyiragongo, Jan 10th,* Bull.-Volcanol. **40,** 189-200.

D. Tedesco, P. Papale, V. Orlando, J. Durieux, D. Wafula, E. Pilger, L. Flynn and P.Baxter (2002): *Nyiragongo (DR Congo) Report of Field Work; MODIS imagery from January 2002 Eruption*, Bull. Global, Volcan. Netw. **27, No 3,** 3-4

Vila, J., R. Ortiz, M. Tarraga, R. Macià, A. Garcia, D. Kumar and A. M. Correig (2008): *Near-Real time analysis of seismic data of active volcanoes: Software implementation of time sequence data analysis*, Nat. Hazards Syst. Sci. **8**, 789-794.

Wafula, M., M. Kasereka, K. Rusangiza, K. Kavuke, K. Mukambilwa, T. Mavonga N. Lukaya, K. Kavotha, M. Yalire, M. Ciraba and M. Bagalwa (2009): *The Nyamulagira Volcanic Eruption on November 27, 2008, Virunga Region, D.R. Congo*, Cahier du CERUKI, Numéro spécial, 108-115.

Zana, N. (1992): *Rapport sur l'éruption actuelle du Nyamulagira (Mikombe)*, Rapport de Mission, CRSN-Lwiro, 2pp.

The 2007 rifting event in Northern Tanzania studied by C- and L-band interferometry

A.M. Oyen[a], C. Wauthier[b,c], N. d'Oreye[d]

[a]*Delft Institute of Earth Observation and Space Systems, Delft University of Technology, Kluyverweg, 1, 2629HS Delft, The Netherlands*
[b]*Royal Museum for Central Africa, Leuvensesteenweg, 13, 3080 Tervuren, Belgium*
[c]*Dept. ARGENCO, University of Liège, Sart Tilman B52, 4000 Liège, Belgium*
[d]*National Museum of Natural History, Rue Josy Welter 19, 7256 Walferdange, G.D.-Luxembourg*

Abstract

July-August 2007, Lake Natron, Northern Tanzania. Part of the eastern branch of the East African Rift (EAR) is struck by a series of moderate earthquakes, culminating with a 5.9 Mw earthquake on July 17, 2007. Thanks to the co-operation of several teams, active in different areas of expertise, this earthquake swarm is recognised to be the first dyking event in a youthful continental rift captured by space-born remote sensing techniques as well as ground based measurements (Calais et al., 2008; Baer et al., 2008; Biggs et al., 2009).

This study focuses on an in-depth analysis of the C- and L-band interferograms covering this event by means of the two multi-acquisition InSAR approaches, proposed by Oyen et al. (2008). The supervised ambiguity cycle slip correction focuses on the correction of unwrapping errors in the interferogram. The second strategy - the multi-acquisition InSAR cascading based on numerical modelling - allows to combine interferograms from different acquisition geometries in order to improve the insights in certain complex geological phenomena, such as rifting events. The resulting artificial interferograms with decreased temporal baselines show less complex deformation patterns and hence facilitate the interpretation of the deformation signal. The availability of L-band radar images, with higher coherence level and fewer phase cycles, significantly improved the interpretation.

Keywords: *East African Rift, continental rifting, radar interferometry, numerical modelling*

1 Introduction

The East African Rift (EAR) is an approximately North-South oriented geological feature that runs all the way through the African continent. The EAR is the result of continental stretching leading to the divergence of the African plate and is characterised by intense seismicity and active volcanism. Spreading velocities for the

Somalian plate w.r.t. the Nubian plate range from 1.5 to 6.5 mm/yr in the south and the north of the rift respectively, (Stamps et al., 2008).
This study focuses on an area in northern Tanzania along the eastern branch of the rift. The area of interest contains a salt lake (the Lake Natron) in the northwest and two main volcanoes (Ol Doinyo Lengai and Gelai) located to the south and east of the lake respectively (see Figure 1).

From July to August 2007 this area was struck by a seismic swarm centred on the southern flank of the Gelai volcano. The crisis was accompanied by renewed activity of the nearby Ol Doinyo Lengai volcano, with some unusual explosive eruptions in September 2007. This event was captured by GPS measurements, a local seismic network, and by two radar remote sensing instruments onboard Envisat and ALOS satellites. The GPS station, located west of Lake Natron, measured a displacement of approximately 5.6 cm vertically and 5.7 cm horizontally (Calais et al., 2008). This displacement was linked to the signal captured by the seismic network, but was much larger than expected at such a large distance from the earthquake's epicentres. The radar interferograms were able to reveal the size of the deformed area.

Figure 1: Screenshot of the East African Rift (northern Tanzania). (Source: Google Earth)

Based on the coherence level and deformation signal, eight potentially interesting interferograms from four different acquisition geometries are selected in Section 2 in order to analyse the observations. Amongst the selected interferograms, two interferograms are acquired in L-band. The two multi-acquisition InSAR approaches, which are introduced by Oyen et al. (2008), will be applied on this data stack in Sections 3 and 4.

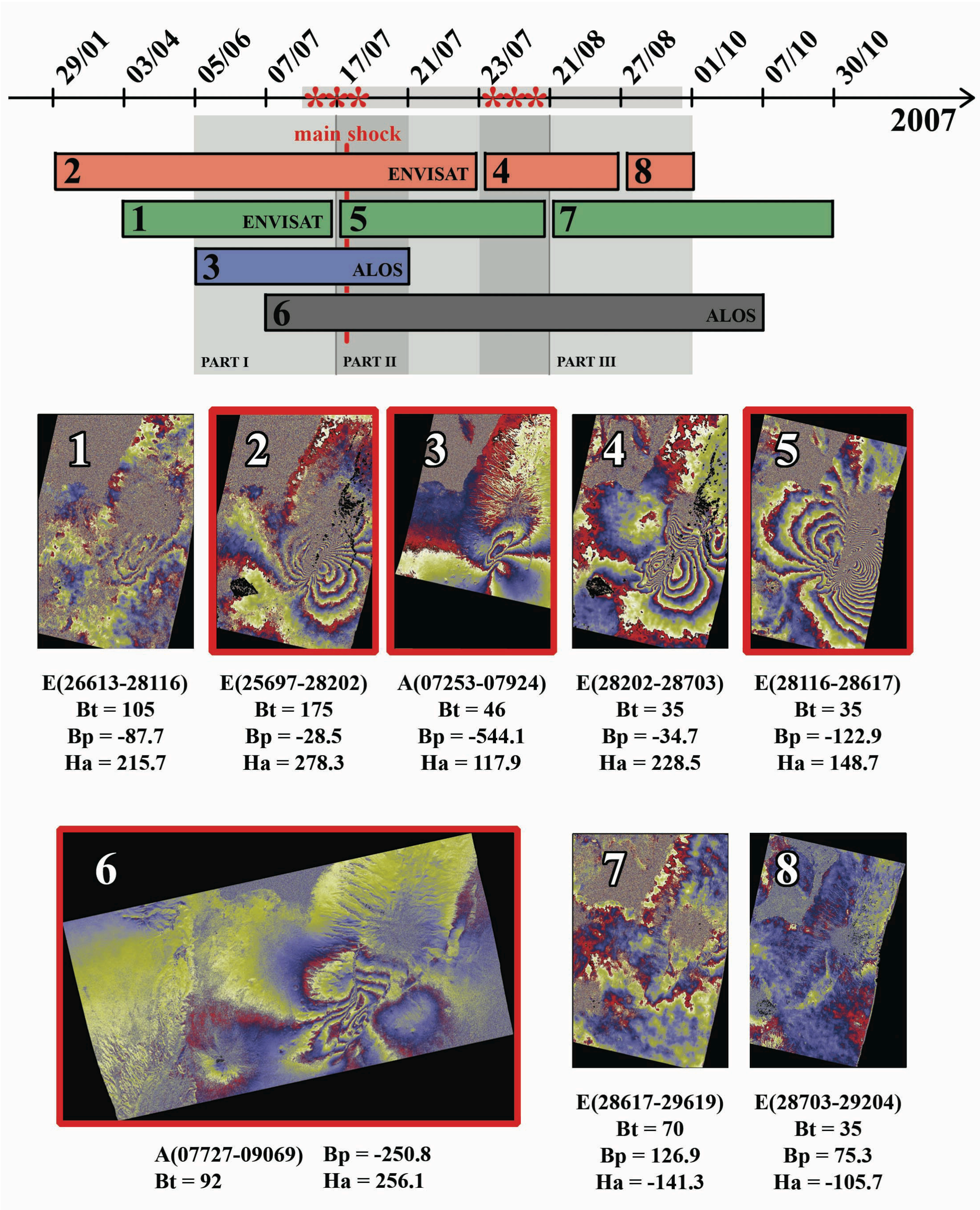

Figure 2: Summary of the differential interferometric results from 29/01/2007 to 30/10/2007. Green and red indicate respectively the Envisat track 6 (swath is6) and the Envisat track 92 (swath is2) interferograms. The descending and ascending ALOS interferograms are represented by blue and black respectively. Some important parameters of the interferograms, which are named by their respective orbit numbers, like temporal baseline (Bt), perpendicular baseline (Bp) and height ambiguity (Ha) are listed next to each interferogram. The > 5 Mw earthquakes of the seismic swarm, that started in the beginning of July 2007 and lasted up to September 2007, are indicated by the red stars on the time line. More specifically, the main shock is indicated by the vertical red line in the time line. The interferograms that contain this main shock are marked by the red boxes. The seismic swarm itself is indicated by the grey rectangle (July 2007 – September 2007).

The results are discussed in Section 5. The supervised ambiguity cycle slip correction will be applied on two interferograms, one captured by the Envisat ASAR and one by the ALOS PalSAR instruments. The results of the multi-acquisition InSAR cascading approach indicate that this rifting event consisted out of a dyking episode on the central axis of the main graben. Furthermore, the results suggest that a magma-injection is preceded by slip on a fault plane located in the direction of the magma-displacements. Finally, some conclusions are drawn in Section 6.

2 Data availability

The Natron basin is monitored by both the Envisat ASAR and ALOS PalSAR instruments, providing a data set containing radar images from four different acquisition geometries. Amongst these, eight potentially interesting interferograms are selected in order to analyse the deformation pattern and its chronology.
These interferograms, including a time line, are shown in Figure 2. The grey bar in the time line represents the total time span of the seismic swarm, while the red stars indicate the >5 Mw single events. Based on the acquisition dates of the available radar images, the seismic swarm is subdivided into three parts. *Part I* includes the deformation at the beginning of the seismic swarm (July 12-17). *Part II* represents the main part of the dyking episode (July 17-August 21) and *Part III* represents the deformation after the 21st of August. The main shock on July 17th is indicated by the red vertical bar in the time line, while the interferograms containing this earthquake are marked by a red box.
Based on seismic data and more interferograms not included in Figure 2 no significant deformation is assumed before July 12th and after October 1st.

3 The supervised ambiguity cycle slip approach

High noise levels in interferograms can result in unwrapping errors. Unwrapping improvement can be applied by ambiguity cycle slip adjustment. The ambiguity cycle slips are detected by means of peak value detection in the gradient plots along the unwrapped interferogram in both E-W and N-S directions. The outliers, or the single pixels that are selected to be potential unwrapping errors, will be removed and the area to be corrected will be defined. This area will be shifted up or down with respect to the rest of the interferogram by 2p or half the wavelength times an integer number. The term *supervised* refers to the use of a-priori information from other interferograms or geodetic measurements.

This approach is applied on interferograms 2:E(25697-28202) and 6:A(07727-09069). The corrected unwrapped interferograms are shown in Figure 3 and Figure 4. In both figures the black dots indicate the locations of the detected phase jumps. Moreover, these pixels are located in the graben area in both interferograms. It can be assumed that the deformation in graben areas is vertical (subsidence). This implies that the actual phase shift can be determined by cross-comparison of all the interferograms, rescaled to the vertical and temporal baseline, if necessary. Therefore, the interferograms are stacked and calibrated with respect to a chosen reference pixel with no deformation. The chosen pixel is located SW of the Lake Natron, where no deformation is assumed. The ambiguity number to correct for these cycle slips with is

determined from a joint analysis of the cycle slip-free unwrapped interferograms and the field measurements.
Figure 3 And Figure 4 show that the ambiguity cycle slip adjustment is applied successfully. These optimised unwrapped interferograms will be used in the further analysis.

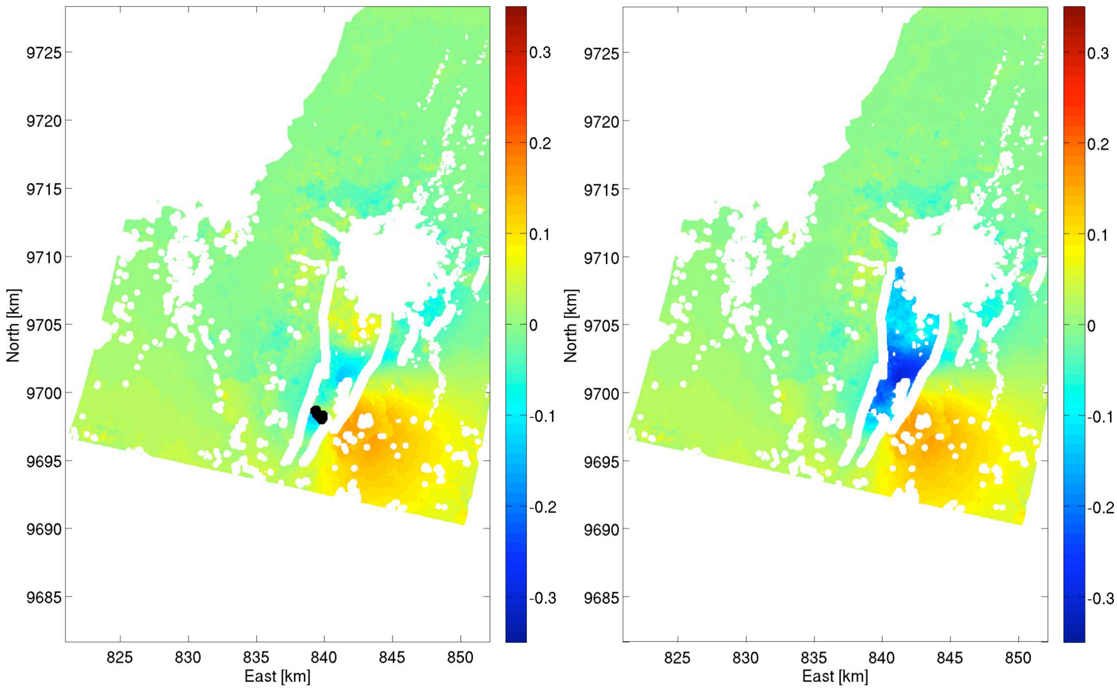

(a) Original unwrapped interferogram with cycle slips. *(b) Corrected unwrapped interferogram*

Figure 3: Unwrapping adjustment of interferogram 2:E(25697-28202). The values in both the colour bars are given in meters.

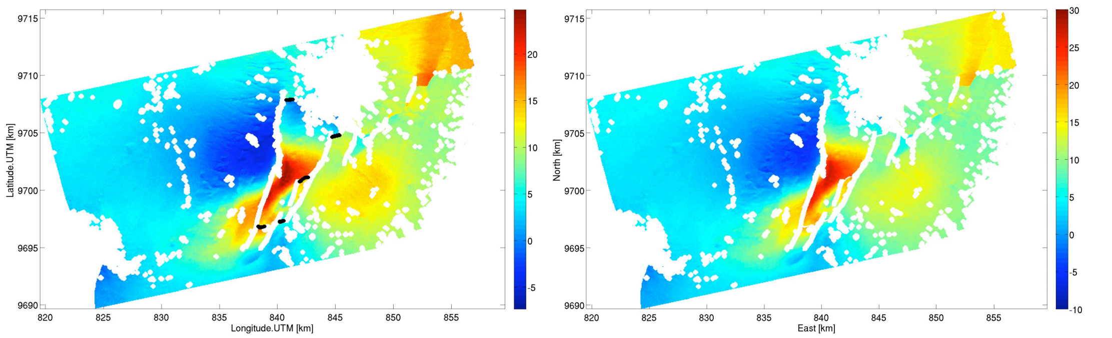

(a) Original unwrapped interferogram with cycle slips. *(b) Corrected unwrapped interferogram*

Figure 4: Unwrapping adjustment of interferogram 6:A(07727-09069). The values in both the colour bars are given in radian.

4 The multi-acquisition InSAR cascading approach based on numerical modelling

In order to improve the detailed analysis of some particular geological phenomena, geodetic observations are utilised as input for a modelling process. In the current study, InSAR data is used as input for a combination of the 3D Mixed Boundary Element Method (3D-MBEM) (Cayol and Cornet, 1996) and a neighbourhood algorithm (NA) (Sambridge, 1999a,b). The 3D-MBEM makes use of any type and number of user-defined sources. These sources are mainly fault planes with 'slip' or 'opening' or de/inflation sources. Furthermore, the 3D-MBEM method takes the topography into account, which avoids misinterpretation of the sources in mountainous areas, as is stated by Cayol and Cornet (1998). The NA is a search algorithm, which is used to invert for the *n* source parameters. It makes use of Voronoi cells in the *n*-dimensional space to converge to a certain number of optimal sets of source parameters.

In order to retrieve an in-depth analysis of this continental rifting process, in particular the chronology of the process, each interferogram, as presented in Figure 2, will be explained. Due to the large temporal sampling of the radar images, the complexity of the observed displacements of such geological events as observed in northern Tanzania is too high to provide accurate and realistic models of the traditional interferograms. Therefore, a method to decompose these displacements in smaller time periods has to be applied. The chosen method utilises several interferograms of different acquisition geometries with overlapping temporal baselines in order to create artificial, cascading interferograms.

This multi-acquisition InSAR cascading approach will be applied on *Part I*, *Part III*, and *Part II* respectively:

- *Part I* considers the deformation prior to the actual dyking episode and is fully covered by interferogram 1:E(26613-28116). The model of this interferogram is referred to as artificial interferogram 20070712-20070717.
- The modelling optimisation method for *Part III*, which represents the deformation after the dyking episode, will be applied as follows: the oldest interferogram 8:E(28703-29204) is modelled and subtracted from interferogram 7:E(28617-29619) in order to create the artificial interferogram 20070821-20080827.
- Subtracting the 20070712-20070717 deformation from interferogram 3:A(07253-07924) results in the artificial interferogram 20070717-20070721 or in *Part* II_a. And, subtracting interferograms 4:E(28202-28703) and 20070821-20080827 results in interferogram 20070723-20070821 or *Part* II_c. The remaining *Part* II_b will be modelled by three artificial interferograms simultaneously.

The fringe discontinuities and linear oriented decorrelated pixels, which are observed in the wrapped interferograms and coherence image respectively, indicate the location of the surface ruptures and are confirmed by field observations. Combining the information of these three sources resulted in the fracture map as presented in Figure 5. These fractures will be used in the modelling process.

Considering the graben bounding faults, Angelier et al. (1997) described a simple model relating the horizontal (Dh) and vertical (Dn) offsets to the dip angle (z) of the scarp as follows,

$$\tan z = Dn / Dh.$$

According to this theory and the information resulting from the field observations (Delvaux et al., 2008), the geometry of the graben bounding faults is fixed during the modelling process. The dyke is assumed to be located on the central axis of the main graben and the graben bounding faults dip towards this central axis with a constant dip angle of 65°. The depth of the top of the dyke is determined by the depths of the bottom of the graben bounding faults. Moreover, the dyke is assumed to be vertical. Finally, the shear stress drops on deep buried faults is fixed at 3 MPa, while on the graben bounding faults a shear stress drop of 0 MPa is considered. The latter implies the passive nature of such faults as they are triggered by the stresses resulting from the dyke intrusion and not by pure tension inside the crust.

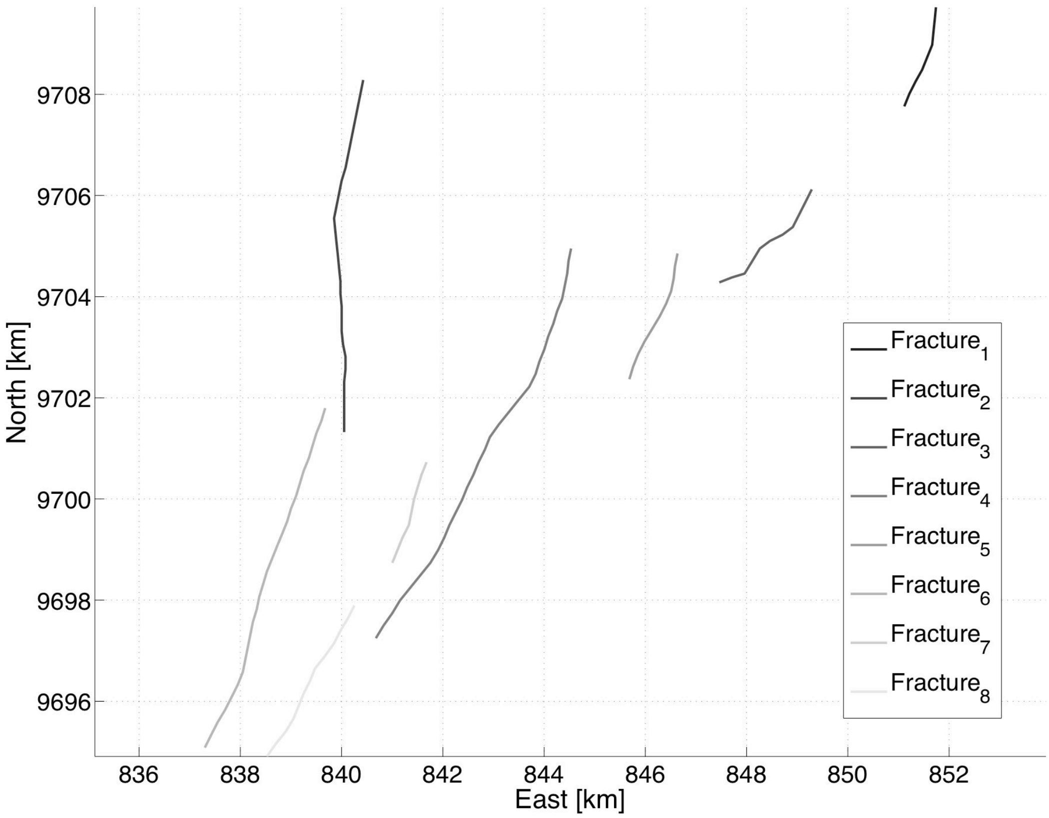

Figure 5: Mapping of the surface ruptures by cross-comparison of the coherence image and wrapped interferogram of interferogram 6:A(07727-09069) and field observations.

4.1 Part I

Part I, which contains the deformation prior to the dyking episode, is modelled by a 9.7 km long normal fault. The fault dips towards the NW at an angle of 54° with an average slip of 1.5 m between between depths of 4 km and 5.5 km below mean sea level (MSL). The dip and strike angle were determined by the seismic data, as obtained by a local seismic network, (Calais et al., 2008). The model, referred to as interferogram 12072007-17072007, is shown in Figure 6. The residual phases indicate that model simulates very well the observed displacements. The residual fringes are a result of atmospheric effects and are neglected in this study.

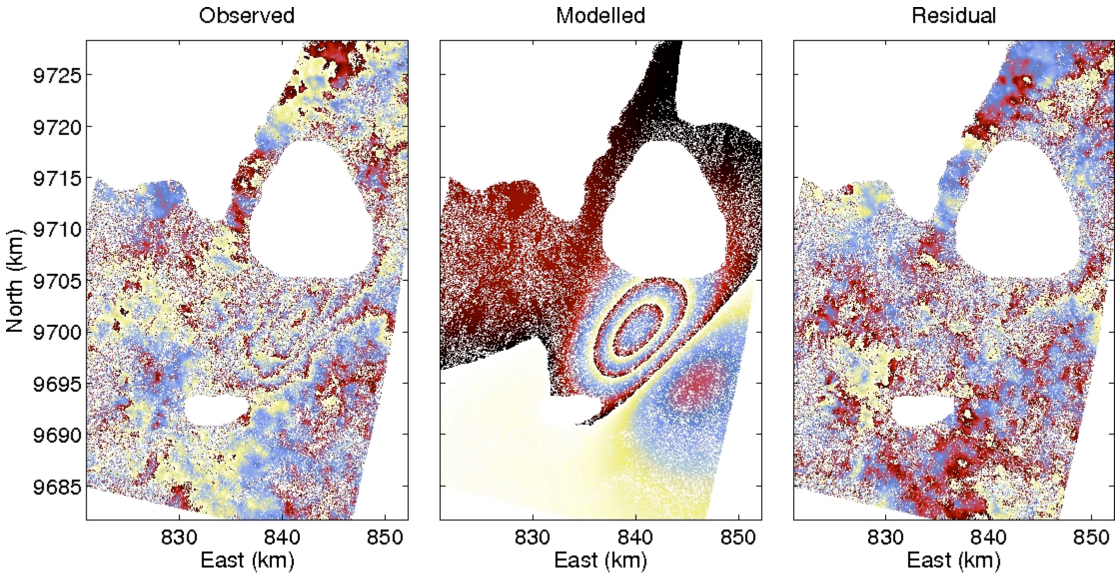

Figure 6: From left to right: observed deformation field from interferogram 1:E(26613-28116), best fit model, and residual displacements. (RMS: 11 mm)

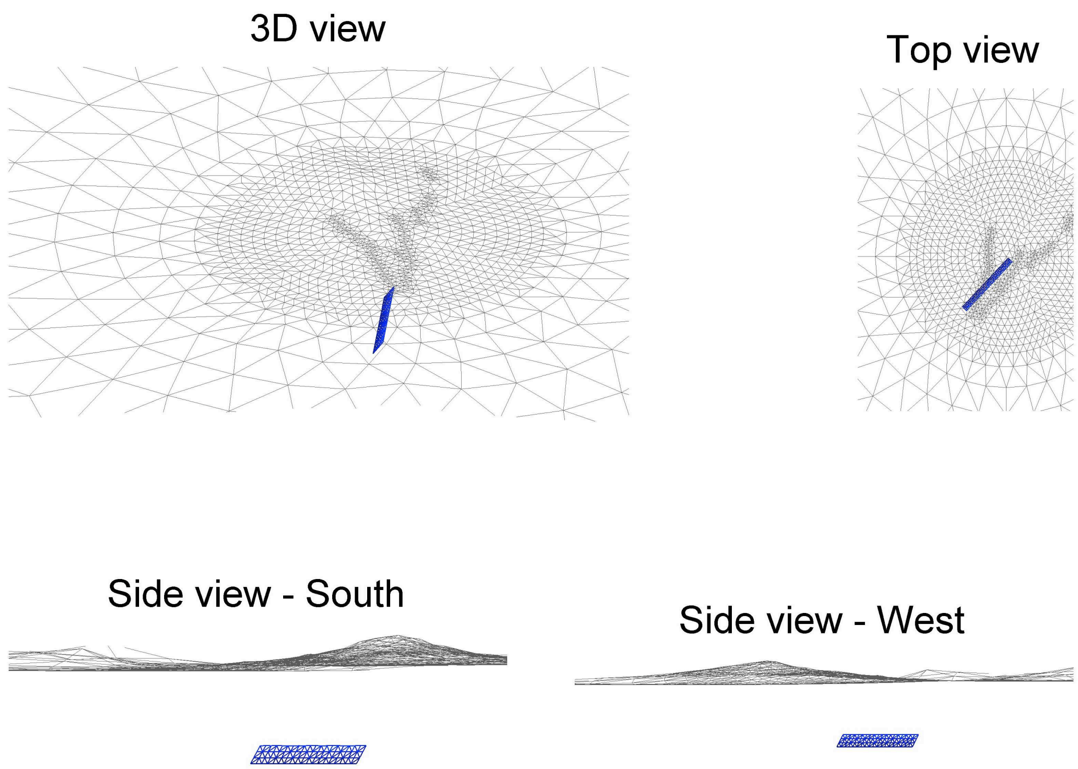

Figure 7: Interferogram 1:E(26613-28116): Sources.

4.2 Part II

The dyking episode is covered by *Part II* of the seismic swarm and is subdivided in three parts *a*, *b*, and *c*. Since no significant earthquake occurred between July 21 and

July 23, both *Part II_a* and *Part II_b* are modelled simultaneously in order to get a more reliable model.

- *Part II_a* and *Part II_b* contain the residual deformation of interferograms 2:E(25697-28202) and 3:A(07253-07924) and 20070712-20070717. The coherence image and the fringes in the wrapped interferograms indicate that $Fracture_4$ has reached the surface and some slip occurred on $Fracture_7$ and $Fracture_8$. In order to simplify the model, the geometry of the graben bounding faults, i.e. $Fracture_{2/4/7/8}$, is fixed. Furthermore, the model is created as a summation of two separated models: (*i*) one covering the dyke intrusion and the slip on the graben bounding faults and (*ii*) another one representing the slip on a normal fault plane, which corresponds to the July 17 main earthquake. The best fitting model suggests a dyke with an opening of 3 m at a depth of 2 km below MSL. The normal fault, associated to the main shock, has slipped 2 m in average at 3.4 km below MSL. The corresponding model is shown in Figure 8. The residual phase in Figure 8 indicate that the most of the observed displacements is explained by the modelled sources. These sources are visualised in Figure 9. However, the modelled displacements near the surface ruptures deviate from the observations. The residuals also show that the displacements inside the graben area are also underestimated.
- *Part II_c* covers the last phase of the dyking episode. During Part II_c the western graben bounding faults, indicated by $Fracture_2$ and $Fracture_6$ in Figure 5, as well as $Fracture_4$ have formed up to the surface. The model of that *Part II_c* is not yet considered in the present preliminary study.

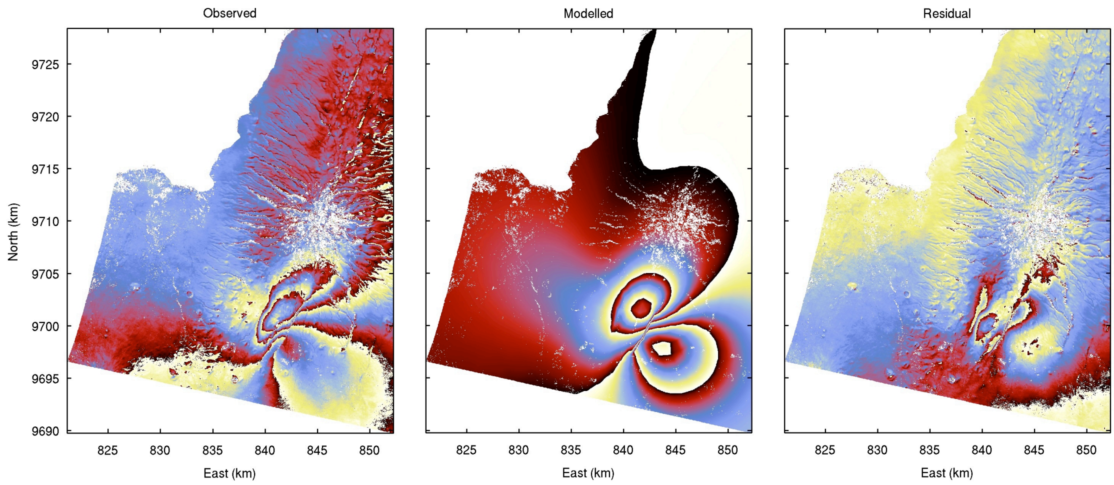

Figure 8: From left to right: observed deformation field from interferograms 2:E(25697-28202) and 3:A(07253-07924), best fit model, and residual displacements. (RMS: 37 mm).

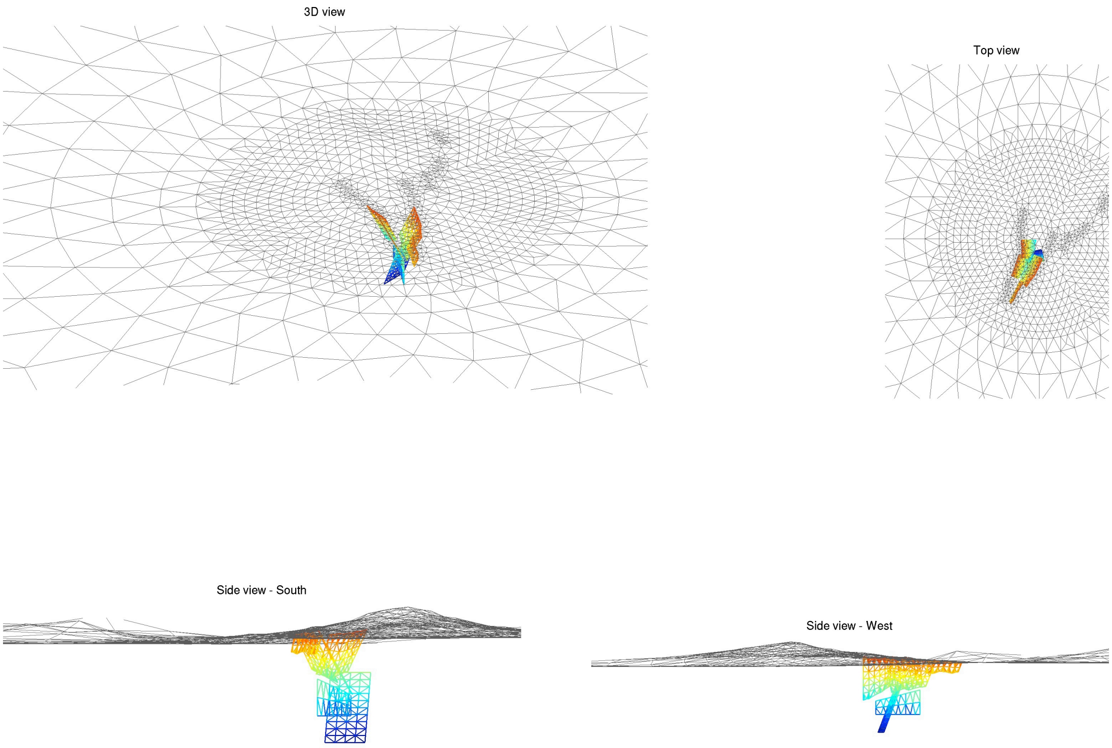

Figure 9: Interferograms 2:E(25697-28202) and 3:A(07253-07924): Sources.

4.3 Part III

The interferograms covering *Part III* show few fringes of deformation on the eastern and southeastern flank of the Gelai volcano. Furthermore, some slight subsidence is observed in the main graben area, which can be linked to either visco-elastic relaxation of the earth or deformation due to the cooling down of the injected magma.

Interferogram 8:E(28703-29204) and interferogram 7:E(28617-29619) are both modelled by an east-dipping normal fault located on the southeastern flank of the Gelai volcano, with two superficial parts reaching the surface in Fracture$_1$ and Fracture$_3$ (see Figure 5). Since interferogram 7:E(28617-29619) is easy to interpret and it fully covers the displacements mapped in interferogram 8:E(28703-29204), interferogram 8:E(28703-29204) will not be modelled in this study. However, in terms of chronology it is clear that the slip on the fault plane located on the southeast flank of the Gelai volcano migrated northwards.

The resulting model (Figure 10) suggests an east-dipping fault with two superficial segments that reach the surface. The average slip on the fault is 4c m.
According to the residual phase in Figure 10, the model explains the main fringe pattern southeast of the Gelai volcano. However, again the fringes near the surface ruptures are not perfectly reproduced by the model.

5 Discussion

The results that are described in Section 4 can be compared to three existing studies performed on the same case study. Since Calais et al. (2008), Baer et al. (2008), and Biggs et al. (2009) made use of the Okada modelling technique it is not straightforward to make a comparison between the modelling results. The Okada method inverts the slip on individual patches along the fault and applies a certain smoothing factor, while the 3D-MBEM superimposes a homogeneous distribution of the shear stress drop on the whole fault plane and derives the global slip.

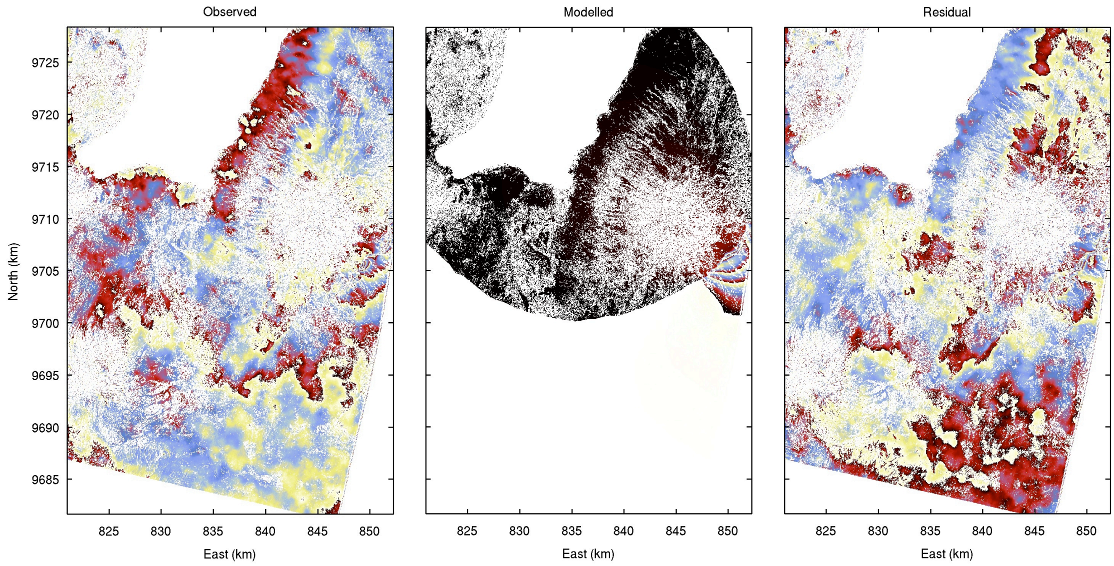

Figure 10: From left tot right: observed deformation field from interferogram 7:E(28617-29619), best fit model, and residual displacements. (RMS: 25 mm).

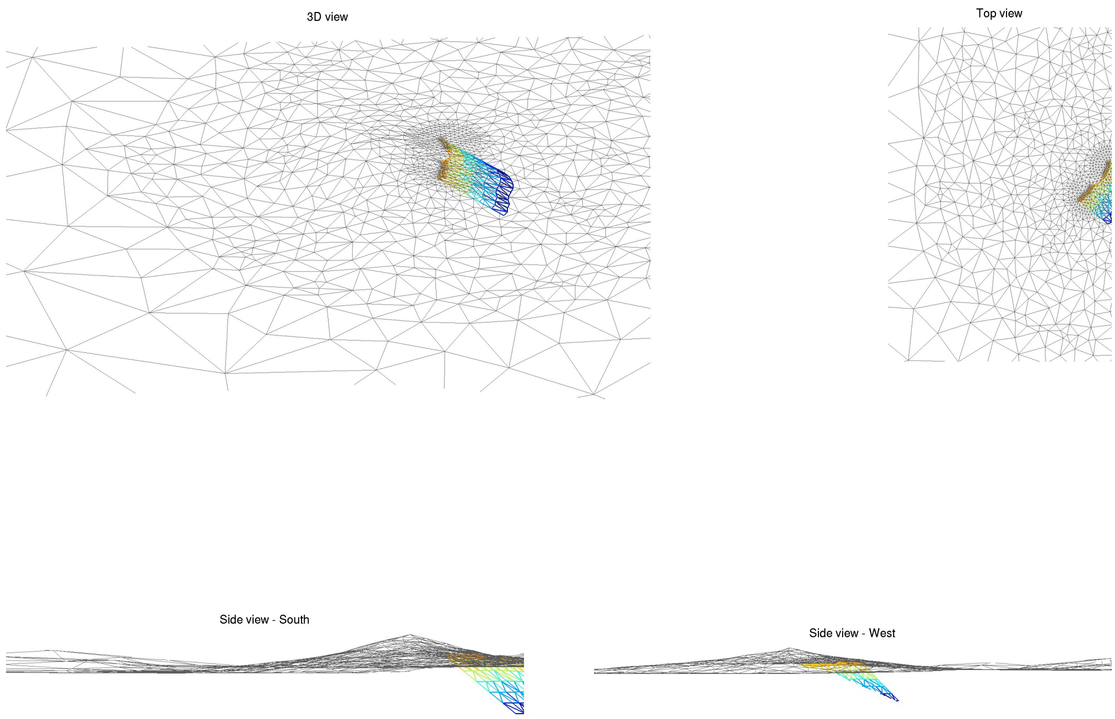

Figure 11: Interferogram 7:E(28617-29619): Sources.

Calais et al. (2008) utilised the earthquake's epicentres to define a main fault plane and only takes into account interferograms 1:E(26613-28116) and 5:E(28116-28617). On the other hand, Baer et al. (2008) invert the position of numerous fault planes and apply a similar method to create artificial interferograms with decreased temporal baseline. Biggs et al. (2009) also work with a fixed number of sources, being a dyke located at the southern half of the graben, a fault plane and a deflation source to the east of the dyke. They do not take into account the graben area.

Another difference arises from the InSAR processing software used for these studies. Baer et al. (2008) applies software that makes use of the raw data provided by the instruments (the JPL/Caltech ROI-PAC software and GAMMA software to perform the ALOS PalSAR processing). Like for the current study, Calais et al. (2008) used the open source DORIS software to process the C-band and L-band data. The DORIS software makes use of the so-called Level 1 data distributed by ESA, which are the focused single look complex data. As a result of the focussing algorithm used for that pre-processing by ESA, some data is lost near the edges of the radar images and the surface covered by the SAR images are slightly smaller. Since the Gelai volcano is located at the near range of the radar image, part of the displacements on the eastern flank of the Gelai volcano cannot be mapped.

5.1 Part I

Interferogram 1:E(26613-28116) is modelled in all studies by a west-dipping normal fault. An overview is given in Table 1. The differences between the source parameters are mainly due to the difference in orientation of the fault plane.

The suggested fault plane is slightly shallower and has a length and slip which are both approximately three times as much as in the former studies. This is mainly due to the difference in fault slip calculations of both the methods as stated earlier. In addition the topography has a large influence on the modelled displacements in this area.

Table 1: Overview of the difference in modeling parameters of the fault plane covering Part I of the seismic swarm. Study I: Calais et al. (2008), Study II: Baer et al. (2008), Study III: Biggs et al. (2009), Study IV: this study.

	Study I	**Study II**	**Study III**	**Study IV**
depth [km]	7,5	6	3,6	4,8
length [km]	20	32	16	9,7
height [km]	5	2	5	1,4
dip [°]	60	40	53	54
strike [°]	213	226	223	223
slip [cm]	50	30	40	151

5.2 Part II

The modelling would be more accurate and reliable when multiple observations, preferably from different acquisition geometries, are available. Therefore, interferograms 2:E(25697-28202) and 3:A(07253-07924) are modelled simultaneously as a single data set. This assumption is supported by the fact that Part II_b spans only two days and no significant earthquakes occurred during that time.

The graben bounding faults are assumed to be fully triggered by the dyke intrusion, introducing the idea of passive faulting.

Baer et al. (2008) model Part $II_{a/b}$ as a combination of a dyke intrusion located in the southern part of the graben and slip on three fault planes. Two of these faults coincide with the graben bounding faults used in this study. The third fault plane is located below the Gelai volcano and corresponds to the main event on July 17. It has a length of approximately 7 km. The dyke has a length of 12 km and opens up to 1 m at a depth of 2 km.
Biggs et al. (2009) model a slip of 50 cm along the same fault as modelled in Part I and a dyke opening of 1.5~m at a depth of 4.25 km. In addtion a deflation source is needed to explain the surface displacements.
This study suggests a fault with similar length, but with a larger strike angle. The dyke has a length of 4.5 km but shows an opening of 2 m at a depth of 4.5 km.

The difference between the results is remarkable in this stage. As it was the case in Part I, this difference can be explained by the modelling techniques. The opening of the dyke intrusion as modelled by Baer et al. (2008) occurred in one main patch which is smeared out from north to south. The significant opening is only present in the northern half of the dyke. This reduces the length of the dyke to 6 km, which is closer to the result obtained by this study. Also the choice of the elastic properties plays an important role.

5.3 Part III

The deformation in both interferograms 7:E(28617-29619) and 8:E(28703-29204) is minor compared to that observed in the other interferograms. Therefore, Calais et al. (2008) did not consider these observations in the dyking episode analysis. Though, it is analysed by Baer et al. (2008). According to their research, interferogram 7:E(28617-29619) can be modelled by 5 fault segments and a dyke intrusion at the location of $Fracture_2$. Three of these faults are not detectable in our interferograms, and the graben is not considered in Part III of the swarm.

Therefore, it can be concluded that both studies agree on the location of the fault southeast of the graben. According to Baer et al. (2008), the maximum amount of slip is approximately 20 cm, which is twice the maximum slip on the fault plane modelled in this study. However, it is not clear on which of the 5 fault planes this maximum slip would occur in Baer et al. (2008)'s analysis.

6 Concluding remarks and recommendations

This study applied both the supervised ambiguity cycle slip correction and the multi-acquisition InSAR cascading approaches (Oyen et al., 2008) to the 2007 Tanzanian seismo-magmatic event. It was concluded that the second proposed strategy facilitated the interpretation of the observed displacements. However, in terms of modelling the deformation observed in the artificial interferograms was not simplified up to the preferred level. Increasing the number of sources would increase the number of parameters to invert. Therefore, in the current study several assumptions were considered for the modelling. As outlined in Section 4, these assumptions were related to the geometry of the graben bounding faults and the dyke depth. The other assumptions are related to the shear stress drop superimposed on the faults.

The interferograms that span both the period prior to the dyking episode and the dyking episode itself (Part I and Part II of the seismic swarm respectively) show a remarkable temporal pattern. The displacements in Part I are the result of slip along a fault plane located where the dyke intrusion modelled in Part $II_{a/b}$. Furthermore, during Part $II_{a/b}$ and Part II_c two west-dipping faults, located in the northern and southern part of the graben respectively, have slipped. This behaviour indicates the occurrence of fault slip prior to the dyke intrusion as a result of the stresses imposed by the upcoming magma.

Remarkable is the northward migration of fault motion on East-dipping faults on the southeastern flank of the Gelai volcano. A possible hypothesis of the driving forces triggering these faults is as follows. Since these faults are neither graben bounding faults nor faults indicating any dyke intrusion/migration, their orientation implies that it is very likely that they are a result of the remaining tensional forces in the earth's crust. Due to the large surface load implied by the Gelai volcano, it is not expected that any faulting would appear on the mountain flank. However, faulting is expected at the foot of the volcano, as is observed in these interferograms.

The dyking episode that occurred at the southern flank of the Gelai volcano in the summer of 2007 was accompanied by renewed activity of the Lengai volcano. The relatively small distance between the two volcanoes suggests a most probable link between the two events. Therefore, it is preferable to perform an InSAR time series analysis on the Lengai volcano in order to detect any deformation of the volcano or it surroundings prior to and during the dyking episode. Detecting such unusual behaviour of the earth's surface might help to predict new magmatic episodes and improve our knowledge about continental rifting.

Since the 3D-MBEM considers an elastic medium, the modelling of faults that reach the surface might be problematic. This is also observed in the models covering the dyking episode (Part II of the seismic swarm). An in-depth analysis the application of such faulting within the 3D-MBEM modelling method is also recommended.

Recent research consider the most recently (re)located hypocenters, which are computed by Albaric et al. (2009), and give new insights in this seismo-magmatic event. Areas with dense clusters of hypocenters indicate the presence of magma displacements, either in magma chamber or through dykes. As such, three main areas of magmatic activity can be distinguished: one at the southern half of the graben, a second one at the axis from the Lengai volcano to the Kerimasi volcano, located south of the Lengai, and a third one to the east-southeast of the Gelai. The deepest earthquakes are located at the southern half of the graben and below the Lengai volcano. The third cluster near the Gelai contains shallow earthquakes only. Remarkable is the high seismic activity in Part III of the swarm, which does not result in any significant surface displacements. This implies that more research should be performed on the low frequency signal in the inferograms covering the months after August 2007.

7 Acknowledgements

The radar images presented in this study are captured in the frame of the ESA Cat-1 project CT-3224 and the ESA-JAXA ALOS project 3690. The InSAR processing was

performed by the DORIS software, developed by the Delft institute of Earth Observation and Space Systems (DEOS) of the Delft University of Technology (DUT). Orbital and topographic data are provided by DUT and SRTM respectively.
The authors would like to thank P. Marinkovic for his assistance on the ALOS data processing and V. Cayol and Y. Fukushima for the use of the modelling codes and helpful suggestions.

8 References

Albaric, J., J. Déverchère, C. Petit, J. Perrot, and B. L. Gall (2009). Crustal rheology and depth ditribution of earthquakes: Insights from the central and southern east african rift system. Tectonophysics 468, 28–41.

Angelier, J., F. Bergerat, O. Dauteuil, and T. Villemin (1997). Effective tensionshear in extensional fissure swarms, axial rift zone of northeastern iceland. Journal of Structural Geology 19, 673–685.

Baer, G., Y. Hamiel, G. Shamir, and R. Nof (2008, April). Evolution of magma-driven earthquake swarm and triggering of the nearby oldoinyo lengai eruption, as resolved by insar, ground observations and elastic modeling, east african rift, 2007. Earth and Planetary Science Letters 272 (doi:10.1016/j.epsl.2008.04.052), 339–352. Issue 1-2.

Biggs, J., F. Amelung, N. Gourmelen, T. H. Dixon, and S.-W. Kim (2009, May). Insar observations of 2007 tanzania rifting episode reveal mixed fault and dyke extension in an immature continental rift. Geophy. J. Int. 179(doi:10.1111/j.1365-246X.2009.04262.x), 549 —558.

Calais, E., N. d'Oreye, J. Albaric, A. Deschamps, D. Delvaux, J. D´everch`ere, C. Ebinger, R. W. Ferdinand, F. Kervyn, A. S. Macheyeki, A. Oyen, J. Perrot, E. Saria, B. Smets, D. S. Stamps, and C. Wauthier (2008, December). Strain accomodation by slow slip and dyking in a youthful continental rift, East Africa. Nature 456 (doi:10.1038/nature07478), 783–788.

Cayol, V. and F. H. Cornet (1996). 3d mixed boundary elements for elastostatic deformation fields analysis. Int. J. Rock Mech. Min. Sci. and Geomech. Abstr. / 34, 275–287.

Cayol, V. and F. H. Cornet (1998). Effects of topography on the interpretation of the deformation field of prominent volcanoes - application to etna. Geophysical Research Letters 25, 1979–1982.

Delvaux, D., B. Smets, C. Wauthier, and A. S. Macheyeki (2008). Brief scientific report of the october 2007 field work in northern tanzania. Field mapping of the surface ruptures associated to the July-August 2007 Gelai volcano-tectonic event.

Oyen, A. M., P. Marinkovic, C. Wauthier, N. d'Oreye, and R. F. Hanssen (2008). A continental rifting event in Tanzania revealed by Envisat and ALOS InSAR observations. In ALOS PI Symposium, Rhodes, Greece, 3–7 Nov 2008, pp. 8.

Sambridge, M. (1999a). Geophysical inversion with a neighbourhood algorithm - i: Searching a parameter space. Geophysical Journal International 138, 479–494.

Sambridge, M. (1999b). Geophysical inversion with a neighbourhood algorithm - ii: Appraising the ensemble. Geophysical Journal International 138, 727–746.

Stamps, S., E. Calais, E. Saria, C. Hartmady, J.-M. Nocquet, C. J. Ebinger, and R. M. Fernandes (2008, March). A kinematic model for the east african rift. Geophysical Research Letters 35 (doi:10.1029/2007GL032781).

The Mount Cameroon volcano and its sedimentary basement.

J. P. F. Tsafack [1], P. Wandji [2], J. M. Bardintzeff [3,4]

(1) Département des Sciences de la Terre, Faculté des Sciences, Université de Yaoundé I, BP 812, Yaoundé, Cameroun.
(2) Laboratoire de Géologie, Ecole Normale Supérieure, Université de Yaoundé I, BP 47, Yaoundé, Cameroun.
(3) Laboratoire de Pétrographie-Volcanologie, bât. 504 et équipe Planétologie, UMR CNRS IDES 8148, Université Paris-Sud, 91405 Orsay, France.
(4) IUFM, Université de Cergy-Pontoise, 95000 Cergy-Pontoise, France.

Abstract

Mount Cameroon volcano (4095 m asl) that has erupted seven times in the last 100 years remains the most active volcano of the Cameroon Volcanic Line (CVL). It is located at the boundary between the oceanic and the continental segments of the CVL.

The lavas constitute a weakly differentiated alkaline series: mainly basanites, basalts, hawaiites and rare mugearites. The Bomana phreatomagmatic crater which is the subject of this study is situated to the NW of Mount Cameroon, and is dated at 2.83 ± 0.11 Ma by the K/Ar method (alkali basalts). The basement of Mount Cameroon consists of sandstone that are composed of fine grains (1-3 mm, essentially quartz) set within a clay cement as observed in the Bomana crater. The composition of this sand indicates that it has a different origin from the black sands (products of basalt alteration) that are widespread along the coastal beaches around Mount Cameroon. It is possible that these sandstones constitute the sedimentary basement on which lie the first products erupted from Mount Cameroon.

Keywords: Mount Cameroon; Bomana crater; phreatomagmatic; sandstone.

I. Introduction

In central Africa, the Cameroon volcanic line (CVL) (~ 1600 km long) is the most important active alkaline volcanic province. It is oriented NE-SW (Fitton, 1987). Seismic refraction data and gravity lows (Stuart et al., 1985 ; Fairhead and Okereke 1987 ; Poudjom Djomani et al., 1997) indicate that the Cameroon line rest on crust and lithosphere 20-30 km and 80-120 km thick, respectively. Mount Cameroon volcano, 4095 m high with a volume of 1200 km^3, is the largest edifice along the CVL. It is located at the boundary between the oceanic and the continental segments of the CVL (Fig. 1a). Three main structural trends in the basement, evidenced by both field observations and digital elevation model (DEM) studies, seem to control the location of volcanic activity in the CVL: Batoke axis (30°-40°), Debundscha axis (60°-70°) and Limbé axis (140°-150°).

Mount Cameroon's activity is characterized by passive effusion of lava (basanite, alkali basalt, hawaiite) as well as explosive strombolian activity (basanite, alkali basalt, hawaiite and rare mugearite). The most recent eruptions occurred in 1999 (27 March - 22 April) and 2000 (28 May - 19 June) (Déruelle et al., 2000 ; Suh et al.,

2003) (Fig. 1b). It is worth noting that:

- it is the most active volcano of the line;
- its lavas are not differentiated or only slightly differentiated, that is common in the other volcanic graben areas all along the CVL.

The aim of this study is to demonstrate that Mount Cameroon volcano has a sedimentary substratum by examining the eruptive products and entrained lithics from the Bomana crater.

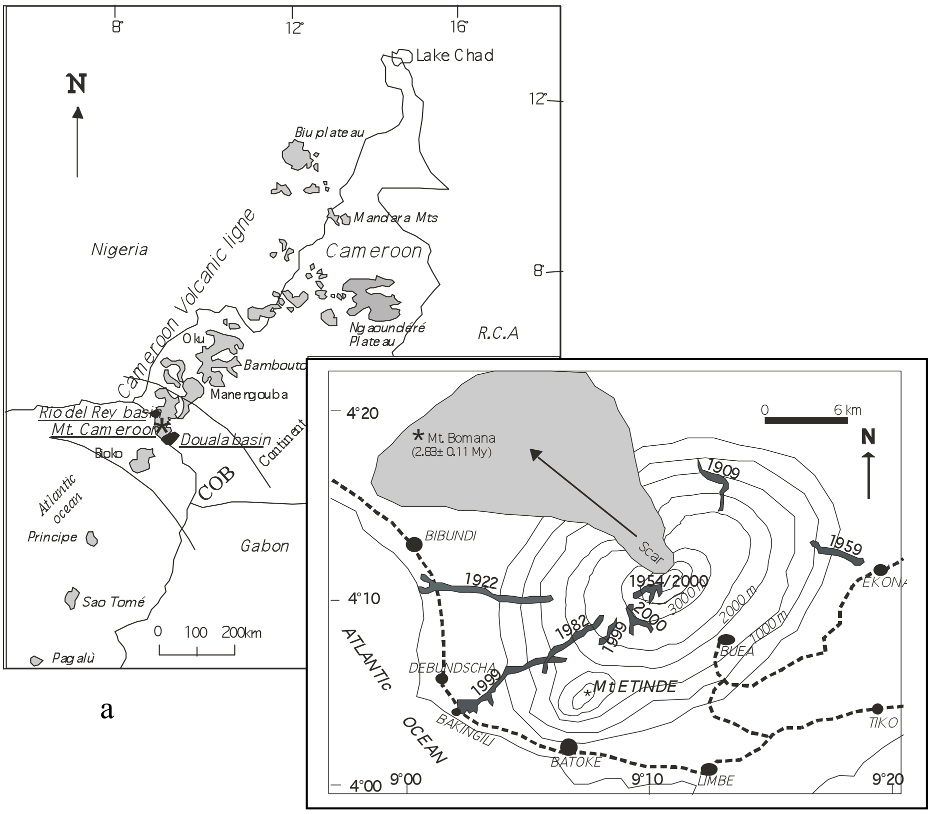

a

b

Figure 1: a. The Cameroon Volcanic Line (CVL) showing the location of Mount Cameroon. COB = Continental Ocean Boundary. b. Location of Bomana crater on the NW flank of Mount Cameroon. Arrow indicates the flow path of the debris (purple colour) inferred to have been derived from the collapse of the scar extending from the summit of the edifice. Lava flows and dates of eruption are indicated.

II. Petrography and mineralogy

The lavas from the Bomana area were analyzed and are named according to the TAS classification of Le Maitre (2002). They are mafic lavas, including basanites, basalts, hawaiites and mugearites. The main minerals in these lavas are olivine (Fo50-85), clinopyroxene, plagioclase (bytownite, labradorite, andesine) and Fe-Ti oxides (titanomagnetite, magnetite and ilmenite). Sparse alkali feldspars including anorthoclase and sanidine are found in the basanites, basalts and mugearites. Two oxides generations are observed. Early oxides are included in the olivines or pyroxenes, while late crystallizing oxides are interstitial to the principal phenocrysts phases in the groundmass.

III. The Mount Cameroon basement

The lithostratigraphic correlations between the Cameroonian sedimentary basins show that Rio Del Rey basin, situated in the NW of the massif, is a continuation of the Douala Atlantic coastal basin (Fig. 2), situated in the SE (Njike Ngaha et al., 2001). The sedimentary products that constitute the Mount Cameroon basement have been observed in the crater of the Bomana maar. They are covered by a mud flow. Otherwise, it was thought for a long time that the big scar on the NW at 3000 m altitude above the sea level was a cauldron subsidence. But, the recent field works show that it might be a landslide scar from where voluminous debris were derived (Fig. 1b). This debris covered the sedimentary formations along the E bank of Sanje river near the Bomana locality.

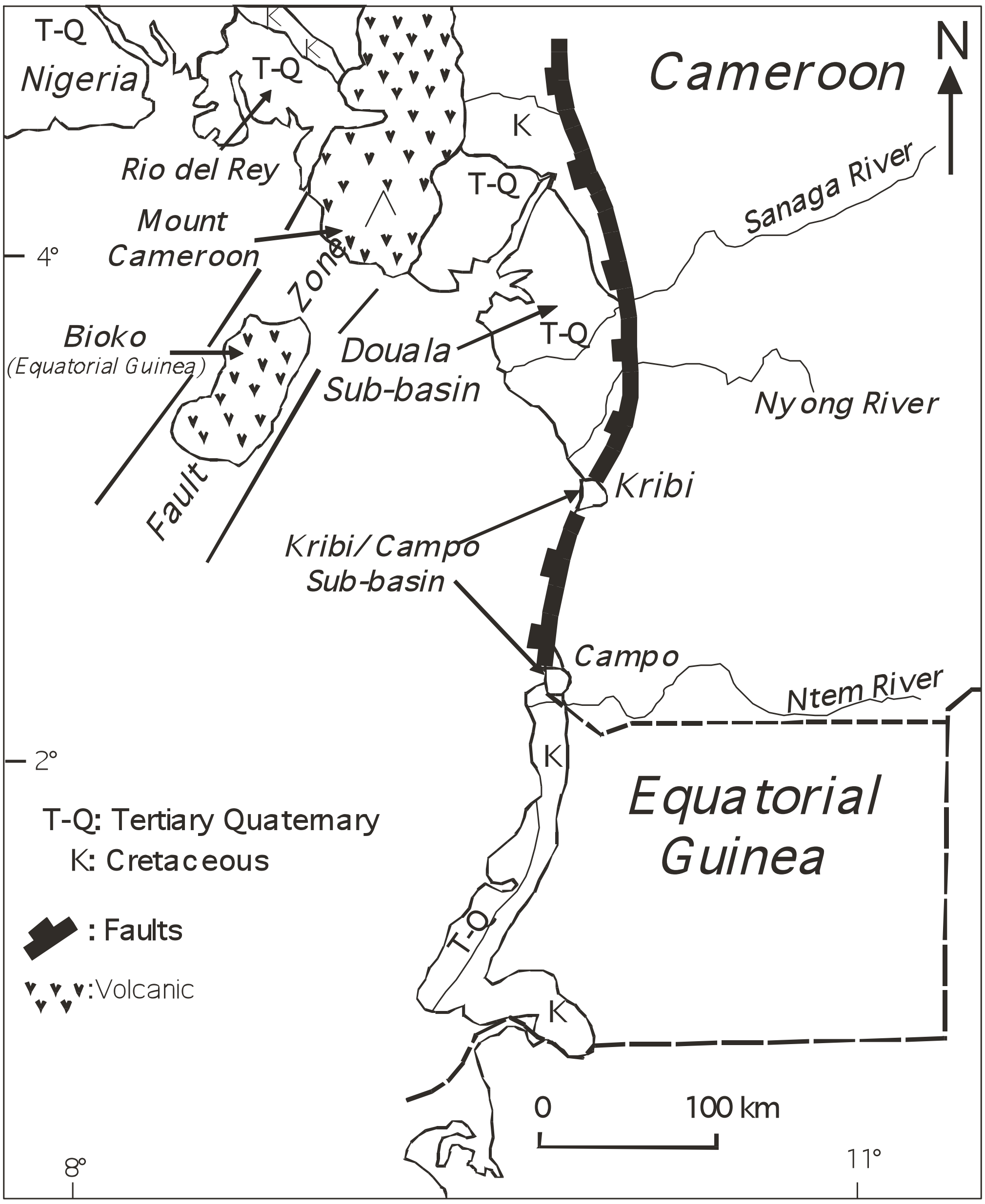

Figure 2: General geologic setting of the Douala-Kribi/Campo basin and Rio del Rey basin (Hourcq, 1955).

The tephrastratigraphic section (Fig. 3) in the Bomana maar shows the following succession, from the top to the base:

- C_1 level: mud flow stratum, composed of pebbles and blocks whose sizes vary from one centimetre to about five centimetres;
- C_2 level: the same mud flow sequence made up of thick blocks. This stratum lies on the sandstone basement (Photo 1). The block sizes vary from 4 to 30 cm and are partially rounded and blunt indicating that they have been transported.
- C_3 level: sedimentary basement (Photos 1, 2), made up of a sand of fine grains (1-3 mm, essentially quartz) with sparse clay cement.

IV. Conclusion

Mount Cameroon volcano (2.83 ± 0.11 Ma) located at the boundary between the oceanic and the continental segments of the CVL remains the most active and the most prominent horst of the CVL. Lavas from this volcano are mostly basaltic.

Its sedimentary substratum is composed of sandstones covered by the debris as observed at the Bomana maar crater to the NW of the edifice. The composition of the sand which constitutes this sandstone indicates that it is anterior to the volcanic activity of the Mount Cameroon, and that it has a different origin of that of the black sands of the coastal beaches along the massif :

- Sand of the substratum is clear. Quartz grains are abraded and glossy that witness of fluviatile transport. Reversely, sand of the beach is black and not abraded (blunt) that witness of local origin.
- Sand of the substratum contains quartz, feldspar and mica while black sand of the beach essentially contains olivine, pyroxene and Fe-Ti oxides.

This would be therefore the sedimentary basement on which lie the first products emitted by the Mount Cameroon. The important historical activity of the Mount Cameroon would be therefore responsible, during Pliocene, of the separation of the two basins i.e. Rio Del Rey basin (situated at the NW of the Mount Cameroon) and Douala basin (situated at the SE of the Mount Cameroon) (Fig. 1a and 2). Before, the two basins were joined and form only one basin. This basin formed during lower Cretaceous, linked up to the South Atlantic opening.

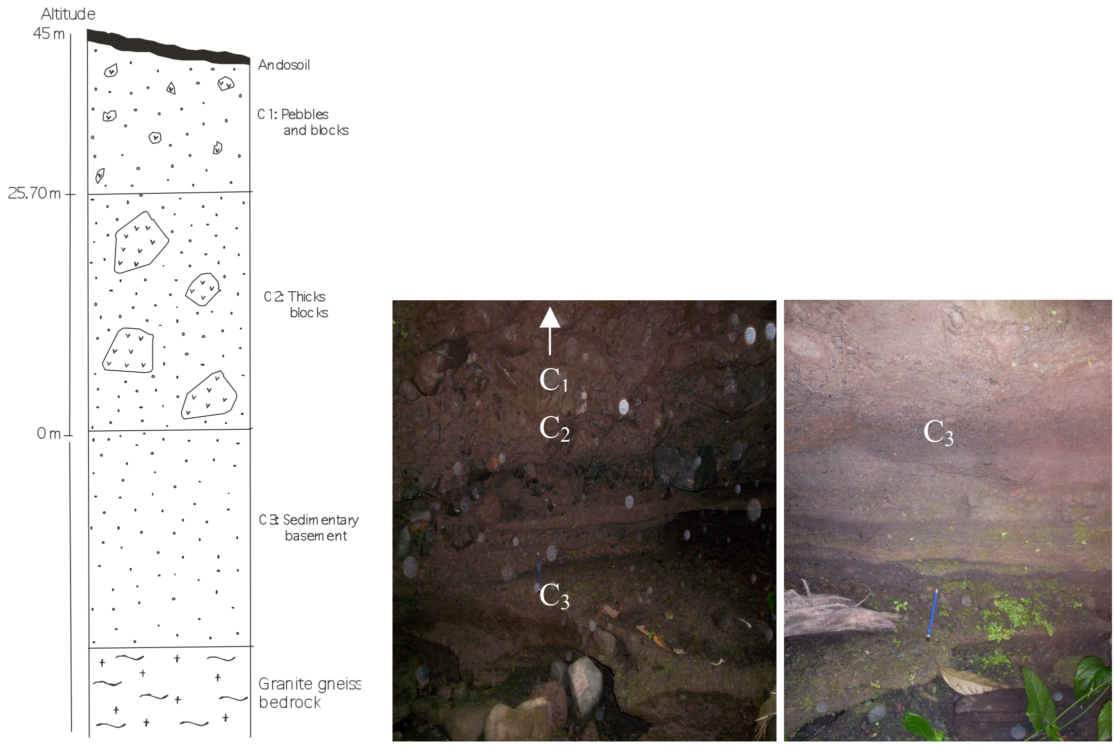

Photo 1 Photo 2

Figure 3: Tephrastratigraphic section of the Bomana cone.

References

Déruelle, B., Bardintzeff, J. M, Cheminée, J. L., Ngounouno, I., Lissom, J., Nkoumbou, C., Etamé, J., Hell, J. V., Tanyileke, G., N'ni, J., Ateba, B., Ntepe N., Nono, A., Wandji, P., Fosso, J., Nkouathio, D. G., 2000. Eruptions simultanées de basalte alcalin et de hawaiite au mont Cameroun (28 mars-17 avril 1999). C. R. Acad. Sci. Paris, Sciences de la Terre et des planètes / Earth and planetary Sciences, 331, 525-531.

Fairhead, J. D., Okereke, C. S., 1987. A regional gravity study of the West African rift system in Nigeria and Cameroon and its tectonic interpretation. Tectonophysics, 143, 141-159.

Fitton, J. B., 1987. The Cameroon Line, West Africa: a comparison between oceanic and continental alkaline volcanism. In: Fitton J. G., Upton B. G. J. (Eds.) Alkaline igneous rocks. Geol. Soc. Lond. Spec. Publ., 30, 273-291.

Hourcq, V., 1955. Les bassins sédimentaires du Cameroun. Symposium sobre yacimientos de petroleo y gas. XX Congreso geologico internacional.

Le Maitre, R. W. (Ed), 2002. Igneous Rocks, A Classification and Glossary of Terms. (Recommendations of the International Union of Geological Sciences Subcommission on the Systematics of Igneous Rocks), Cambridge University Press, Cambridge, UK, 236 p.

Poudjom Djomani, Y. H., Diament, M., Wilson, M., 1997. Lithospheric structure across the Adamawa plateau (Cameroon) from gravity studies. Tectonophysics, 273, 317-327.

Njike Ngaha, P. R., Eno Belinga, S. M., Ndjeng, E., Hell, J. V., Tsafack, J. P. F., 2001. Contexte tectogénétique de la mise en place des bassins sédimentaires camerounais du Sud au Nord. GSAf12: Geo-Environmental Catastrophes in Africa (Abstracts), p. 96.

Stuart, G. W., Fairhead, J. D., Dorbath, L., Dorbath, C., 1985. A seismic refraction study of the crustal structure associated with the Adamawa plateau and Garoua rift, Cameroon, West Africa. Geophysical J. R. Astron. Soc., 81, 1-2.

Suh, C. E., Sparks, R. S. J., Fitton, J. G., Ayonghe, S. N., Annen, C., Nana, R., Luckman, A., 2003. The 1999 and 2000 eruption of mount Cameroon: eruption behaviour and petrochemistry of lava. Bull. Volcanol., 65, 267-281.

Monitoring of volcanic activity in the Goma region (N-Kivu, Democratic Republic of Congo) and mitigation of related risks by both spaceborne and ground-based techniques: experience of the GORISK project.

A.-C. van Overbeke[1], M. Bagalwa [2], J. Durieux[3], D. Kavotha[2], F. Kervyn[1,4], A. Kies[5], F. Lukaya[2], P. Mitangala[6], N. d'Oreye[7], E. Osodundu[2], B. Smets[1], D. Tedesco[8], C. Wauthier[1,9], M. Yalire[2]

[1]Royal Museum for Central Africa (RMCA), Belgium – anne-catherine.van.overbeke@africamuseum.be
[2]Goma Volcanological Observatory (GVO), Democratic Republic of Congo
[3]United Nation Risk Management Unit, Democratic Republic of Congo
[4]Centre d'Informations Géographiques, Democratic Republic of Congo
[5]University of Luxembourg (UniLux), Luxembourg
[6]*Centre scientifique et médical de l'ULB pour ses activités de coopération* (CEMUBAC), Belgium
[7]National Museum of Natural History (NMNH), Luxembourg
[8]Second University of Naples (UniNap), Italy
[9] Dept. ArGEnCo,University of Liège, Belgium

1. Introduction

The Nyiragongo and Nyamulagira volcanoes, which are amongst the most active in Africa, are sources of several hazards that threaten the region of Goma (N-Kivu, D.R. of Congo). The Nyiragongo eruption that occurred in January 2002 produced spectacular lava flows that destroyed about 15% of the city of Goma. Although the amount of casualties was limited, hundred thousands of inhabitants were forced to evacuate in difficult conditions, which added more pressure in a highly politically sensitive area.

This paper presents an overview of the ongoing "GORISK" project. Launched in 2007, GORISK is a multidisciplinary project involving scientific teams from Belgium, Luxembourg and Italy and 3 local DRC end users (the Goma Volcanological Observatory - GVO, the Belgian NGO CEMUBAC active in public health and the United Nation Risk Management Unit in Goma - UGR) and is oriented towards the implementation and improvement of ground-based and spaceborne tools for volcanic risk and health impact assessment. The main activities are the monitoring of ground deformations, the sampling, the analysis and the monitoring of geochemical parameters in water and gas vents, the study of the volcanic plume dispersion and its possible impact on human health, the updating of the map of Goma and the implementation of a GIS platform integrating all the results.

2. Ground Deformation Monitoring

The ground deformation monitoring is addressed by both spaceborne (InSAR) (Figure 1) and ground based techniques. A network of 5 telemetred tiltmeters has been installed in the frame of the project (Figure 2). A geodetic GPS network of 7 permanent stations (loaned by the National Museum for Natural History) is under development. This complements the existing seismic network installed by the Istituto Nazionale di Geofisica e Vulcanologia (INGV, Italy) after the 2002 eruption and maintained by the Goma Volcanological Observatory, providing a (near)-real time monitoring with continuous and high resolution measurements .

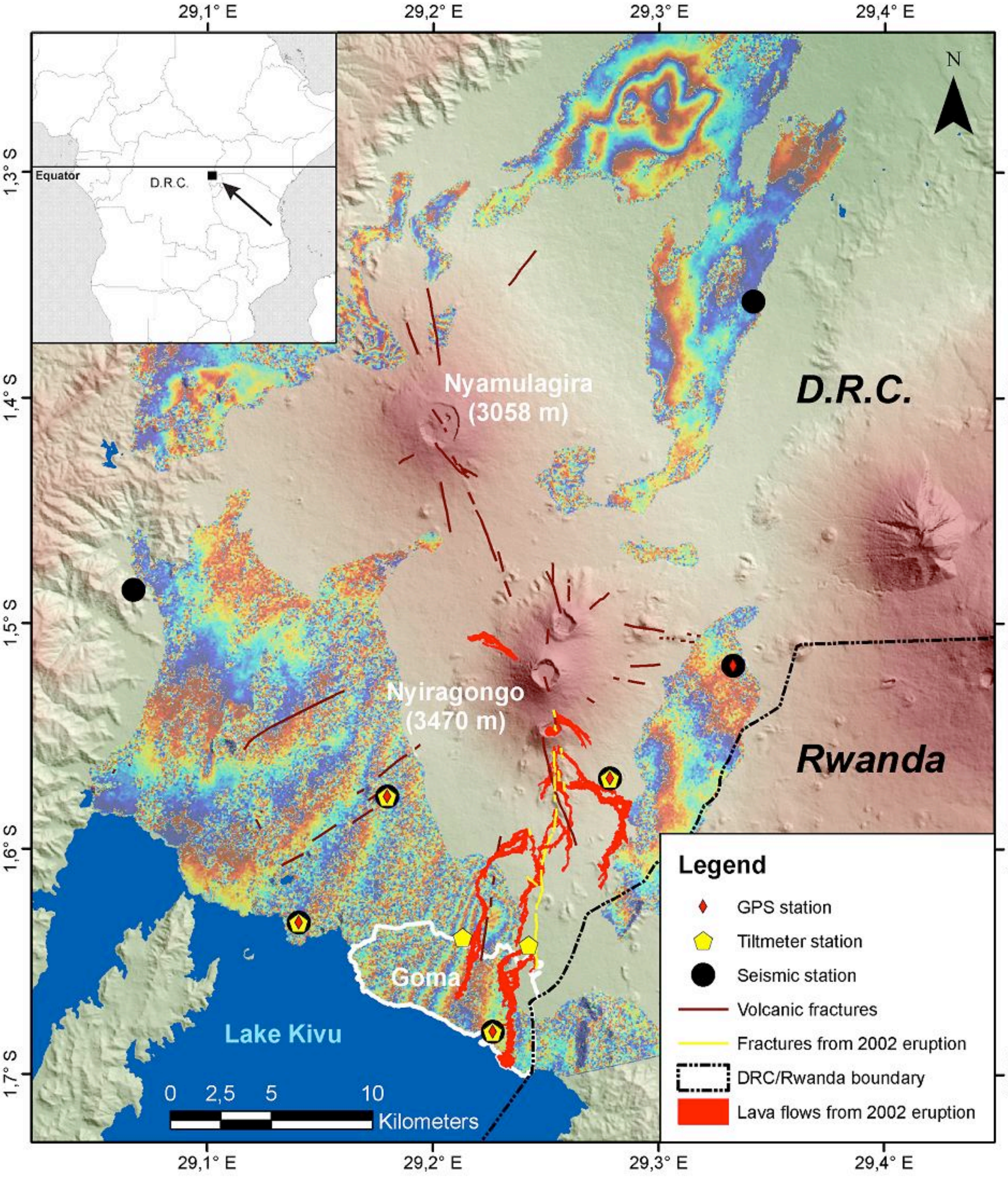

Figure 1: ground deformations associated with the January 2002 eruption of the Nyiragongo. Deformation interferogram (time span: 6th September 2000 to 3rd July 2002) wrapped on the colour-coded SRTM digital elevation model. The 2002 eruption produced a 15km long network of fractures (yellow lines) and two of the lava flows (in plain red) intruded into the city of Goma. Each fringe (one full colour cycle) represents a 2.83 cm ground displacement (or range change) in the satellite line of sight (LOS). Note that the dense vegetated areas that are decorrelated (absence of interferometric significant signal) had been masked. Narrow fringes in the Goma area, indicating a range increase, correspond mainly to subsidence with a maximum ground displacement of about 15cm in LOS. Symbols mark the location of the permanent stations networks.

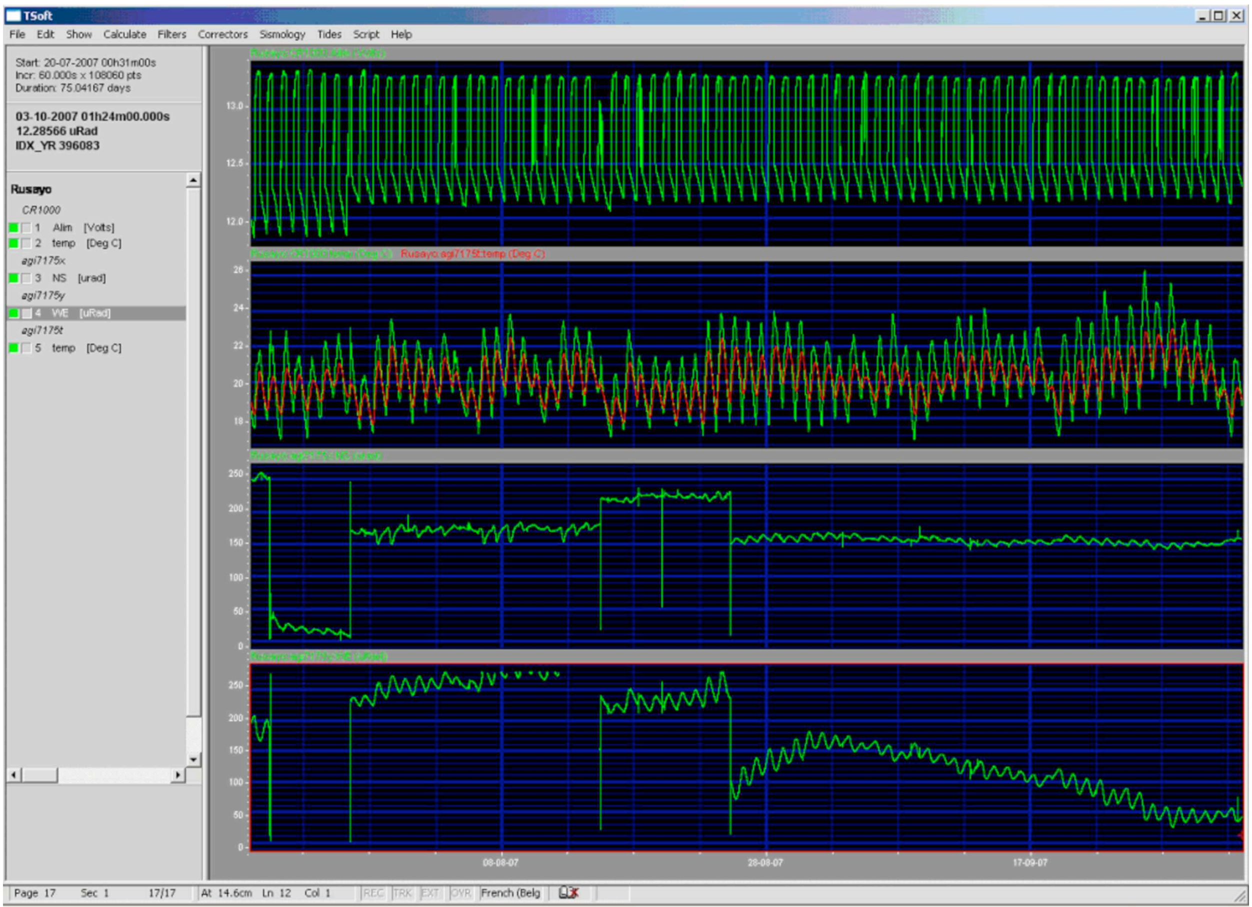

Figure 2: Example of tilt records at Rusayo station from July 2007 to October 2007. Curves from top to bottom: Supply voltage (volts); acquisition system (green,°C) and tiltmeter temperature (red, °C); North-South tilt (µRad); West-East tilt (µRad). One can clearly identify the daily ~1 Volt charge/discharge cycle of the solar power supply, the daily temperature variations of ~5 degrees inside the station damped to ~2 degrees within the sensor, and the diurnal tilt cycles. Large amplitude steps on the tilt records are related to drift corrections applied by the operator while spikes are earthquakes signatures. Data are transmitted automatically to the GVO by mobile phone.

The capacity to detect efficiently ground deformations by InSAR in densely vegetated volcanic environment has been evidenced by previous works [1]. The systematic InSAR monitoring of the Goma region is performed using ENVISAT ASAR data acquired in a routine mode (~ one acquisition per week). The hundreds of satellite radar images (including ERS archives) have been processed and more than 1400 interferograms have been computed out of that ~15-years long database with the open source DORIS software [2]. As a result, ground deformations associated to the Bukavu 2008 Mw 5,9 earthquake [1, 3] and to the most recent eruptions of the Nyiragongo (2002) and Nyamulagira (2002 and 2006) were successfully detected (figure 1) and studied into details [4, 5]. For example, concerning the 2002 Nyiragongo eruption, preliminary modeling studies show that a dyke and a normal fault can explain most of InSAR data close to Nyiragongo and city of Goma [1, 4].

3. Geochemistry and Health

Monitoring water quality and gas emanations from the sub-surface involves a network of 3 continuous Radon and CO_2 measuring stations and the sampling and analyses of both water and gas.

Special attention has also been paid to the study of *mazuku*, these dry and cold-ambient CO_2-rich gas vents that correspond to depressions where carbon dioxide, being heavier than air, accumulates by gravity at high – often lethal – concentrations (figure 3). Abundant in Goma and its vicinity, and more generally in the area South of Nyiragongo and Nyamulagira volcanoes, *mazuku* are known since a long time [6, 7 & 8]. Yet the process of formation had never been studied in detail and scientists still debate about their origin. However, fieldworks allowed us to distinguish some preferential areas where gas escapes from the ground and accumulates. Geochemical studies on gas isotopes (C and He ratios) are also performed to understand the origin(s) of gas and highlight or not a relationship with the volcanic activity. *Mazuku* are also a serious hazard. People are killed by gas every year and given the important demographic and urban growths of the region of Goma coupled with the current insecurity situation that cause sudden migration of population, the risks associated to *mazuku* are increasing accordingly. A location map with all known *mazuku* areas was produced as a tool both for scientific studies and risk management.

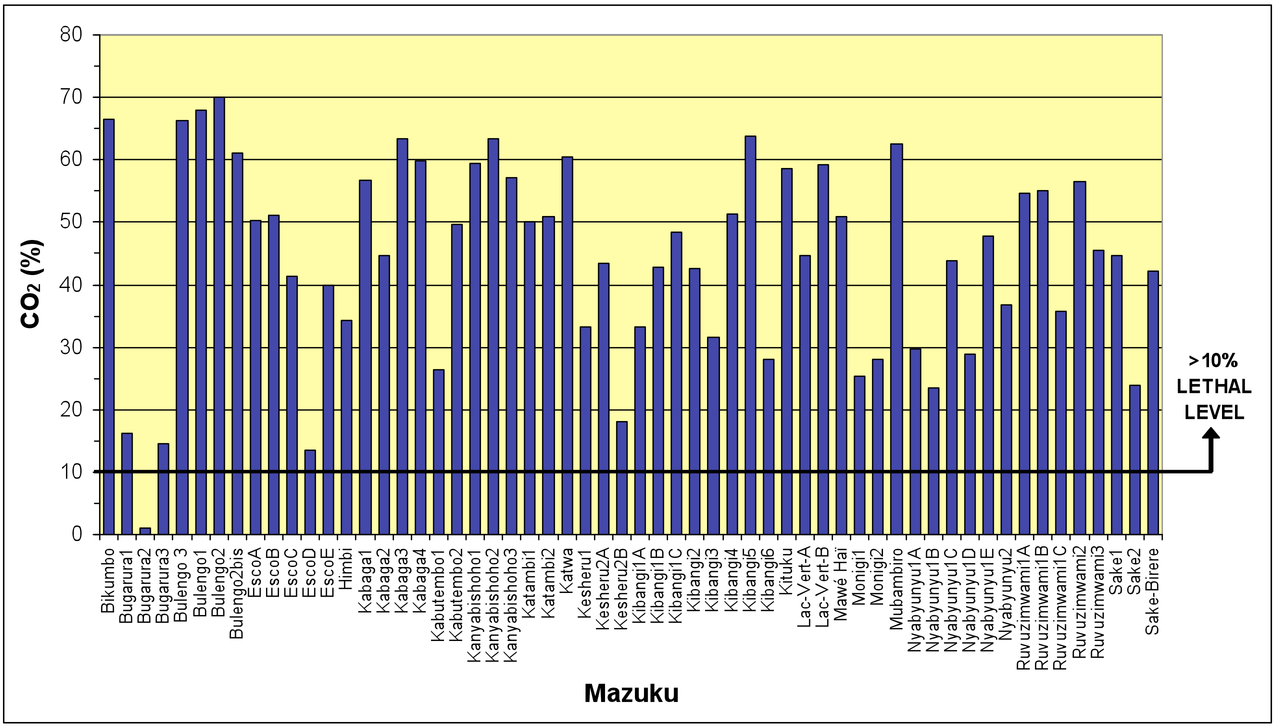

Figure 3: CO_2 concentration (%) in mazuku in the Goma area - the graphic shows that more than 98% of surveyed mazuku exceed the deadly concentration level at ground surface for a short term exposure [7].

Epidemiological data are studied to assess the possible impact on health of the volcanic activity and especially the influence of the permanent SO_2 plume emanating from the Nyiragongo and the episodic plume of Nyamulagira. To achieve this objective, GORISK takes benefit from the ongoing EU-FP6 project NOVAC [9] and US-NSF project ViSOR [10] that are focused respectively on ground-based and spaceborne monitoring of the volcanic gas plume. VISOR provides SO_2 dispersion maps created from OMI satellite sensor, whereas NOVAC uses DOAS systems for SO_2 concentration measurements from the ground. Health data are provided by the Belgian NGO CEMUBAC and are gathered in health centers scattered all over the province in both plume-prone and plume-free areas. These quarterly data include four pathologies (breath disease, skin and eye infections and diarrhea) for 2 age categories (<5 years and ≥ 5 years). The SO_2 dispersion maps are put together with these epidemiological indicators of water or air related diseases in order to attest for a possible relationship between volcanic activity and human health. Such a correlation is nevertheless not always clear and the preliminary results are evidencing that other parameters such as sanitary conditions, urban pollution, meteorological data and access to health centers need to be taken into consideration.

4. Map updating

Until recently, the map for the urban area of Goma did virtually not exist. There is an archive map created in colonial time when Goma was still a very small locality but it strongly contrasts with the size of the actual ~5 to 700.000 inhabitants city.
A new map was created locally by an NGO project [11] based on Quickbird image dated from February 2005. But since then important demographic movements related to unstable political situation and to the war were responsible for rapidly increasing urban growth. Acquisition of STEREO PRECISION IKONOS images was planned at the beginning of the project but remained unsuccessful because of the poor visibility due to atmospheric conditions. As an alternative, we acquired recently archive non-stereo IKONOS images dated from June and July 2008. Differential GPS field measurements for ground control point acquisition were performed in order to orthorectify the images and the digitalization of the urban area has started.

5. GIS platform

The implementation of a tool with analysis capability to support the data interpretation is realized through the integration of all the collected data into a GIS platform. Data are stored into a common database that can be exploited by the local end users. It contains base maps created through other initiatives, the GORISK layers associated to instruments records (tilt, GPS, geochemistry,…), the InSAR deformation and coherence maps, the updated map of the urban and infrastructure networks and the epidemiological data.

6. Training

To ensure the sustainability of the methods and to improve the capacity building of the end-users, seminars have been organized in Goma during field campaigns by the different European partners to train local staff to the maintenance and use of the tilt- and GPS-networks, to some GIS and InSAR basics as well as to the collection of water and gas (mazuku) and to the recovering of the Rn/CO_2 data.
One member of GVO and one member of UGR spent four months (Sept. – Dec. 2007) at the Royal Museum for Central Africa (RMCA) to be trained in GIS and remote sensing.

7. Conclusion

During the past two years, we improved the ground-based deformation monitoring tools by installing real time permanent GPS and tiltmeters networks. However these networks, as well as the seismic and geochemical networks and the fieldwork campaigns, suffered from serious problems related to the local, economical, security and political context. Looting episodes, inaccessibility to stations and to the field because of the war, records interruptions due to unexpected station dismantling, power supply and data transmissions interruptions are indeed so many factors preventing the continuous data collection.
On the other hand spaceborne techniques proved to be the most reliable tool for long term and systematic studies in that specific and unfavorable context. However spaceborne methods cannot replace ground based monitoring for early warning purposes to mention the least.

8. Acknowledgements

Authors acknowledge support of the Belgian Science Policy under the project GORISK (SR/00/113) and the National Research Fund of Luxembourg under the project FNR/STEREOII/06/01.

9. References

[1] N. d'Oreye, F. Kervyn, E. Calais, V. Cayol, J. Fernández, C. Frischknecht, P. Gonzales, S. Heleno, A. Oyen, C. Wauthier, "Systematic InSAR monitoring of African active volcanic zones: what we have learned in three years, or a harvest beyond our expectations", Proc. of 2008 Second workshop on USE of Remote Sensing techniques for Monitoring Volcanoes and Seismogenic Areas *(USEReST 2008)*, Naples, Italy, November 11-14, 2008, 1-4244-2547-1/08/$20.00 ©2008 IEEE, pp57-62, 2008

[2] B. Kampes, S. Usai, "Doris: The Delft Object-oriented Radar Interferometric software," *Proc. ITC 2nd ORS symposium*, August 1999, The Netherlands, 1999.

[3] N. d'Oreye, P.J. González, A. Shuler, A. Oth, L. Bagalwa, G. Ekström, D. Kavotha, F. Kervyn, C. Lucas, F. Lukaya, E. Osodundu, C. Wauthier, J. Fernández, Source parameters of the 2008 Bukavu-Cyangugu earthquake estimated from InSAR and teleseismic data. *Submitted*

[4] C. Wauthier, V. Cayol, N. d'Oreye, F. Kervyn, "Modelling of InSAR displacements related with the January 2002 eruption of Nyiragongo volcano (DRC)," *Proc. of 4th ESA Fringe2007 workshop*, ESA-ESRIN, Frascati, Italy, 26-30 November 2007. See also contribution in this issue.

[5] V. Cayol, N. d'Oreye, F. Kervyn and the GVO Team (2008) InSAR displacements associated to the November 2006 Nyamuragira eruption. *Abstr. IAVCEI 2008 general assembly, 18-22 August 2008, Reykjavik, Iceland.*

[6] O. Vaselli, B. Capaccioni, D. Tedesco, F. Tassi, M.M. Yalire, M.C. Kasereka. "The "Evil's winds" (mazukus) at Nyiragongo volcano (Democratic Republic of Congo)". Acta Vulcanologica 14-15, The January 2002 eruption of Nyiragongo Volcano and the socio-economical impact, 123-128, 2004.

[7] B. Smets "Etude des *mazukus* dans la région de Goma (RDC) et gestion des risques", Master thesis (D.E.S. interuniverstaire en gestion des risques naturels), Liège University, Belgium, 2007.

[8] B. Smets, D. Tedesco, F. Kervyn, A. Kies, O. Vaselli, M.M. Yalire, "Dry gas vents ("mazuku") in the Goma region (North-Kivu, Democratic Republic of Congo): formation and risk assessment. Journal of African Earth Sciences, AVCoR Special Issue, 2009, *in press*.

[9] http://www.novac-project.eu/

[10] http://userpages.umbc.edu/~scarn/virunga/index.htm

[11] Centre d'Informations Géographiques, "Carte de Goma" mai 2008, ONG SODERU Goma Nord-Kivu. www.soderu.org

Environmental impact of the Nyiragongo volcanic plume after the January 2002 eruption

Orlando Vaselli[1,2], Franco Tassi[1], Dario Tedesco[3,4], Emilio Cuoco[3]
Barbara Nisi[5], Matthieu M. Yalire[6]

[1]Department of Earth Sciences, Via G. La Pira, 4, 50121 Florence (Italy)
[2]Institute of Geosciences and Earth Resources, CNR, Via G. La Pira, 4, 50121 Florence (Italy)
[3]Department of Environmental Sciences, Via Vivaldi 43, 81100 Caserta (Italy)
[4]Institute of Geology and Geoengineering, CNR, Piazzale Aldo Moro, 00100 Rome (Italy)
[5]Institute of Geosciences and Earth Resources, Via Moruzzi, 1, 56124 Pisa (Italy)
[6]Volcanological Observatory of Goma, Goma (Democratic Republic of Congo)

Abstract

During the January 2002 eruption at Nyiragongo volcano (Democratic Republic of the Congo), a NS-oriented fracture system of about 15 km long opened in the southern flank of the volcanic apparatus and several lava flows were emitted. Since May 2002, volcanic activity resumed in the main edifice (ca. 1.3 km in diameter), forming in the western part of the crater a lava lake that is still active nowadays. From this period a huge and visible plume, up to two km high, is releasing in the atmosphere up to 60,000 ton/day of SO_2.

The prevailing winds, mainly oriented to the W and SW, usually displace the plume for several hundreds of kilometers, carrying solid (volcanic ash, lapilli, Pelee's hairs) material and causing acidic rains that affect the equatorial forest, the crops and the villages in the surrounding of the volcano, where about 50,000 people are living. The consequences of the dispersion of the volcanic plume in the atmosphere pose severe problems in terms of water supply, since these populations only rely in the meteoric water.

Rain water samples, discontinuously collected at the crater rim from 2002 to 2007, are characterized by pH values as low as 2 and high F^- (up to 2,400 mg/L), Cl^- (up to 1,750 mg/L) and SO_4^{2-} (up to 10,000 mg/L) contents, unequivocally related to the interaction with the volcanic plume. Both pH and salinity values tend to be re-established to those typical of meteoric waters to the West, but unfortunately in the villages of Rusayo and Mudja, at about 10 km from the crater summit, low pH values and relatively high contents of F^- were occasionally recorded. Although the future volcanic activity of Nyiragongo volcano is by far to be assessed, the activity of the lava lake at the Nyiragongo may be long-lasting and water resources and crops in the villages located in the western and southwestern flanks may be jeopardized.

Key-words: Nyiragongo volcano – Democratic Republic of Congo – Meteoric waters – Volcanic plume - Fluoride

Introduction

Volcanic degassing activity has recently been recognized as a threatening phenomenon that may affect wide areas from months to years (e.g. Oppenheimer et al., 2003). The resulting impact on the environment and human health may be devastating (e.g. Thorarinsson, 1979; Cronin & Sharp, 2002). Acidic rains, crop destruction, cattle deaths, contamination and pollution of the superficial and ground water systems are examples of the pressure that the degassing activity may locally induce (e.g. Delmelle et al., 2002). The Nyiragongo volcanic edifice (3,470 m high, with a 1.3 km wide crater) belongs to the Virunga Volcanic Province and is located at the border between the Democratic Republic of the Congo and Rwanda. The volcanic activity at Nyiragongo is mainly dominated by effusive events with lava flows that show a silica-undersaturated, ultra-alkaline, alkalic-mafic composition (e.g. Chakrabarti et al., 2009 and references therein).

A recent eruptive event on January 17, 2002 discharged, through a NS-oriented fracture system on the southern flank of the volcano, about 20 x10^6 m^3 of highly fluid lava flows (Tedesco et al., 2007b), two of which reached the city of Goma (ca. 500,000 inhabitants, 15 km away from the crater summit). Subsequently, volcanic activity resumed few months later in the main crater, forming since May 2002 a stable lava lake and a gas-rich volcanic plume that has been detected as far as several thousands of kilometers to the West, mainly displaced by EW-oriented winds (Fig. 1). Since 2002, SO_2 flux from the Nyiragongo main crater was estimated by TOMS (Total Ozone Mapping Spectrometer) to be up to 60,000 ton/day (Carn et al., 2002/2003), although in May/June 2005 and January 2006, Sawyer et al. (2008) reported average emission rate of SO_2 up to 3300 ton/day by ultraviolet spectroscopic measurements.

In this work, a geochemical survey on meteoric waters interacting with the volcanic plume has been carried out. The main aim is to assess the effects induced by the volcanic plume in the surrounding areas of Nyiragongo volcano by field observations and chemical analysis of meteoric waters collected in a span of time of more than 4 years (2002-2007).

Figure 1 – The volcanic plume of Nyiragongo displaced to the West. The crater of Baruta is in the foreground.

Sampling collection and analytical methods

Meteoric waters were collected in different locations (Fig. 2), i.e. from i) the crater summit, ii) the Goma Volcanological Observatory (GVO), and iii) the villages of Sake, Mudja, Rusayo and Kunene (West of Nyiragongo volcano) and Kibati and Bulengo (South of Nyiragongo volcano) (Table 1). In the villages of Mudja and Rusayo meteoric waters were also collected from the tanks with a capacity of several cubic meters into which rainwater is conveyed. These represent the only water supply for the local populations living at more than 10 km North of Lake Kivu (one of the biggest water reservoirs in central Africa).

For comparison anionic compositions of Lake Kivu and of a fumarolic condensate, sampled from a fumarolic emission located in the 1st platform (cooled lava lake from 1977; e.g. Tazieff, 1979; Durieux, 2002/2003) of the presently active crater, were also included (Table 1). A meteorological station was set on the top of the crater but owing to the difficult political and socio-economical situations it was looted few days after the installation. As a consequence, no systematic collection was carried out and the presented analytical data cannot be related to the amount of rainfall neither to a single event, as the samples often represent the integration of more events.

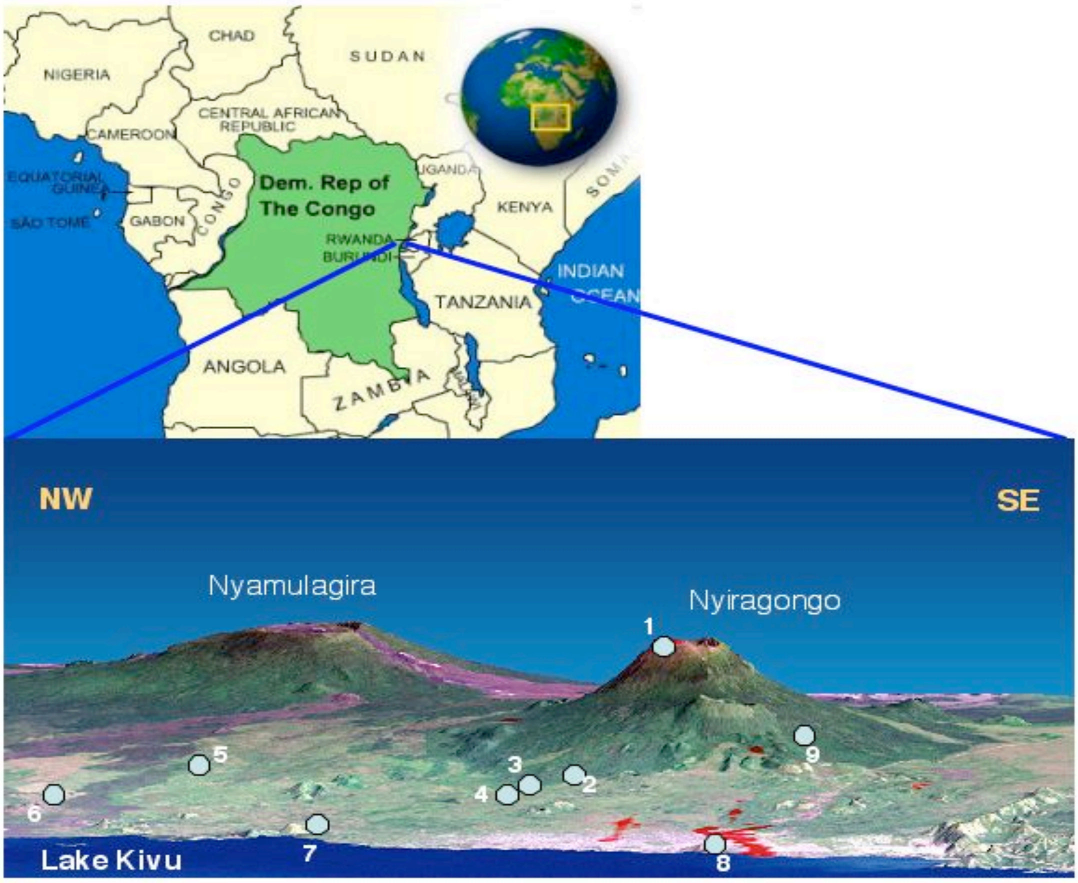

Figure 2 – Location of meteoric water sampling point: 1. Nyiragongo crater; 2. Mudja, 3. Rusayo water tank, 4. Rusayo; 5. Kunene; 6. Sake; 7. Bulengo; 8. GVO (Goma Volcanological Observatory); 9. Kibati. According to Sawyer et al. (2008), the prevailing wind directions are towards W-SW and SSW, respectively.

It is expected that the very first rainfall should produce the lowest pH values and the highest contents of anions resulting from interactions of the acidic gases (SO_2, HF and HCl) of the volcanic plume with meteoric waters; this was confirmed by local people from Rusayo who assessed that their skins are "bitted" by the very first drops of any meteoric event. Concentrations of SO_4^-, Cl^-, F^-, NO_3^- and Br^- were determined by ion-chromatography using three cross-calibrated different instruments: Dionex 100 and 120 and Metrohm 761. Repeated analysis of samples and standards indicates that analytical precision and accuracy are better than 3%.

Field observations and analytical results

Under volcanic plume conditions, the cooling process let many gas species condensing into fine particles that act as condensation nuclei for steam. As a consequence, ash particles and atmospheric water form acidic areosol. S-, Cl- and F-compounds, as a function of the temperature, able to adhere to the tephra particles (Oskarsson, 1980).

Therefore, rainwater can remobilize the chemical components constituting the volcanic plume into the hydrological cycle (e.g. Aiuppa et al., 2001; 2006). Meteoric waters interacting with the volcanic gases are thus responsible of scavenging processes of the volcanic gases.

The effects of the acidic rains by the Nyiragongo plume were visible since September 2002 when the activity of the lava lake, although small, became more effective and stable (Tedesco et al., 2007a,b). The equatorial forest on the western flank was the first to be heavily affected, showing the heads of the trees partly destroyed by both the volcanic material and acidic rainfalls. Similarly, crops (e.g. Mudja and Rusayo, Fig. 2) and vegetation westwards the volcanic plume displayed severe damages (Fig. 3) that are still seriously affecting the local economy. Values of pH and concentrations of F^-, Cl^-, NO_3^-, Br^- and SO_4^{2-} (in mg/L) from selected sampling sites (Fig. 2) are reported in Table 1 along with the water composition of Lake Kivu and a fumarolic condensate (Fracture 2; Tassi, Vaselli and Tedesco, unpublished data) located on the 1st platform (Durieux, 2002/2003).

Figure 3 – Effects of acid rains below the volcanic plume of the Nyiragongo volcano: a) beans; b) colocasia; c) banana trees.

Meteoric water samples collected on the top of the Nyiragongo crater rim show the lowest pH values (down to 2.4) and the highest anion concentrations (up to 2,400, 1,750 and 10,000 mg/L, for F^-, Cl^-, and SO_4^{2-}, respectively). Water samples from other localities at increasing distance from the Nyiragongo summit crater show a dramatic decrease in the plume-related components, although those collected below the volcanic cloud (i.e. Mudja, Rusayo, Kunene), independently by the period of sampling, have systematically higher anion contents than those sampled in the southern part (i.e. GVO, Kibati, Bulengo; Fig. 2), suggesting a stronger and prolonged interaction between meteoric waters and volcanic gases. Significant enrichments in F^-, Cl^- and SO_4^{2-} up to 5.9, 12 and 13 mg/L, respectively, likely due to south-oriented winds, have been measured in December 2002 at GVO. Bromide and NO_3^- contents are usually below 1.5 and 2.0 mg/L. The only exception is a sample collected at Rusayo (Febraury 2004) where 10 mg/L of NO_3^- were detected, likely due to anthropogenic influence. As no control on the amount of rainwater collected during this survey was carried out, to compare the water sample data set and to envisage the volcanic contribute it is more convenient to refer to F^-/Cl^-, F^-/SO_4^{2-} and Cl^-/SO_4^{2-} ratios instead of absolute values (Table 1). The large variability observed in this respect mainly indicates a large heterogeneity of the sampled waters. The F^-/Cl^- ratios of the meteoric waters from the Nyiragongo crater summit cluster slightly above 1 and are similar to those of the fumarolic condensate (Fracture 2). Conversely, rainwater from the sites below the plume is systematically lower than 1, and comprised between 0.08 (Mudja: May 2003) and 0.66 (Mudja: February 2003) (Table 1). Similar considerations do not apply for the F^-/SO_4^{2-} and Cl^-/SO_4^{2-} ratios as they vary from 0.10 (GVO, Dec. 2006) to 3.00 (Bulengo) and from 0.09 (Nyiragongo. Sept. 2002) and 9.29 (Bulengo), respectively. Such a large variability, at least in terms of Cl^-/SO_4^{2-} ratio, has been already observed in the meteoric waters interacting with the volcanic plume of Etna (Aiuppa et al., 2001) and may be ascribed different oxidation processes in the volcanic cloud of the S-bearing species, although short-term temporal fluctuations were observed in SO_2-HF-HCl plume composition and related to shallow degassing processes (Sawyer et al., 2008).

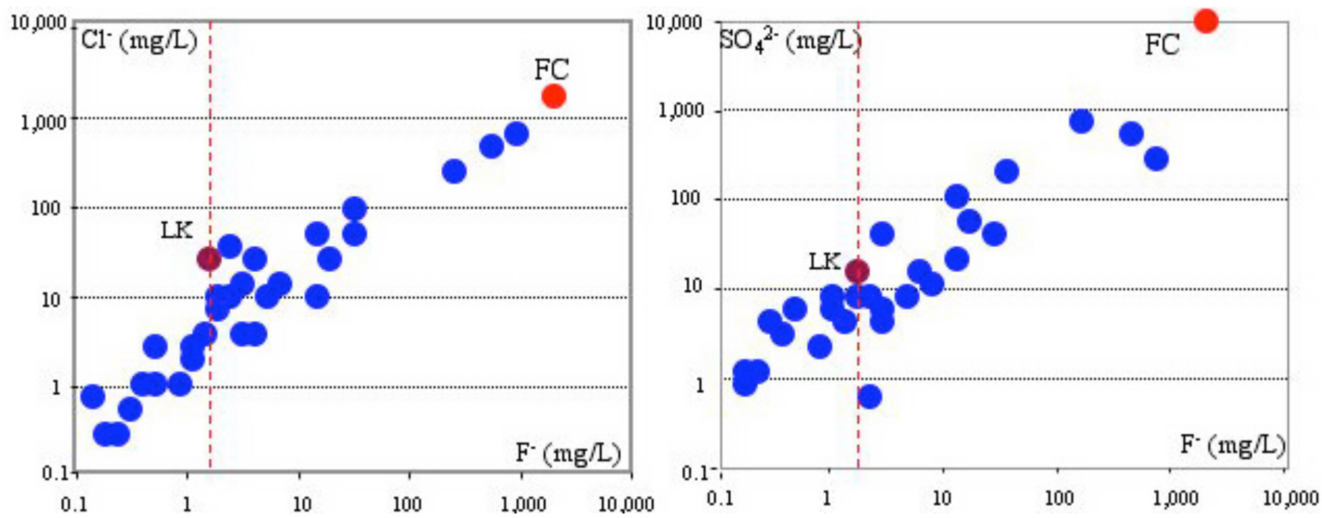

Figure 4 – Cl^- and SO_4^{2-} versus F^- for the meteoric waters collected at Nyiragongo crater and surrounding areas. The composition of a fumarolic condensate (FC) from the inner crater and of Lake Kivu (LK) is also reported. The red line indicates the maximum admissible concentration for F^- in drinking water according to the World Health Organization (WHO).

The direct dependence of the volcanic plume on the meteoric waters can be visualized in Fig. 4 where SO_4^{2-} and Cl^- vs. F^- (in mg/L) binary plots are reported. The maximum admissible concentration for F^- contents in drinkable water, according to the World Health Organization (WHO), is reported (1.5 mg/L). Setting aside the summit crater meteoric waters, F^- concentrations often overcome those recommended by WHO, particularly in those villages where rainfalls are the only water resource supply, whereas Cl^- and SO_4^{2-} concentrations are relatively low (Table 1). This situation may pose serious healthy since fluoride is toxic, provoking dental to skeletal fluorosis, when >1.5 mg/L waters are daily used.

Table 1 – Values of pH, anionic concentrations (in mg/L) and F^-/Cl, F^-/SO_4^{2-} and Cl^-/SO_4^{2-} ratios for selected rain waters collected in the sites reported in Fig. 2. Chemical data and halide/sulphate ratios from Lake Kivu and a fumarolic condensate from the Nyiragongo crater (1st platform) are also reported for comparison.

Locality	**Sampling date**	**pH**	**F**	**Cl**	**Br**	**NO_3**	**SO_4**	**F/Cl**	**F/SO_4**	**Cl/SO_4**
Nyiragongo	14-09-02	<4.00	13.8	9	0.05	2.00	96	1.54	0.14	0.09
Nyiragongo	04-10-03	4.11	565	638	1.5	<0.01	500	0.89	1.13	1.28
Nyiragongo	23-05-04	3.73	246	260	<0.01	<0.01	645	0.95	0.38	0.40
Nyiragongo	15-07-04	4.02	2400	1750	<0.01	<0.01	10000	1.37	0.24	0.18
Niyragongo	01-12-06	nd	28	42	0.07	0.26	41	0.67	0.68	1.02
Niyragongo	24-02-07	2.40	36	74	0.09	1.31	244	0.49	0.15	0.30
Mudja water tank	18-02-03	9.15	5.5	8.3	0.02	1.3	15	0.66	0.37	0.55
Mudja water tank	11-05-03	8.71	2.8	33	<0.01	0.40	5.0	0.08	0.56	6.60
Mudja water tank	11-05-03	6.28	2.8	5.0	0.01	0.23	7.3	0.56	0.38	0.68
Mudja water tank	18-02-04	6.46	1.2	3.8	<0.01	2.0	6.5	0.31	0.18	0.58
Rusayo water tank	28-10-03	7.22	2	7.4	0.015	2.4	9.5	0.27	0.21	0.77
Rusayo	18-02-04	6.48	14	55	<0.01	10.0	53	0.25	0.26	1.04
Rusayo	Sept. 2005	4.03	1.1	2.6	0.00	0.41	5.1	0.42	0.22	0.51
Kunene	26-11-02	6.42	2.5	7.5	<0.01	0.55	9.8	0.33	0.25	0.77
Kunene	13-05-03	5.83	13	24	<0.01	<0.01	19	0.54	0.68	1.26
Kunene	03-12-06	nd	4.8	24	<0.01	<0.01	9.4	0.20	0.51	2.55
Sake	27-11-02	5.79	0.6	1.1	<0.01	0.15	5.5	0.55	0.11	0.20
Sake	27-03-03	6.38	2.9	19	<0.01	1.84	42	0.15	0.07	0.45
Bulengo	25-03-03	8.23	2.1	6.5	<0.01	0.11	0.7	0.32	3.00	9.29
GVO	21-12-02	6.42	5.9	12	<0.01	0.01	13	0.49	0.45	0.92
GVO	16-02-03	6.70	0.2	0.4	<0.01	0.01	1.3	0.50	0.15	0.31
GVO	12-05-03	6.65	0.8	1.0	<0.01	0.75	2.5	0.80	0.33	0.41
GVO	07-12-06	nd	1.1	3.2	<0.01	<0.01	9.3	0.34	0.12	0.34
GVO	13-12-06	nd	0.6	2.7	<0.01	<0.01	5.9	0.22	0.10	0.46
Kibati	16-02-03	6.15	0.4	1.1	<0.01	1.2	2.8	0.36	0.14	0.39
Kibati	Sept. 2005	7.00	0.3	0.6	<0.01	3.9	3.4	0.50	0.09	0.18
Kibati	07-12-06	nd	0.1	0.9	<0.01	<0.01	1.3	0.17	0.11	0.66
Lake Kivu	24-06-03	8.70	1.6	23	0.09	0.08	13	0.07	0.12	1.77
Fracture 2	21-06-03	nd	870	760	nd	nd	300	1.14	2.90	2.53

It has to be mentioned that most water reservoirs from Virunga Volcanic Province, similarly to those of other East African regions, are characterized by high F^- concentrations (see for example Lake Kivu in Table 1) (e.g. Baxter & Ancia, 2002, Vaselli et al., 2007, Rango et al., 2009 and references therein, Tassi et al., 2009), likely resulting by water-rock interactions with F-rich and Ca-poor volcanic rocks. In fact, as fluoride enters the aqueous solution, the low Ca contents and the usually high pH (>8) values do not allow the formation of insoluble CaF_2 that would favor the removal of F^- ions. Consequently, fluorosis might be relatively common in this region, although at our best knowledge proper statistical investigations and careful diagnosis have not yet been carried out.

Conclusions

The 50,000 people living in the villages around the western flank of Nyiragongo volcano have no direct access to good-quality drinkable water. As a consequence, they are forced to use rainwater stored into water tanks, that is frequently spoiled by volcanic plume-related acidic gases (SO_2, HF and HCl) that are easily dissolved in meteoric waters.

The Goma Volcano Observatory is sporadically trying to carry out chemical analysis on both meteoric and superficial waters to control their quality. However, so far no systematic investigations are carried out and people from those villages located below the volcanic plume are constantly drinking potentially contaminated rainwater.
Lack of financial support and analytical facilities and difficulties in establishing international collaborations are related to the unstable political and socio-economical situations, thus hampering simple and low-cost in situ measurements (at least, pH and F concentrations) that should be performed before any use. Moreover, in case of poor water quality, fluoride can be removed by flocculation and adsorption (Zevenberger et al., 1996), although their exercise costs are likely difficult to be incurred by third world countries. Affordable defluorinization methods are however available and include calcite, activated saw dust, activated coconut shell carbon, groundnut shell, coffee husk, rice husk, magnesia, serpentine, bone charcoal and so forth (Meenakshi and Maheshwari, 2006 and references therein).
Finally, it should also be taken into serious account the possibility to provide medical controls on the population and, particularly, on the kids since they may develop symptoms of dental and/or crippling fluorosis, the latter being a lethal disease.

Acknowledgements

Many thanks are due to G. Bianchini who improved an early version of the manuscript.

During the revision of this paper our friend Jacques Durieux (Chief of the Volcanological Observatory of Goma) passed away. He devoted his life to explore volcanoes from around the world and we like to remember him on the top of the Nyiragongo Volcano admiring and challenging the powerful of the nature. We will miss him.

Jacques Durieux (1949 – 2009) at Nyiragongo Volcano.

References

Aiuppa, A., Bellomo, S., Brusca, L., D'Alessandro, W., Di Paola, R., M. Longo, R., 2006. Major ion bulk deposition around an active volcano (Mt. Etna, Italy), Bull. Volcanol. 68, 255–265.

Aiuppa, A., Bonfanti, P., Brusca, L., D'Alessandro, W., Federico, C., Parello, F., 2001. Evaluation of the environmental impact of volcanic emissions from the chemistry of rainwater: Mount Etna (Sicily). Appl. Geochem., 16, 985-1000.

Baxter, P.J., Ancia A., 2002. Human health and vulnerability in the Nyiragongo volcanic crisis. Final report to the World Health Organization, p. 49, 13 figures, http://www.who.int/disasters/repo/7828.pdf.

Carn, S.A. 2002/2003. Eruptive and passive degassing of sulphur dioxide at Nyiragongo volcano (D.R. Congo): the 17 January 2002 eruption and its aftermath. Acta Vulcanol., 14-15, 75-85.

Chakrabarti, R., Basu, A.R., Santo, A.P., Tedesco, D., Vaselli, O., 2009. Isotopic and geochemical evidence for a heterogeneous mantle plume origin of the Virunga volcanics, Western rift, East African Rift system. Chem. Geol., 259, 273-289. doi:10.1016/j.chemgeo.2008.11.010.

Cronin, S.J., Sharp, D.S., 2002. Environmental impacts on health from continuous volcanic activity at Yasur (Tanna) and Ambrym, Vanuatu. Internation. J. Environ. Health Res., 12, 109-123.

Delmelle, P., Stix, J., Baxter, P.J., Garcia-Alvarez, J., Barquero, J., 2002. Atmospheric dispersion, environmental effects and potential health hazard associated with the low-altitude gas plume of Masaya volcano, Nicaragua. Bull. Volcanol., 64, 423-434.

Durieux J. 2002/2003. Volcano Nyiragongo (D.R.Congo): evolution of the crater and lava lakes from the discovery to the present. Acta Vulcanol., 14-15, 137-144.

Meenakshi and R.C. Maheshwari, 2006. Fluoride in drinking water and its removal. J. Hazard. Mat., 137, 456-463.

Oppenheimer, C., Pyle, D.M., Barclay, J. (Eds.), 2003. Volcanic Degassing, Geological Society Special Publication 213, Geological Society Publishing House.

London, U.K.
Óskarsson, N., 1980. The interaction between volcanic gases and tephra: fluorine adhering to tephra of the 1970 Hekla eruption. J. Volcanol. Geotherm. Res. 8, 251–266.
Rango T., Bianchini G., Beccaluva L., Ayenew T., Colombani N., 2009. Hydrogeochemical study in the Main Ethiopian Rift: new insights to the source and enrichment mechanism of fluoride. Environ. Geol., 58, 109-118, doi: 10.1007/s00254-008-1498-3.
Sawyer, G.M., Carn, S.A., Tsanev, V.I., Oppenheimer, C., Burton, M., 2008. Investigation into magma degassing at Nyragongo volcano, Democratic Republic of the Congo. Geochem. Geophys. Geosystem., 9, doi:10.1029/2007GC001829.
Tassi, F., Vaselli, O., Tedesco, D., Montegrossi, G., Darrah, T., Cuoco, E., Mapendano, M.Y., Poreda, R., Delgado Huertas, A., 2009. Water and gas chemistry at Lake Kivu (DRC): geochemical evidence of vertical and horizontal heterogeneities in a multi-basin structure. Geochem. Geophys. Geosyst, 10(2). DOI:10.1029/2008GC002191.
Tazieff H. (1979). Nyiragongo: The Forbidden Volcano . Barron's Educational Series, 288 pp.
Tedesco, D., Badiali, L., Boschi, E., Papale, P., Tassi, F., Vaselli, O., Kasareka, C., Durieux, J., De Natale, G., Amato, A., Cattaneo, M., Ciraba, H., Chirico, G., Delladio, A., De Martin, M., Favalli, G., Franceschi, D., Lauciani, V., Mavonga, G., Monachesi, G., Pagliuca, N.M., Sorrentino, D., Yalire, M., 2007a. Cooperation on Congo volcanic and environmental risks. EOS, Transactions, Am. Geophys. Un., 88, 177-178.
Tedesco, D., Vaselli, O., Papale, P., Carn, S., Voltaggio, M., Sawyer, G., Durieux, J., Kasereka, M., Tassi, F., 2007b. The January 2002 volcano-tectonic eruption of Mt. Nyiragongo, Virunga Volcanic Chain, (Democratic Republic of Congo). J. Geophys. Res., 112, B09202, doi:10.1029/2006JB004762.
Thorarinsson, S., (1979), On the damage caused by volcanic eruptions with special reference to tephra and gases, in Sheets, P.D. and Grayson, D.K. (Eds.), *Volcanic activity and human ecology*, Academic Press, 125-156.
Vaselli, O., Tassi, F., Nisi, B., Tedesco, D., Capaccioni, B., 2007. Gas discharges from the Nyiragongo Volcano (D.R. Congo) and surrounding areas: implications for environmental impact and CO_2-related risks from dry vents. 9th Intl. Conf. on Gas Geochemistry (ICGG), 1-8 October, 2007, Taipei (Taiwan), 220-223.
Zevenberger, C., van Reeuwijk, L.P., Frapporti, G., Louws, R.J., Schuling, R.D., 1996. A simple method for defluorinization of drinking water at village level by adsorption on Ando soil in Kenya. Sci. Tot. Environ., 188, 225-232.

Volcanology and petrochemical aspects of Mount Manengouba volcano, Cameroon

P. Wandji[(1)], P. J. Chakam Tagheu[(2)], J. M. Bardintzeff[(3,4)], H. Bellon[(5)]

(1) Laboratoire de Géologie, Ecole Normale Supérieure, Université de Yaoundé I, BP 47 Yaoundé, Cameroun. pierrewandji@yahoo.fr
(2) Département des Sciences de la Terre, Faculté des Sciences, Université de Yaoundé I, BP 812 Yaoundé, Cameroun.
(3) Laboratoire de Pétrographie-Volcanologie, bât. 504 et équipe Planétologie, UMR CNRS IDES 8148, Université Paris-Sud, 91405 Orsay, France.
(4) IUFM, Université de Cergy-Pontoise, 95000 Cergy-Pontoise, France.
(5) UMR 6538 Domaines océaniques, IUEM, Université de Bretagne Occidentale, Université européenne de Bretagne, 6 av. Le Gorgeu, CS 93837, 29238 Brest Cédex 3, France.

Abstract

Lavas with a mantle origin at Mount Manengouba define two distinct geochemical evolution trends: (i) a basanite-alkaline basalt-hawaiite-mugearite-benmoreite-trachyte series on the flanks of Eboga volcano; (ii) a basanite-alkaline basalt-hawaiite-mugearite series on the flanks of Elengoum volcano. New Sr-Nd-Pb isotopic data for lavas from this edifice show that old trachytes (13.56 My), phonolites (7.55 My) and rhyolites (1.02 My) do not share a common parental magma with the series that include basalts and recent trachytes.

Keywords: Mount Manengouba; Cameroon Volcanic Line; Alkaline volcanism; K/Ar Ages; Isotopes (Sr, Nd, Pb); Mantle reservoir.

Introduction

Mount Manengouba (2 411 m asl) is one of the three large volcanoes of the continental sector of the Cameroon Volcanic Line (CVL) along with Mount Cameroon (4 100 m asl) and Mounts Bambouto (2 740 m asl). CVL (Fig. 1a) is a major structural feature oriented N30 in Central Africa, that stretches from the Atlantic Ocean to Lake Chad. Mount Manengouba is a stratovolcano covering about 500 km² and has two distinct calderas: Elengoum and Eboga. Recent field data on Manengouba (Itiga et al., 2004; Chakam Tagheu, 2006) allow us to propose a new stratigraphy for the volcanic successions and further investigate them by using new $^{40}K/^{40}Ar$ ages and Sr-Nd-Pb isotopic compositions.

Volcanology and geochronology

The Mount Manengouba is a stratovolcano linked to a horst and slightly elongated in the N40 direction. It lies between the Mbo plain to the north and the Tombel graben to the south. The basement (Pan-African granites and gneisses) is affected by a series of sub parallel strike slip faults oriented N30.

More than 70 strombolian cones of variable size (300-980 m basal diameter) are scattered on this huge stratovolcano and many have breached craters. The main directions of lava flows are N70 and N120, while the cones follow N150, N120 and N70 alignments.

The Manengouba stratovolcano has been built during two main volcanic stages:

The first stage was effusive, initially producing basaltic lavas dated at 30 My (in Chakam Tagheu, 2006) probably corresponding to the beginning of the volcanic activity of the Manengouba. This was followed by a phase characterized by the eruption of trachytic lavas (13.56 My) at Essom, phonolites (7.55 My) in the North-West of Bangem and rhyolites (1.02 My) at Ekom. This phase corresponds to the construction of the Elengoum volcano, followed by the formation of its caldera.

During the second stage, two volcanic phases are observed: (1) an effusive episode produced intermediate lavas such as hawaiites at Mboassoum (0.45 My) and Melong (0.47 My), mugearites at Enyandong (0.43 My) and later trachytes to the north-west of Bangem (0.21 My); and (2) an explosive episode with minor effusive activity that erupted basanites observable at Passim and dated at 0.11 My and hawaiites to the south of Nkongsamba dated at 0.2 My (Fig. 1b).

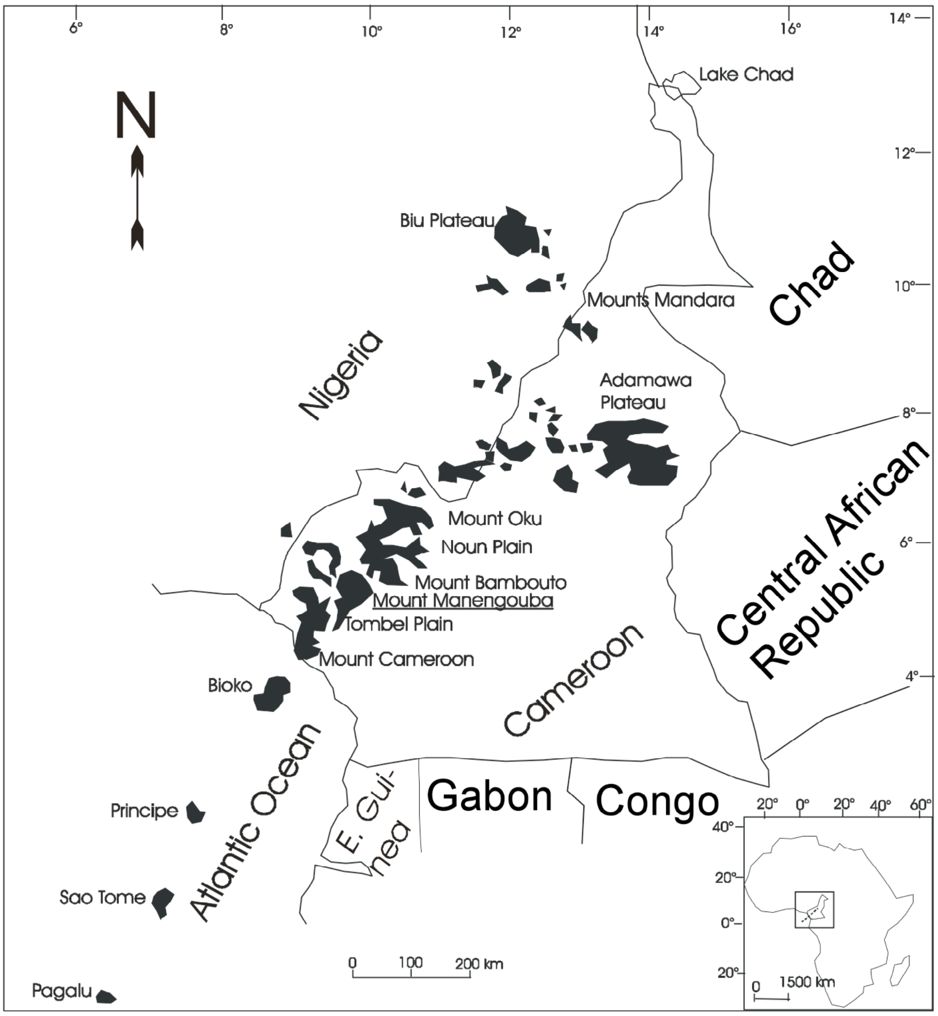

Fig. 1a : Location of Mount Manengouba in the Cameroon Volcanic Line

Petrography and mineralogy

The petrographic study shows that the lavas of the Manengouba stratovolcano are of varied nature: trachyte, phonolite, rhyolite and basalt. More than 350 mineral analyses reveal that the principal minerals in these rocks are olivines, clinopyroxenes, feldspars, Fe-Ti oxides, amphiboles, micas and feldspathoids. The minerals crystallized according to the following order of crystallization: Fe-Ti oxides-olivine-clinopyroxene-plagioclase for basalts with olivine and for basalts with olivine and clinopyroxene; olivine-opaque-clinopyroxene-feldspar-amphibole-mica for basalts with clinopyroxene, with amphibole or without amphibole; apatite-clinopyroxene-amphibole-feldspar-feldspathoïd for phonolites; olivine-clinopyroxene-feldspar-opaque-amphibole for trachytes; and clinopyroxene-amphibole-mica-feldspar for rhyolites.

Geochemistry

New data on representative samples confirm that the basaltic lavas of the Manengouba volcano are alkaline and sodic ($Na_2O/K_2O > 2$), while the felsic lavas are alkaline, but slightly potassic ($Na_2O/K_2O < 2$). The basaltic lavas define a differentiation trend from basanites to benmoreites (27 < D.I. < 76) and to trachyte (D.I. = 81).

Primitive mantle-normalised multi element patterns (McDonough and Sun, 1995) show important negative anomalies (Fig. 2a) for Ba, Sr and Ti in the felsic lavas. These negative anomalies are due to fractional crystallization of alkali feldspars (Ba, Sr) and amphiboles (Ti). Such negative anomalies are described in other felsic lavas of the CVL (Wandji et al., 2008).

Chondrite-normalised REE patterns of lavas from Mount Manengouba are presented in Fig. 2b. The ratios of some incompatible trace elements of the basaltic lavas show only weak variations. That suggests only one source or several identical magmatic sources in the mantle for the genesis of mafic magmas, that then could evolve to felsic magmas.

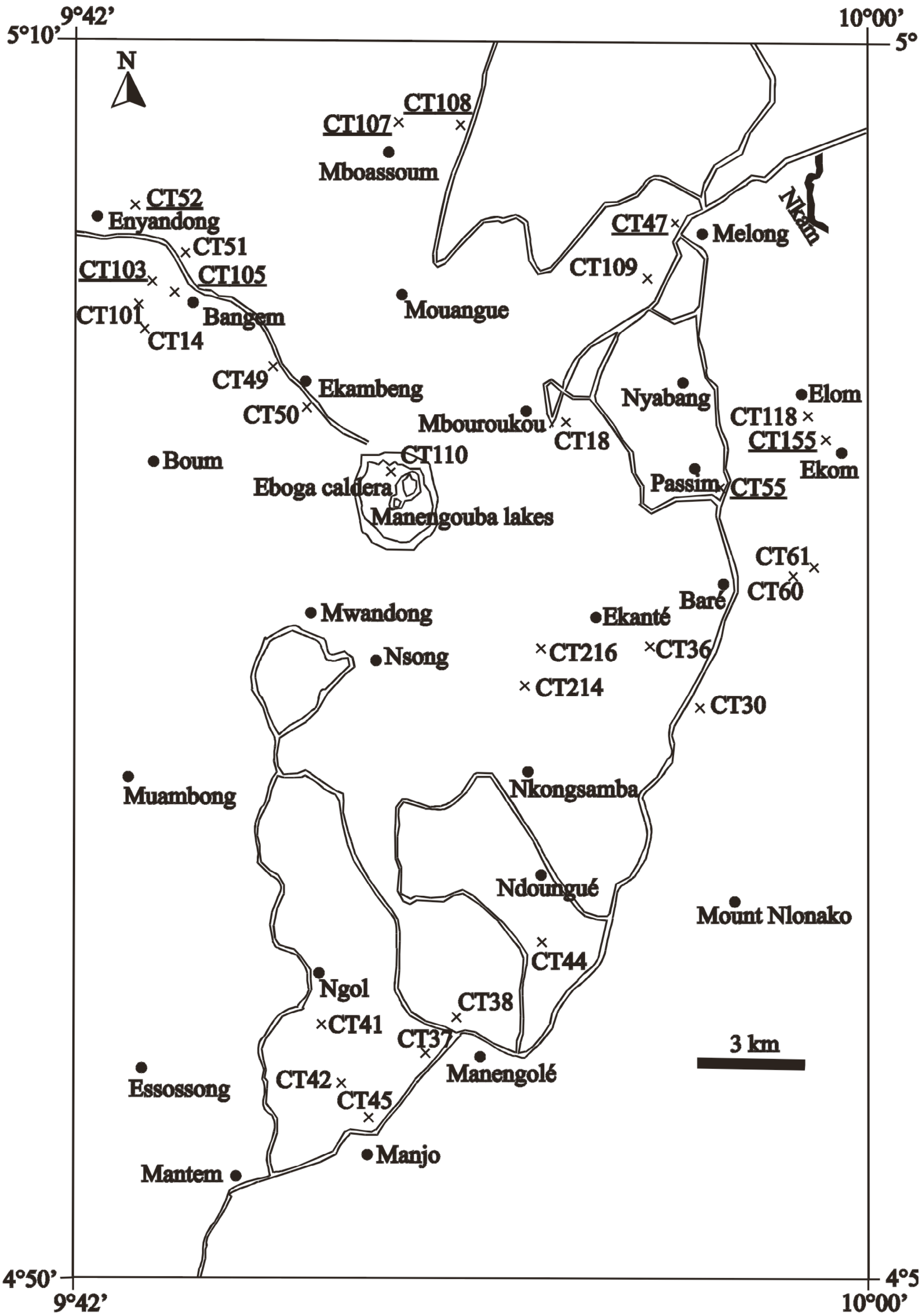

Fig.1b : Sampling map of Mount Manengouba. Numbers of studied rocks samples are underlined (CT47, CT52, CT55, CT103, CT105, CT107, CT108, CT155).

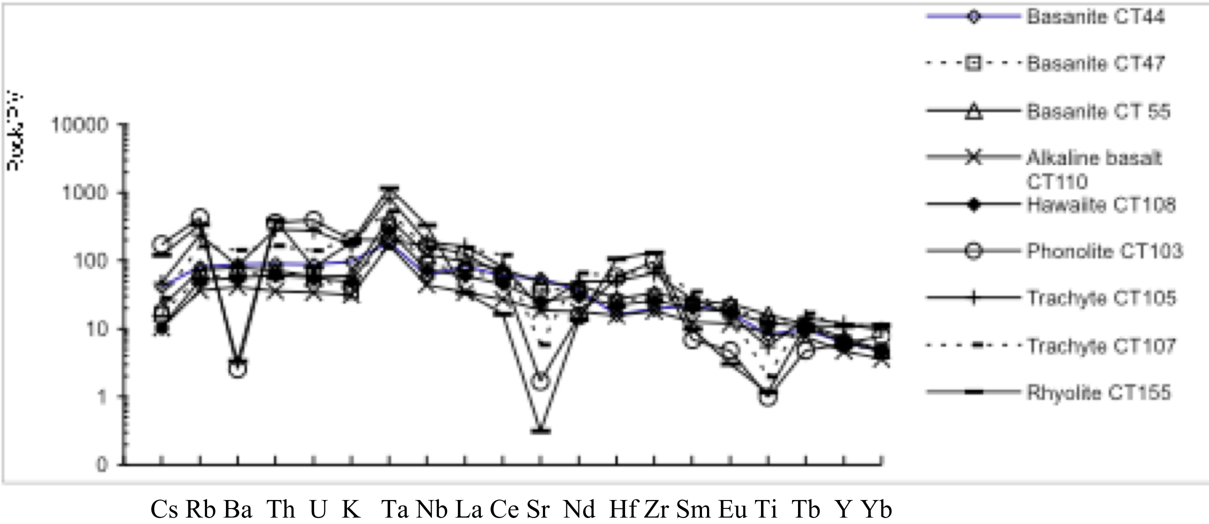

Fig. 2a : Compositional distribution of mafic and felsic lavas of Mount Manengouba (using normalizing values to primitive mantle according to McDonough and Sun, 1995).

Isotopic data

New isotopic data ($^{87}Sr/^{86}Sr$, $^{143}Nd/^{144}Nd$) (Table I) (analyses by D. Demaiffe at the Laboratoire de Géochimie Isotopique, Université Libre de Bruxelles, Belgium) confirm that there is no magmatic association between:

(i) the recent basalts ($^{87}Sr/^{86}Sr$ = 0.703041 - 0.703055; $^{143}Nd/^{144}Nd$ = 0.512933 - 0.512948) and the recent trachytes ($^{87}Sr/^{86}Sr$ = 0.703042; $^{143}Nd/^{144}Nd$ = 0.512869) that share a common mantle origin;

(ii) the Miocene trachytes ($^{87}Sr/^{86}Sr$ = 0.706216; $^{143}Nd/^{144}Nd$ = 0.512558), Miocene phonolites ($^{87}Sr/^{86}Sr$ = 0.707574; $^{143}Nd/^{144}Nd$ = 0.512756) and Pleistocene rhyolites ($^{87}Sr/^{86}S$ = 0.708554, $^{143}Nd/^{144}Nd$ = 0.512764) that all have a crustal origin.
The Mount Manengouba samples have extreme radiogenic Pb isotope signatures ($^{206}Pb/^{204}Pb$ = 18.4508 - 19.7784, $^{207}Pb/^{204}Pb$ = 15.5936 - 15.6300, $^{208}Pb/^{204}Pb$ = 38.8500 - 39.4840).

The ratios of Sr-Nd-Pb isotopic compositions in these rocks show no evident variation with age (Fig. 3).

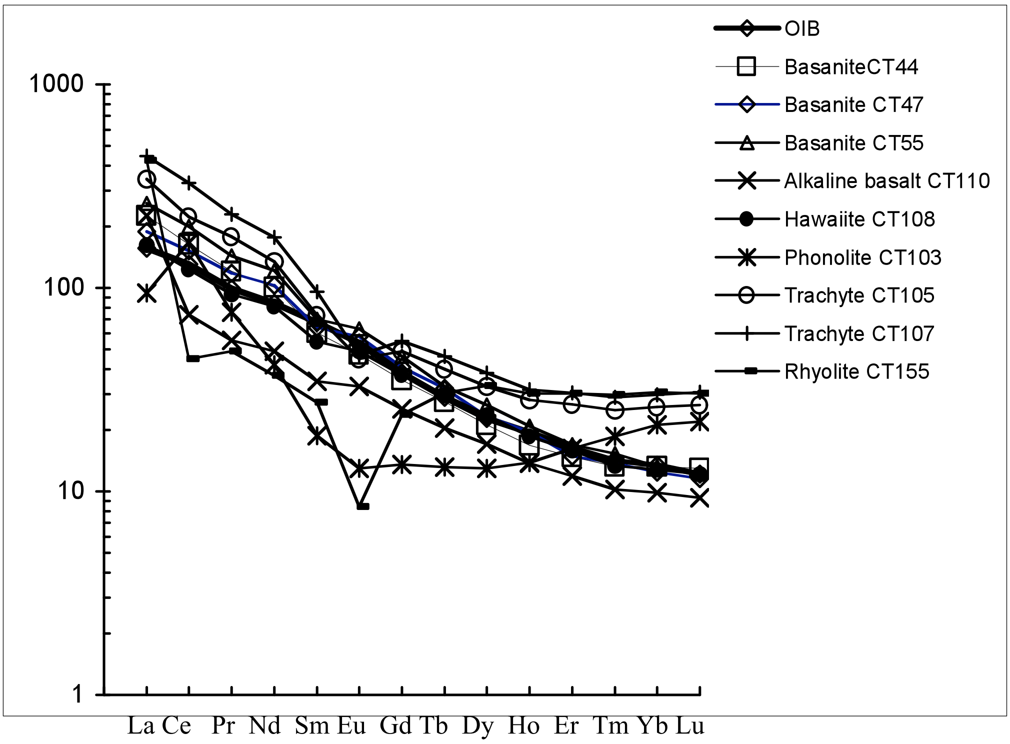

Fig. 2b : REE distribution of mafic and felsic lavas of Mount Manengouba and OIB (using chondrite normalizing values after McDonough and Sun, 1995).

Table I : $^{40}K/^{40}Ar$ ages and Sr-Nd-Pb isotopes in lavas of Mount Manengouba.

Sample	**Ages (My)**	**$^{87}Sr/^{86}Sr$**	**$^{143}Nd/^{144}Nd$**	**$^{206}Pb/^{204}Pb$**	**$^{207}Pb/^{204}Pb$**	**$^{208}Pb/^{204}Pb$**
CT107 Trachyte	13.56±0.39	0.706216	0.512558	18.4508	15.5936	38.8500
CT103 Phonolite	7.55±0.18	0.707574	0.512756	-	-	-
CT155 Rhyolite	1.02±0.03	0.708554	0.512764	18.7909	15.6011	39.0392
CT47 Hawaiite	0.47±0.04	-	-	-	-	-
CT108 Hawaiite	0.45±0.07	0.703055	0.512948	19.7502	15.6296	39.4532
CT52 Mugearite	0.43±0.24	**-**	-	-	-	-
CT105 Trachyte	0.21±0.02	0.703042	0.512869	19.7784	15.6300	39.4840
CT55 Basanite	0.11±0.03	0.703041	0.512933	-	-	-

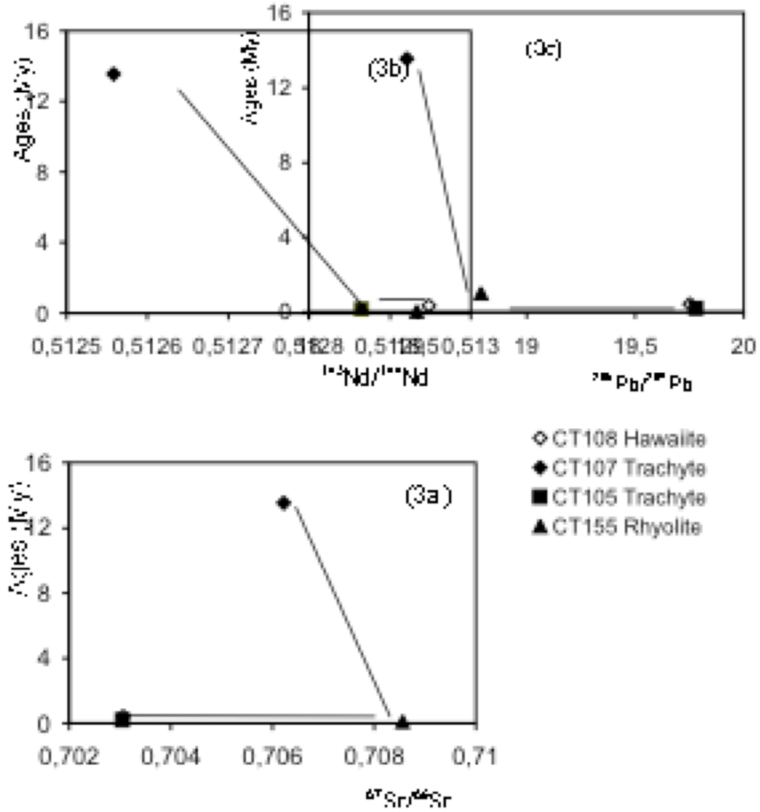

Fig. 3: Sr, Nd and Pb isotopic compositions as a function of the 40K / 40Ar ages (My) for lavas of Mount Manengouba.

Conclusion

The volcanological history of the Manengouba stratovolcano appears more complex according to the recent ages obtained on the basaltic and trachytic lavas. The isotopic ratios show that trachytes (except recent trachytes), phonolites and rhyolites do not belong to the same series as the basalts. They were not derived from basaltic magmas through simple fractional crystallization.

The most recent lavas, emitted by lateral fissures, have a mantle origin and define two distinct evolutionary trends: (i) basanite-alkaline basalt-hawaiite-mugearite-benmoreite-trachyte on the flanks of Eboga; (ii) basanite-alkaline basalt-hawaiite-mugearite on the flanks of Elengoum.

References

Chakam Tagheu P.J. 2006. Le volcanisme néogène à quaternaire des régions du stratovolcan Manengouba (Ligne du Cameroun): volcanologie, pétrologie, géochimie et ressources hydrologiques. Thèse 3e cycle, Univ. Yaoundé I, Cameroun, 228 p.

Itiga Z., Chakam Tagheu P.J., Wotchoko P., Wandji P., Bardintzeff J.M., Bellon H. 2004. La Ligne du Cameroun: Volcanologie et géochronologie de trois régions (mont Manengouba, plaine du Noun et Tchabal Gangdaba). Géochronique, 91, 13-16.

McDonough W.F., Sun S.S. 1995. The composition of the Earth. Chemical Geology, 120, 223-253.

Wandji P., Tchokona Seuwui D., Bardintzeff J.M., Bellon H., Platevoet B. 2008. Rhyolites of the Mbépit Massif in the Cameroon Volcanic Line: an early extrusive volcanic episode of Eocene age. Mineralogy and Petrology, 94, 3-4, 271-286.

Modeling of InSAR displacements related with the January 2002 eruption of Nyiragongo volcano

C. Wauthier[1,2], V. Cayol[3], F. Kervyn[1,4], N. d'Oreye[5]

[1] Dept. of Geology, Royal Museum for Central Africa, Leuvensesteenweg 13, 3080 Tervuren, Belgium, christelle.wauthier@africamuseum.be
[2] Dept. ArGEnCo, University of Liège, Sart Tilman B52, 4000 Liège, Belgium
3 Lab. Magmas et Volcans, Université Blaise Pascal – UMR 6524, rue Kessler 5, 63038 Clermont-Ferrand, France
[4] Centre d'Informations Géographiques SODERU, Goma, North-Kivu, DRC
[5] Dept. of Geophysics/Astrophysics, National Museum of Natural History, Rue Josy Welter 19, 7256 Walferdange, Luxembourg

Abstract

On 17th January 2002, Nyiragongo erupted along an approximately 20 kilometers long fracture system extending from the volcano to the city of Goma and its airport. InSAR data from the ERS-2 satellite show that complex ground displacements, with several overlapping fringe patterns were associated with this eruption. In order to determine the sources of these displacements we use a method that combines a 3D boundary element numerical modeling and a Monte Carlo Inversion algorithm. Complexity of the observed displacements in vicinity of Nyiragongo and in Goma area leads us to assume that they result from the combination of two deformation sources. Because of the tectonic, geologic and magmatic context, three source combinations are studied and compared: (1) a subvertical dike and a deflating reservoir, (2) a subvertical dike and an east-dipping normal fault, (3) a subvertical dike and a west-dipping normal fault. We determine that a subvertical dyke associated to the eruptive fissures and a 15 kilometers long low angle west dipping normal fault parallel to the East African rift is the most likely combination of sources. The low angle west dipping normal fault is aligned with the known horst structures of the Idjiwi Island located on Lake Kivu, so that it could be the continuation of one of the horst faults. It could also correspond to the interface between sedimentary layers tilted by the half graben associated with the East African rift.

1. Introduction

With Nyamulagira, Nyiragongo is one of the two active volcanoes of North Kivu located east of the Democratic Republic of Congo. It is located in the western branch of the East African rift, in the Virunga alkaline volcanic province. This area is affected by a combination of tectonic and volcanic activities [1]. In North Kivu, the rift is most likely a half-graben including a minor transfer zone induced by the rift segmentation along the rift main axis [2, 3]. Nyiragongo hasn't been much studied, in great part due to political tensions taking place in the country. On the 17 January 2002, Nyiragongo erupted along an approximately 20 kilometers long fracture system extending from the southern flank of the volcano to the lake, deeply affecting the city of Goma and its airport [4]. The eruption reactivated part of 1977 fractures network and formed new N-S oriented fractures, parallel to main rift-related tectonic faults (Figure 1). The maximum observed opening along this fracture system is about one meter. Two lava flows entered the town and destroyed about 15% of the houses and infrastructures. The eruption was associated with precursory signals in the months preceding the January 2002 eruption, such as increased fumarolic activity following seismic events. Between 4 and 16 January 2002, seismic activity remained high [5]. Interestingly, the seismicity remained high after the effusive activity had stopped and about 100 tectonic earthquakes with magnitudes larger than 3.5 were recorded in the five days following the January 2002 eruption [6]. Unfortunately, the seismic network that operated during the eruption did not allow an accurate assessment of the location or depth of the seismic events. The erupted volume is estimated approximately at 14-34.10^6 m^3 [6]. A rise of the Lake Kivu water level was also identified after this eruption, most likely linked with a subsidence of the ground in the lake area [3].

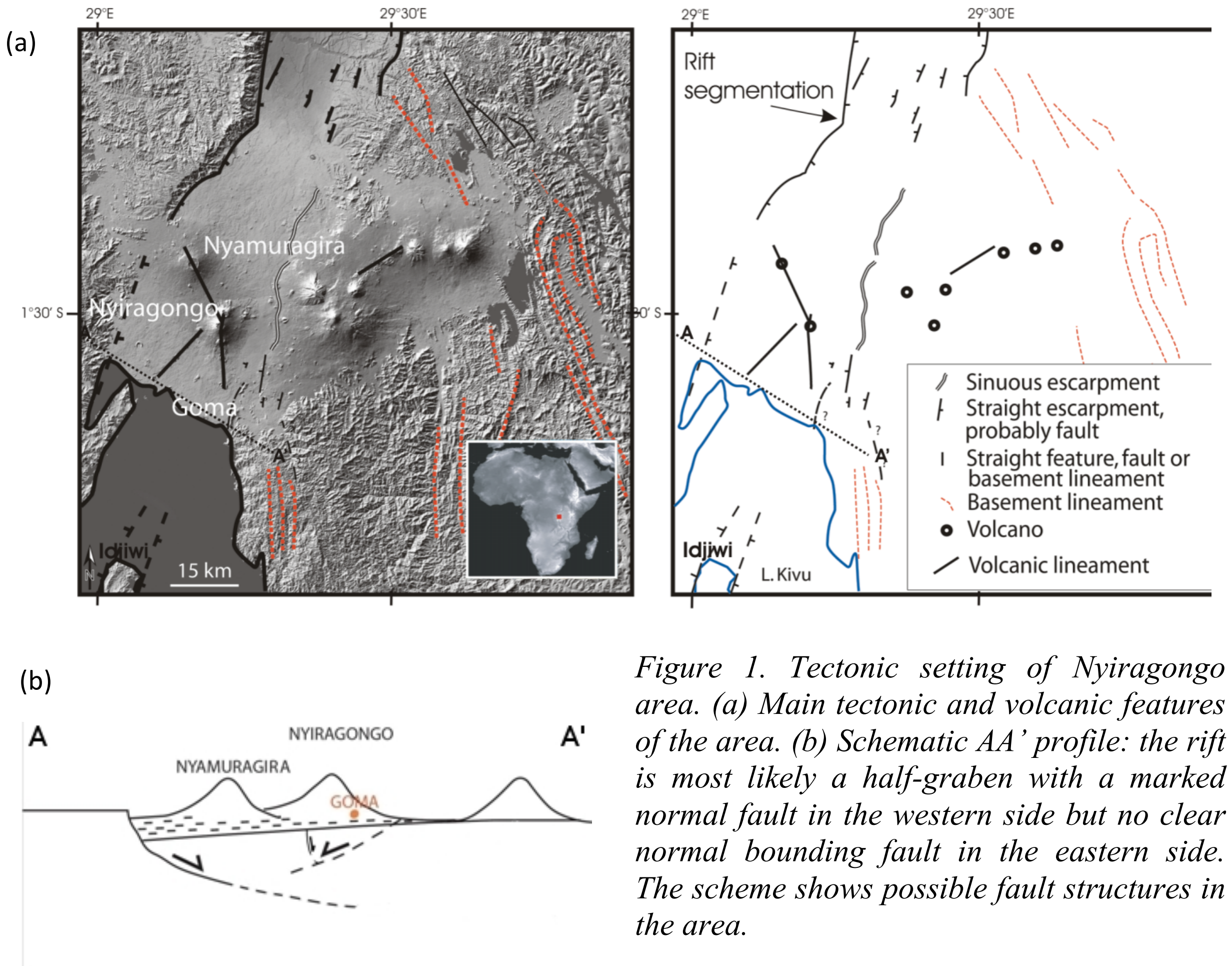

Figure 1. Tectonic setting of Nyiragongo area. (a) Main tectonic and volcanic features of the area. (b) Schematic AA' profile: the rift is most likely a half-graben with a marked normal fault in the western side but no clear normal bounding fault in the eastern side. The scheme shows possible fault structures in the area.

2. Methods

2.1 InSAR data and processing

Displacements associated with 17 January 2002 eruptive event were captured by radar data from the ERS-2 satellite. Combining radar images acquired before and after the event, five independent interferograms were computed, giving displacements along the satellite Line Of Sight (LOS), from the south west of the volcano. In order to obtain large signal to noise data, stable characteristics of the ground surface from a radar acquisition to the next are needed. As the available interferograms have large time spans, characteristics of the ground surface change and the quality (characterized by the coherence of pixels with the surrounding pixels) of interferograms was sometimes low, reducing the number of exploitable interferometric data. The reduced number of available data is also due to the occurrence of Doppler frequencies anomalies in 2001 or too large perpendicular distances (baseline) between acquisitions [7], leading to low signal to noise data. The interferograms were generated with the Doris open-source software [8] using precise orbits from Delft University. The most coherent interferogram, hence in principle the one of highest quality, was selected for further interpretation using numerical modeling and inversions (Figure 2). Because the radar wavelength of the ERS satellite is 5.6 cm, it is sensitive to vegetation, and a loss of coherence is obtained in vegetated areas. In this study, incoherent areas are masked. Studying the available ERS interferograms with a pair-wise logic approach [7], and comparing these data with interferograms captured by the RADARSAT satellite [9], confirms that the observed InSAR signal is actual deformation and not an atmospheric or topographic artefact. The acquisition times of the various interferograms indicate that all the observed ground deformation took place between January 14 and February 13 [10].

2.2 Data analysis

In order to determine the sources of the observed displacements, we use a method that combines a 3D numerical modeling method and a Monte Carlo inversion method [12]. The numerical modeling method is a mixed boundary element method (MBEM) [13], based on the combination of two boundary element methods: the direct and displacement discontinuity methods. The direct method allows accurate and fast modeling of structures such as a topography, cavities or reservoirs, whereas the displacement discontinuity method is suitable for fractures. The edifice is assumed to be linearly elastic which is supported by theoretical and field studies of dikes [14, 15] and the lack of time dependant deformation associated to the emplacement of dikes. The medium is also assumed to be homogeneous and isotropic, as no other information is available on the mechanical properties of rocks in the Nyiragongo area. The prescribed boundary conditions are tractions; they represent perturbations of an initial state of stress, and are null on the ground and equal to overpressures or shear stress drops on deformation sources [13]. Boundaries (in our case, the ground surface, a dike, a deflating reservoir and normal faults) are meshed by planar triangle elements. The topographic mesh size is ten times larger (200 km in radius) than the deformation sources, so that the limited extension of the ground surface has a negligible influence on the computed displacements [13].

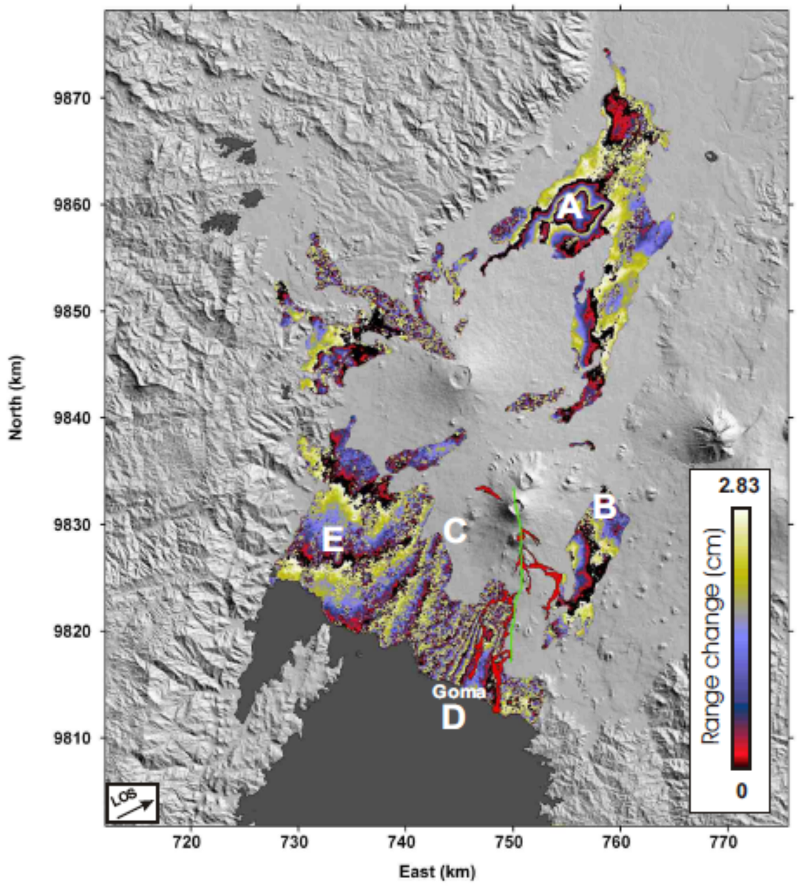

*Figure 2. ERS-2 Best signal to noise ERS-2 deformation interferogram spanning the January 2002 Nyiragongo eruption: Ascending orbit, Incidence Angle (angle from vertical) = 23°, time span: Sept.00 - July 02, H_{amb} (H_{amb} characterizes the sensitivity of the interferogram to errors in the DEM. A DEM error of H_{amb} would result in a fringe in the interferogram) = 148 m. One color fringe corresponds to 2.8 cm range change in the Line Of Sight direction. The interferogram is wrapped on a Digital Elevation Model [11]. Areas with incoherent interferometric signals have been masked. The signal observed in **A** corresponds to the compaction of a well-known Nyamulagira lava flows pile (from 1958, 1967, 1980, 1991-93 eruptions). The asymmetric fringes patterns observed in **B**, **C** is related to the dyke injection. The subsidence of the Goma area is clearly visible in **D** with 5 fringes indicating about 14 centimeters of LOS subsidence. The 2002 lava flows are mapped in red. Fractures used for modeling are in green and correspond to observed eruptive fissures.*

The topographic mesh is dense close to the eruptive fissures and in Goma area where displacement gradients are large and coarse farther away. Displacements created by different sources are compared. Parameters characterizing such sources are shown in Figure 3.

The inversion method used to determine the best-fit model is a near neighborhood inversion algorithm [16]. In order to find the models that best explain the observed data, a misfit function is defined, which quantifies the discrepancy between observed and modeled displacements. It is written as:

$$\chi^2 = (u_o - u_c)^T \, C_d^{-1} \, (u_o - u_c)$$

where u_o and u_c are vectors of observed and modeled line-of-sight (LOS) displacements, respectively, and C_d is the covariance matrix. In order to compare modeled displacements with physically meaningful quantities, fringes shown in the interferogram are converted to displacements leading to LOS displacements maps. This procedure, referred as unwrapping, was performed using the SNAPHU open-source software [17]. As the number of data points in an interferogram is too large to be numerically manageable (6,142,825 pixels), data are subsampled at circular gridded points, in such a way that the number of subsampling points is dense in areas where displacements gradients are large and coarser further away. The unwrapping and subsampling yields to 1147 and 4394 long vectors of observed displacements u_o for single (dike) and multiple sources inversions, respectively. The vector of modeled displacements u_c is constructed by subsampling modeled LOS displacements at the same points as the observed displacements. The covariance matrix C_d is a full matrix, which takes the data noise correlation as well as the modeling uncertainties into account. The near neighborhood searches for models that minimize the misfit within predefined model parameter bounds. The algorithm works as follows: n1 (here about 200) initial acceptable models are randomly chosen. Misfits corresponding to the n1 models are then calculated. Next, at each iteration, n new models are generated in the neighborhood of the n lowest misfit models, and misfits for these new models are calculated. Iterations continue until the misfit is not significantly lowered anymore. The neighborhood around a model is defined by a Voronoi cell which covers the area closer to that model than any other model. When n is small, the search is fast but concentrates to a limited model area; when n is large, the search is slow and the search is conducted in a larger model area. Here when inversions are performed for a single source, n is taken to 30, but when multiple sources are inverted for, we can not afford numerically such a large n and thus n is reduced to 10 (Table 1).

Table 1. Characteristics of typical inversions

	Single source	Multiple sources
Number of inverted parameters	6	10
n (number of new models generated for each iteration)	30	10
Number of forward models calculated	4273	14893
CPU time (minutes)	62	853

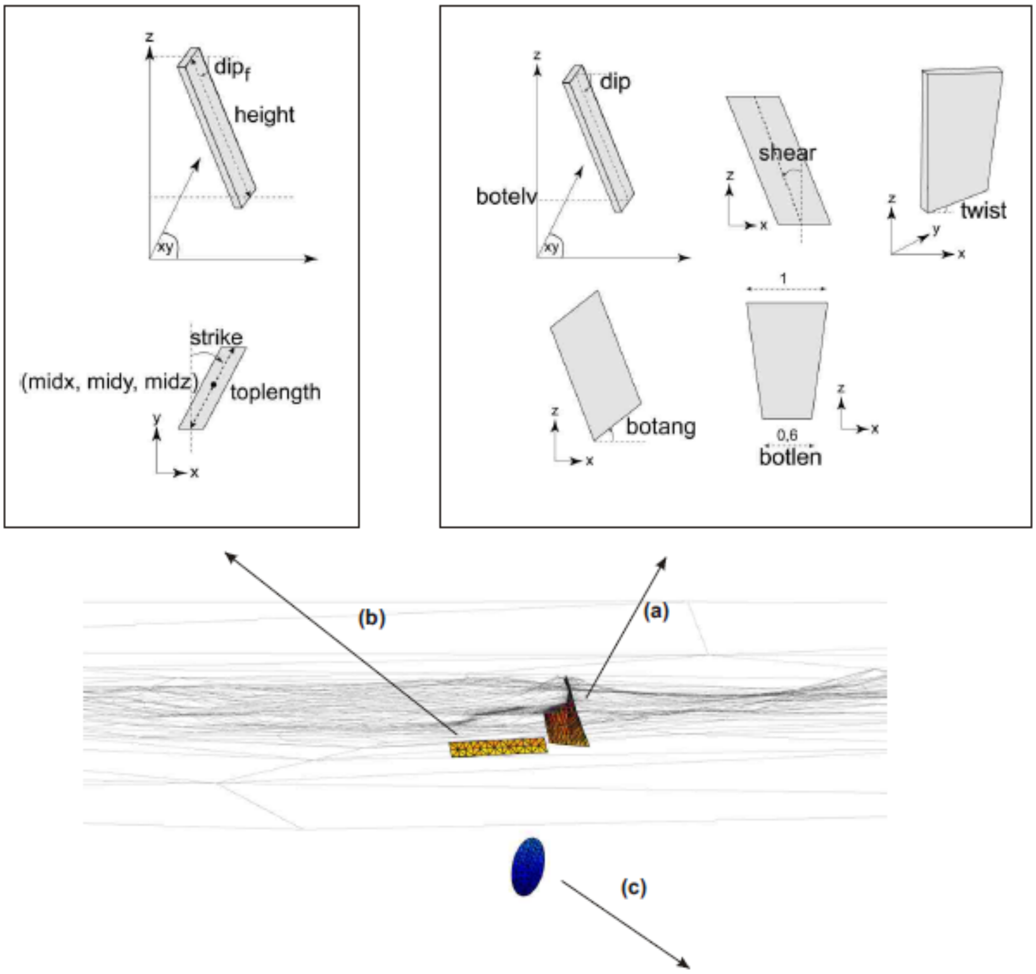

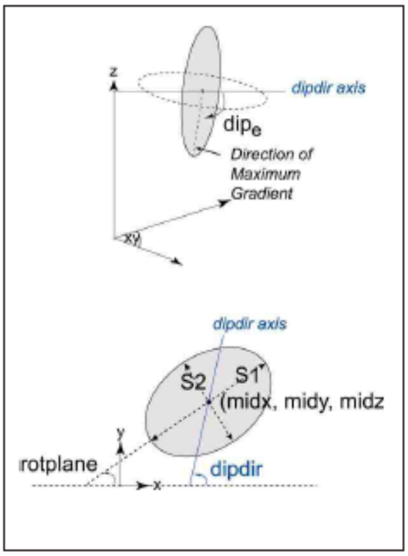

Figure 3. For the modeling, the sources and the topography are meshed. Three types of source are studied: (a) A dike connected to the ground via the eruptive fissure. The dike is roughly a quadrangle defined by six geometrical parameters and an overpressure, P_0. Three of the geometrical parameters determine the position of the line joining the middle of the top and the bottom part of the quadrangle, i.e., the dip angle (dip), the angle from the maximum gradient (shear), the elevation of the bottom point (botelv). Three other parameters determine the location of the end points of the bottom curve, i.e., the length of the lower curve scaled with respect to the length of the top curve (botlen), the angle of this curve from the horizontal direction (botang), the horizontal angle between the bottom curve and the top curve (twist) (b) A normal fault below the ground. The fault is a quadrangle defined by seven geometrical parameters and a value of shear stress drop, S. (c) A deflating reservoir. The reservoir is a planar ellipsoid defined by height geometrical parameters and a pressure drop, P_0. [12, 13]

3. Results

Before combining numerical models and inversions, MBEM forward models were processed to assess the plausible sources and geometries: a dike associated with the eruptive fissure and west and east-dipping normal faults located in the Goma area. These preliminary tests showed that such sources can fit the InSAR data and that a dike produces displacements similar to those measured only in its vicinity. After this step, a single-source inversion with a dike was performed in order to determine the number of parameters that can be discriminated when inverting data captured from a single LOS direction. In order to invert the interferogram for the dike parameters, only data in the vicinity of the dike were considered. These tests confirmed the presence of a subvertical dike associated with the eruptive fissure. Such a dike fits the data observed on both sides of the eruptive fissure, as shown in Figure 4. This inversion indicates that parameters *botlen* and *twist* are close to 1, and 0. Thus, we fix them to these values for the following inversions. This dike is characterized by a low overpressure (0.31 MPa), consistent with the rift context. Such a dike creates 1 meter of maximum opening in the surface, consistent with field observations. The inversion confirmed that this dike does not explain displacements observed further from the eruptive fissure, in the Goma area (D in Figure 2), where there is obviously a superposition of deformation signals related to the various phenomena which occurred during the eruption. As these phenomena occurred at similar times, they probably interacted and thus they have to be simultaneously considered in the models and the inversions. As there were visual observations of an eruptive fissure, a subvertical dike associated with this fissure is always considered in the models. For the simultaneous inversion of two sources, the area considered in the inversion is broader to the west and to the north than for the inversion of a single dike. We investigated three possibilities for the second source: (1) a deflating reservoir, as the Lake Kivu is rich in gas (carbon dioxide, methane…). Indeed, the eruption could have induced a leak in a pre-existing reservoir of planar ellipsoidal shape, as shown in Figure 3. (2) A west or (3) east-dipping normal fault, as such faults are consistent with rift context. The combination of a dyke and an elliptic deflating reservoir poorly fits the data, so we can reject this possibility. Both other possibilities, a dyke and a west or east dipping normal fault, fit the data. The best-fit modeled displacements and the corresponding source geometries are shown in Figure 5 and 6.

Table 2. Characteristics of best fit single dike model showed in Figure 4. *Shear* is fixed to 0°. Rms stands for root mean squared error.

P_0 (MPa)	Dip (°)	Botelv (m)	Botl en	Twist (°)	Botang (°)	Max. opening (m)	V (m^3)	Rms (mm)
0.31	92	-2160	1	-1.7	11	1	5e+07	8.5

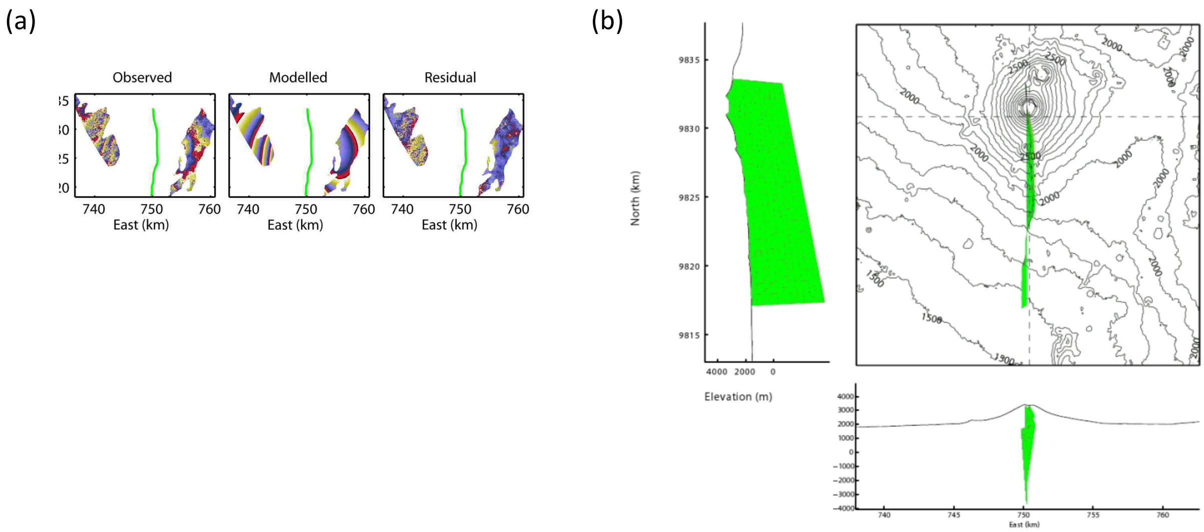

Figure 4. Results obtained for the single dike inversion: (a) Data, Model and Residuals for the best fit single dike model. (b) Geometry of the best fit single dike. Values of model parameters are given in Table 2.

A 2.5 to 3 kilometer high subvertical dyke and a 16 km long narrow east-dipping normal fault extending from the south flank of Nyiragongo to the northern part of lake Kivu fits the data in the Goma area well (rms is 15 mm). However, the interaction between these two sources is mechanically inconsistent, as the fault displacement induces closure of the dyke.

A 1.5 to 2 kilometer high subvertical dyke and a 15 km low angle (25°) west-dipping normal fault extending from the south flank of Nyiragongo to the northern part of lake Kivu fits the data equally well (rms is also 15 mm) but it is a more likely combination of sources, as the opening of the dike is consistent with the fault motion. The dike is submitted to a low overpressure of 0.15 MPa, which is consistent with the rift context. Such a dike creates 0.4 meter of maximum opening in the surface, consistent with field observations. The fault is associated to a low stress drop, but this value is in the range of plausible values for normal faults [18]. The corresponding moment magnitude is 4.9, which is consistent with the magnitude of events observed around Lake Kivu during the period covered by the interferograms, where about 24 events with magnitudes larger than 4, and four events with magnitudes larger than 5 were observed. Modeled displacements induce about 13 cm of maximum LOS subsidence of the lake shore consistent with the observation. The fault is roughly aligned with one of the Idjiwi Island normal faults, a horst structure visible 50 kilometers south on Lake Kivu (see Figure 1). Thus it could be in the continuation on one of the horst normal faults. The low angle of the fault, which is unusual for a normal fault, is consistent with the tilting of sedimentary layers caused by the a-symmetrical opening of the rift. Faulting could results from the reactivation of the contact between tilted lithological (sedimentary and/or volcanic) layers.

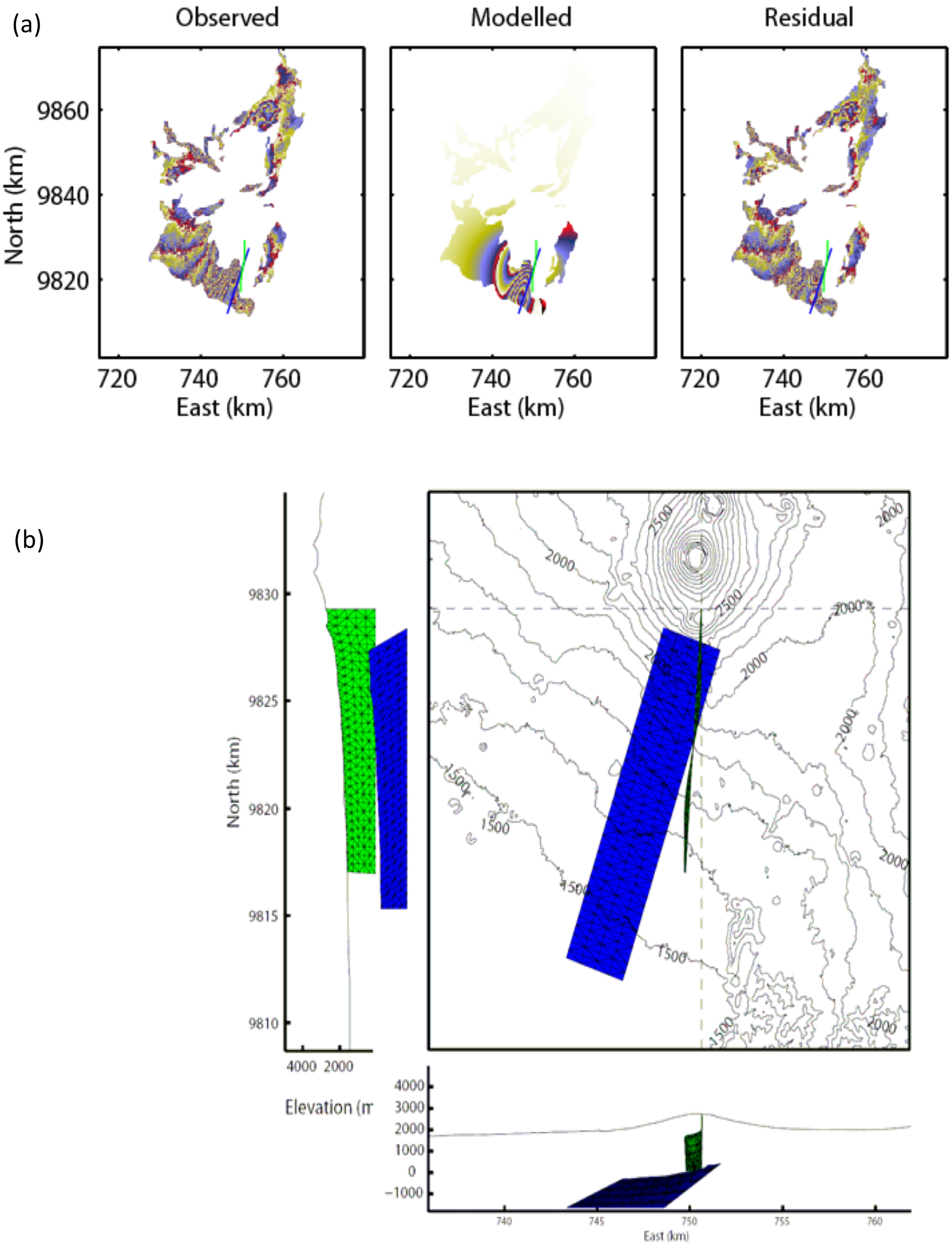

Figure 5. Results obtained for the simultaneous dike and east-dipping fault inversion: (a) Data, Model and Residuals for the best-fit model. (b) Geometry of the best fit dike and fault. Values of model parameters are given in Table 3.

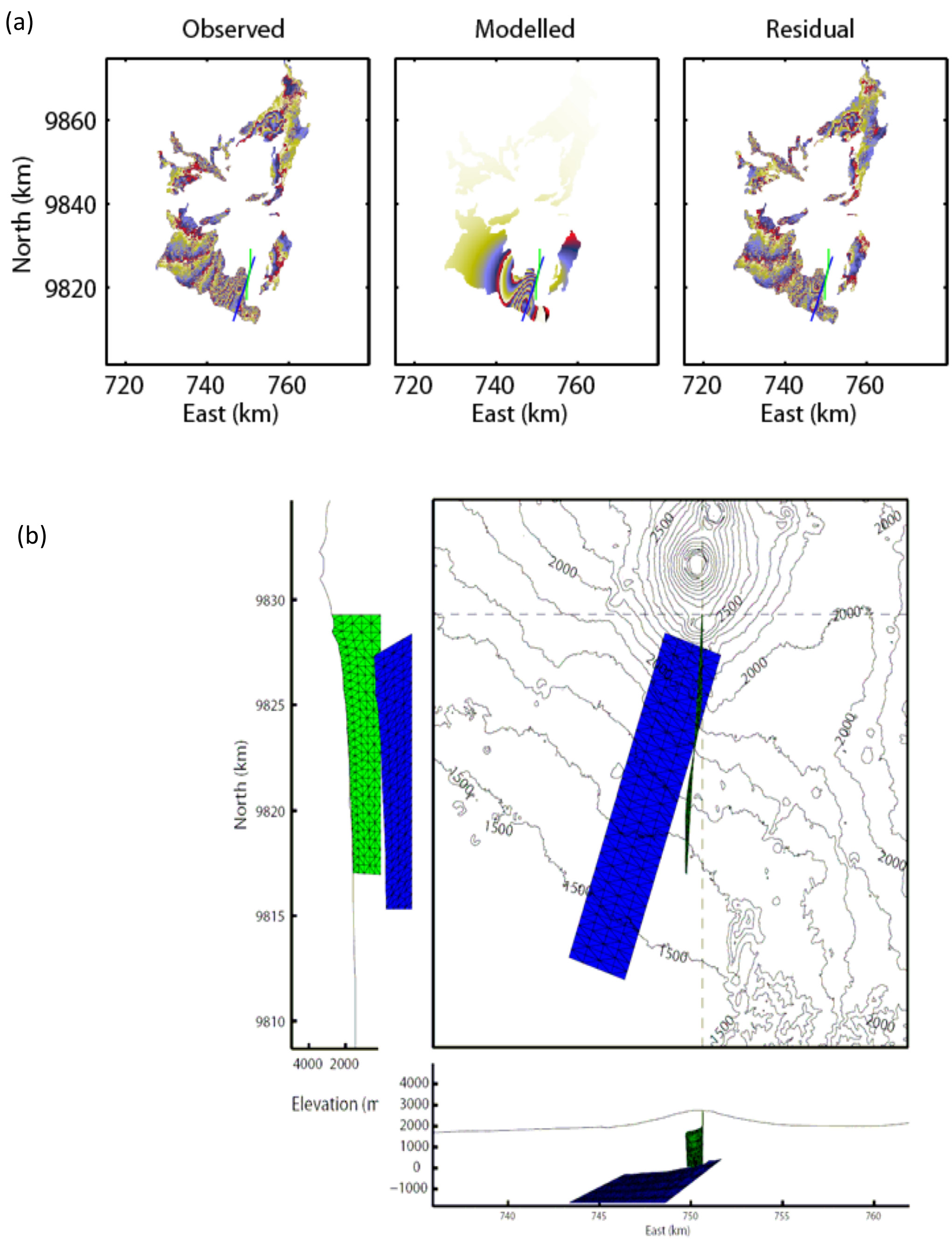

Figure 6. Results obtained for the simultaneous dike and west-dipping fault inversion: (a) Data, Model and Residuals for the best fit model. (b) Geometry of the best fit dike and fault. Values of model parameters are given in Table 3.

The model needs to be improved as data from only one LOS were used. In order to improve the measurement of the co-eruptive displacements, more acquisitions geometries are needed such as those provided by the RADARSAT-1 images. The western part of the study area (E area in Figure 2) can only be explained by the introduction of a third source. Preliminary models showed that a simple deflating spherical source, west of Nyamulagira volcano, can explain this signal. However, the inversion predicts a 24 km deep source. This disagrees with the depth inferred from geophysical and petrological data, which suggested that the magmatic chamber of Nyamulagira is located between 3 and 7 kilometers depth [19, 20]. We are currently exploring other possible sources such as another normal fault in the vicinity of the two neighboring volcanoes.

Table 3. Characteristics of best-fit dike and east-dipping fault model (1) and dike and west-dipping fault (2) showed in Figures 5 and 6 respectively. 10 parameters were inverted for both inversions. For the dike, in both inversions: *Shear* is fixed to 0°, *Botlen* fixed to 1, and *Twist* fixed to 0°. Other fixed parameters are underlined. Mb is the body-wave magnitude.

	P_0 (MPa)	Dip (°)	Botelv (m)	Botang (°)	Max. op. (m)	V (e+06m^3)	Midx; Midy (km)	Midz (m)	Toplength (km)	Height (m)	Strike (°)	Dip$_f$ (°)	S (MPa)	Mw	Rms (mm)
(1)	0.24	70	-1000	3.6	0.9	32	747; 9820	-2300	18.6	970	21	60	3	5.8	15
(2)	0.14	90	69	0	0.4	6	748; 9820	0	15.6	3200	22	25	0.2	4.9	15

4. Conclusions

We determine that the main part of deformation signal observed by InSAR South and East of Nyiragongo between 14 January and 13 February 2002 can be explained by the combined effects of a 2 km high subvertical dike feeding the observed eruptive fissure, and a 15 km long west dipping normal fault extending from the foot of Nyiragongo to the northern part of lake Kivu. The dike is submitted to a low overpressure of 0.14 MPa, consistent wit the rift extension. This fault is in the continuation of the known horst structures of the Idjiwi Island. It could also correspond to the interface between sedimentary layers tilted by the half rift graben opening.

The model has to be refined, first, by taking into account the other InSAR data (RADARSAT data) available for this eruption and then by modeling the western part of the InSAR signal possibly associated to a deflating magmatic reservoir or a deep normal fault.

5. References

[1] Ebinger C.J and Furman T., Geodynamical setting of the Virunga volcanic province, East Africa, In : Acta Vulcanologica, *The January 2002 eruption of*

Nyiragongo volcano and the socio-economical impact, Vol. 14 (1-2) et vol. 15 (1-2), Istituti editorali e poligrafici internazionali, Pisa-Roma, 9-16, 2004.

[2] Corti G., Bonini M., Innocenti F., Manetti P., Mulugeta G., Sokoutis D., and Cloetingh S., Rift-parallel magma migration and localisation of magmatic activity in transfert zones, In : Acta Vulcanologica, *The January 2002 eruption of Nyiragongo volcano and the socio-economical impact*, Vol. 14 (1-2) et vol. 15 (1-2), Istituti editorali e poligrafici internazionali, Pisa-Roma, 17-26, 2004.

[3] Wauthier C., *Modélisation des déplacements InSAR survenus au Nyiragongo en janvier 2002*, Mémoire de Master 2 recherche, Université de Clermont-Ferrand II, 52p. , 2007.

[4] Komorowski J-C, Tedesco D., Kasereka M., Allard P., Papale P., Vaselli O., Baxter P., Halbwachs M., Akumbe M., Baluku B., Briole P., Ciraba M., Dupin J-C, Etoy O., Garcin D., Hamaguchi H., Houli´e N., Kavotha K.S., Lemarchand A., Lockwood J., Lukaya N., Mavonga G., De Michele M., Mpore S., Mukambilwa K., Munyololo F., Newhall C., Ruch J., Yalire M. and Wafula M., The January 2002 flank eruption of Nyiragongo volcano (Democratic Republic of Congo) : Chronology, evidence for a tectonic rift trigger, and impact of lava flows on the city of Goma, In : Acta Vulcanologica, *The January 2002 eruption of Nyiragongo volcano and the socio-economical impact*, Vol. 14 (1-2) et vol. 15 (1-2), Istituti editorali e poligrafici internazionali, Pisa-Roma, 27-62, 2004.

[5] Allard P., Baxter P., Halbwachs M., and J.-C. Komorowski, *The January 2002 eruption of Nyiragongo volcano (Dem. Repub. Congo) and related hazards: observations and recommendations*, Final Report of the Franc-British scientific team, Paris, March 8, 2002.

[6] Tedesco D., O. Vaselli, P. Papale, S. A. Carn, M. Voltaggio, G. M. Sawyer, et al., "January 2002 volcano-tectonic eruption of Nyiragongo volcano, Democratic Republic of Congo", *J. Geophys. Res*., 112, B09202, doi:10.1029/2006JB004762, 2007.

[7] Massonet D. and Feigl K.L., 1998, Radar interferometry and its application to changes in the Earth's surface, *Reviews of Geophysics*, 36(4), 441-500.

[8] Kampes B. and S. Usai, "Doris: The Delft Object-oriented Radar Interferometric software," *Proc. ITC 2nd ORS symposium*, August 1999, The Netherlands, 1999.

[9] Poland M., "InSAR Captures Rifting and Volcanism in East Africa," *Alaska Satellite Facility News & Notes*, Vol. 3:2, 2006.

[10] Wauthier C., V. Cayol, N. D'Oreye and F. Kervyn, "Modeling of InSAR displacements related with the January 2002 eruption of Nyiragongo volcano

(DRC)," *Proc. of 4th ESA Fringe2007 workshop*, ESA-ESRIN, Frascati, Italie, 26-30 November 2007.

[11] Farr, T. G., *et al.*, 2007, The Shuttle Radar Topography Mission, *Rev. Geophys*., 45, RG2004, doi:10.1029/2005RG000183.

[12] Fukushima Y., V. Cayol, and P.Durand, "Finding realistic dike models from interferometric synthetic aperture radar data: The February 2000 eruption at Piton de la Fournaise," *Journal Geoph. Res*., VOL. 110, B03206, 2005.

[13] Cayol V., and F.H. Cornet, "3D mixed boundary elements for elastostatic deformations fields analysis", *Int. J. Rock Mech. Min. Sci. Geomech*. Abstr., 34, 275-287, 1997.

[14] Delaney P. T., D. D. Pollard and J. I. Ziony and E. H. McKee, Field relations between dikes and joints: Emplacement processes and paleostress analysis, J. Geophys. Res., 91, 4920-4938, 1986.

[15] Rubin A. M., Propagation of magma-filled cracks, Annu. Rev. Earth Planet. Sci., 23, 287-336, 1995.

[16] Sambridge M., 1999a, Geophysical inversion with a neighbourhood algorithm - I. Searching a parameter space, *Geophys. J. Int*., 138, 479-494.

[17] Chen C.W. and H.A. Zebker, 2001, Two-dimensional phase unwrapping with use of statistical models for cost functions in nonlinear optimization, Journal of the Optical Society of America, A, vol. 18, 338-351.

[18] Allmann, B. and P. M. Shearer, 2009, Global variations of stress drop for moderate to large earthquakes, J. Geophys. Res., 114, B01310, doi:10.1029/2008JB005821.

[19] Hamaguchi H., 1983, Seismological evidence for magma intrusion during the 1981-1982 Nyamuragira eruption, In : Hamaguchi H. (ed.), *Volcanoes Nyiragongo and Nyamuragira : Geophysical aspects*, Tohoku University, Sendai, Japon, 29-33.

[20] Mishina M., 1983, Gravity survey in and around Volcanoes Nyamuragira and Nyiragongo, In: Hamaguchi H. (ed.), *Volcanoes Nyiragongo and Nyamuragira: Geophysical aspects*, Tohoku University, Sendai, Japon, 69-74.

Table of Contents

Déjà parus

Vol 1:	Seismic Networks and Rapid Digital Data Transmission and Exchange (1990)
Vol 2:	GPS for Geodesy and Geodynamics (1990)
Vol 3:	Non Tidal Gravity Changes: Intercomparison between Absolute and Superconducting Gravimeters (1991)
Vol 4:	Geodynamical Instrumentation Applied to Volcanic Areas (1991)
Vol 5:	Local and National Seismic Networks: On Line Data Processing with Microcomputer Facilities (1992)
Vol 6:	Application of Artificial Intelligence Techniques in Seismology and Engineering Seismology (1992)
Vol 7:	European Macroseismic Scale 1992 (1993)
Vol 8:	New Challenges for Geodesy in Volcanoes Monitoring (1995)
Vol 9:	Dynamical Systems and Artificial Intelligence Applied to Data Banks in Geophysics (1995)
Vol 10:	Accurate Orbit Determination and Observations of High Earth Satellites for Geodynamics (1995)
Vol 11:	Non Tidal Gravity Changes: Intercomparison between Absolute and Superconducting Gravimeters (1995)
Vol 12:	Application of Artificial Intelligence Techniques in Seismology and Engineering Seismology (1996)
Vol 13:	Historical Seismic Instruments and Documents: a Heritage of Great Scientific and Cultural Value (1997)
Vol 14:	Short Term Thermal and Hydrological Signatures Related to Tectonic Activities (1997)
Vol 15:	European Macroseismic Scale (1998)
Vol 16:	Geodynamical Hazards Associated with Large Dams (1998)
Vol 17:	High Precision Gravity Measurements with Application to Geodynamics and Second GGP Workshop (2000)
Vol 18:	Evaluation of the Potential For Large Earthquakes in Regions of Present Day Low Seismic Activity in Europe (2001)
Vol 19:	L'Echelle Macrosismique Européenne 1998 New (version française) (2001)
Vol 20:	Analytical Representation of Potential Field Anomalies for Europe (2003)
Vol 21:	Escala Macrosismica Europea 1998 (spanish version) (2003)
Vol 22:	IMG 2002- Instrumentation and Metrology in Gravimetry (2003)
Vol 23:	The State of GPS Vertical Positioning Precision: Separation of Earth Processes by Space Geodesy (2004)
Vol 24:	Forcing of Polar Motion in the Chandler Frequency Band: A Contribution to Understanding Interannual Climate Variations (2005)
Vol 25:	GOCINA: Improving Modeling of Ocean Transport and Climate Prediction in the North Atlantic Region Using GOCE Gravimetry (2006)
Vol 26:	International Comparison of Absolute Gravimeters in Walferdange (Luxembourg) of November 2003 (2006)
Vol 27:	Escala Macrosismica Europea 1998 (updated spanish version) (2009)
Vol 28:	Seismicity Patterns in the Euro-Med Region (2009)